UNIVERSITÉ DU QUÉBEC À MONTRÉAL

LA DYNAMIQUE DU DIOXYDE DE CARBONE ET DU MÉTHANE DANS UN RÉSERVOIR TROPICAL

THÈSE

PRÉSENTÉE

COMME EXIGENCE PARTIELLE

DU DOCTARAT EN BIOLOGIE

PAR

CYNTHIA SOUEID

DÉCEMBRE 2020

UNIVERSITÉ DU QUÉBEC À MONTRÉAL
Service des bibliothèques

Avertissement

La diffusion de cette thèse se fait dans le respect des droits de son auteur, qui a signé le formulaire *Autorisation de reproduire et de diffuser un travail de recherche de cycles supérieurs* (SDU-522 – Rév.10-2015). Cette autorisation stipule que «conformément à l'article 11 du Règlement no 8 des études de cycles supérieurs, [l'auteur] concède à l'Université du Québec à Montréal une licence non exclusive d'utilisation et de publication de la totalité ou d'une partie importante de [son] travail de recherche pour des fins pédagogiques et non commerciales. Plus précisément, [l'auteur] autorise l'Université du Québec à Montréal à reproduire, diffuser, prêter, distribuer ou vendre des copies de [son] travail de recherche à des fins non commerciales sur quelque support que ce soit, y compris l'Internet. Cette licence et cette autorisation n'entraînent pas une renonciation de [la] part [de l'auteur] à [ses] droits moraux ni à [ses] droits de propriété intellectuelle. Sauf entente contraire, [l'auteur] conserve la liberté de diffuser et de commercialiser ou non ce travail dont [il] possède un exemplaire.»

REMERCIEMENTS

Cette thèse est le fruit non seulement d'un travail personnel, mais surtout d'un effort collectif d'une multitude de personnes sans lesquelles elle n'aurait pas été possible. Un des éléments clés pour mener à bien un projet de doctorat est l'encadrement. C'est pour cette raison que j'aimerais remercier en premier mon superviseur de recherche, le Dr Yves Prairie, qui a été un mentor exemplaire pour moi. Pour ton esprit passionné, ton expertise et ta créativité scientifique, ton habilité et ton enthousiasme à enseigner, et ton support moral infaillible, merci Yves. J'ai eu la chance d'avoir un superviseur qui, malgré sa surcharge de travail, fait de ses étudiants une vraie priorité, gardant toujours la porte de son bureau entre ouverte au cas ou l'un d'eux aurait besoin d'aide.

J'ai aussi eu la chance de travailler dans un groupe de recherche très amical et dynamique, ou l'entraide et la cohésion sociale étaient toujours au rendez-vous. Pour cela je remercie tous les membres de mon labo et des labos connexes pour avoir bâti ensemble cet environnement de travail exceptionnel. Plus particulièrement, Sara Mercier-Blais, Paula Reis, Jihyeon Kim, Shoji Thothattil, Marie Gérardin, Karelle Desrosiers, Martin Desmers, Joan Pere Casas Ruiz et Nicolas Fortin St-gelais, de vraies sœurs et frères scientifiques, qui m'ont soutenu pendant plusieurs années et ont partagé avec moi les bons et les mauvais moments. Aussi, Marie-Pier Hébert, Vincent Fugère, Tonya Delsontro, Patricia Pernica, Matthew Bogard, et Richard Vogt, que je considère avant tout comme des amis, ont été des piliers pour moi durant cette période, autant au niveau scientifique que personnel. Sara, Paula, et Karelle ont été des partenaires d'échantillonnage incroyables, à qui je dois une base de données de grande qualité. D'ailleurs, l'échantillonnage a été possible surtout grâce à nos collaborateurs malaisiens avec qui j'ai vécu des moments inoubliables : Karen Lee Suan Ping, Jenny

Choo Cheng Yi, Jessica Fong Fung Yee, Amar Ma'aruf Bin Ismawi, Gerald Tawie Anak Thomas, Hilton Bin John, et les chauffeurs de bateau. Un merci spécial à Jenny qui a coordonné les campagnes d'échantillonnage et a pris de son temps pour me faire découvrir la culture et les richesses de sa terre natale. Les analyses de labo ont été beaucoup plus faciles et agréables grâce à l'aide Katherine Velghe, Marilyne Robidoux, et Alice Parkes, avec qui c'est toujours un plaisir de travailler.

Finalement, je remercie mes amis et ma famille qui ont toujours été présents pour m'écouter, m'encourager, et me permettre de décrocher quand j'en avais besoin. En particulier, mon conjoint, Stéphane Brucher, qui a vécu à mes côtés et au quotidien les moments les plus difficiles du doctorat. Ton support a été constant, inconditionnel, et essentiel à la réussite de cette thèse, merci du fond du cœur.

TABLE DES MATIÈRES

LISTE DES FIGURES

LISTE DES TABLEAUX

RÉSUMÉ

Les réservoirs sont reconnus comme étant des émetteurs de gaz à effet de serre (GES) vers l'atmosphère, comme le dioxyde de carbone (CO_2) et le méthane (CH_4), pourtant, l'ampleur globale de ces émissions est encore incertaine et débattue. Les GES sont émis à travers plusieurs voies dans les réservoirs (la diffusion en surface, l'ébullition, le dégazage, et les émissions dans l'effluent), cependant, elles ne sont généralement pas toutes prises en compte dans les bilans de carbone des réservoirs. Les flux de GES varient énormément entre les réservoirs, mais aussi au sein d'un même système en fonction de du temps, de l'espace, et de la voie d'émission. Prédire les émissions de carbone à l'échelle de l'écosystème des réservoirs actuels et futurs est donc un défi, et nécessite une bonne compréhension des processus qui sous-tendent les flux de CO_2 et de CH_4. Les flux de GES des réservoirs résultent de la somme des apports horizontaux, des échanges gazeux à l'interface sédiment-eau, du transport vertical des gaz, et du métabolisme dans la colonne d'eau. Ces processus sont rarement quantifiés dans les réservoirs, et sont souvent étudiés séparément. Par conséquent, la connaissance actuelle de la régulation du CO_2 et du CH_4 est fragmentée, n'offrant pas de portrait intégral de l'importance relative des processus et de leurs interactions à l'échelle de l'écosystème. Le but général de cette thèse est de construire un portrait complet des flux de CO_2 et CH_4 et des processus qui les sous-tendent ces émissions dans le réservoir Batang Ai situé sur l'ile tropicale de Bornéo. Cet objectif a été réalisé grâce à une combinaison de techniques : échantillonnage sur le terrain, incubations expérimentales, et modélisation.

Les résultats montrent que les flux diffusifs et ebullitifs sont relativement faibles dans le réservoir, dont l'empreinte carbone est principalement due au dégazage et aux émissions dans l'effluent, de CH_4 surtout (Chapitre I). Les flux mesurés contrastent avec les prédictions des modèles actuels qui surestiment la diffusion de surface et l'ébullition et sous-estiment les flux en aval du barrage. La composition du sol, les patrons de sédimentation, le métabolisme net du CO_2, et la dynamique des GES en eaux profondes ont été identifiés comme éléments clés à investiguer pour améliorer la modélisation des flux de GES des réservoirs. La contribution relative des sources qui soutiennent la diffusion de surface change le long du continuum hydrologique, avec une influence décroissante des apports horizontaux, et diffèrent entre les deux gaz, avec un plus grand apport des sédiments pour le CH_4 versus de la couche profonde pour le CO_2 (Chapitre II). Le métabolisme dans la colonne d'eau joue un rôle majeur, dans le cas du CO_2 et du CH_4, mais est aussi la composante la plus variable et incertaine des budgets épilimnetiques de ces gaz. La modélisation du CO_2 et du CH_4 dans la couche profonde, qui alimente les émissions en aval, suggère que l'accumulation de gaz s'est stabilisée environ 10 ans après la construction du barrage (Chapitre III). La comparaison entre les données modélisées et mesurées a révélé que la production anaérobique de CO_2 et la méthanogenèse dans la colonne d'eau sont des processus peu connus, mais importants dans la dynamique des GES en profondeur. Les patrons de CO_2 et CH_4 en eaux profondes sont étroitement liés à la concentration en oxygène (O_2), qui a un grand impact sur la respiration aérobique et sur l'oxydation du CH_4. Parmi les paramètres du modèle, la diffusivité verticale des gaz joue un rôle fondamental à travers son effet direct sur le transport des gaz, et son impact sur le profile d'O_2, modulant indirectement les processus métaboliques.

La combinaison des résultats des trois chapitres présente un portrait exhaustif permettant une meilleure compréhension du rôle et de l'interaction des voies d'émissions, des processus, et des facteurs qui régissent la dynamique du CO_2 et du CH_4 à l'échelle de l'écosystème. À travers un échantillonnage spatiotemporel détaillé, l'étude montre la variabilité des composantes mesurées, et révèle leurs chagements le long de la transition hydrologique d'une rivière à un réservoir. Cette recherche fournie des informations manquantes sur le cycle des GES dans un réservoir stratifié en permanence, un trait commun dans les régions tropicales sous étudiées et où la construction de barrages est en forte expansion. Les connaissances acquises ici, particulièrement à travers la modélisation, sont aussi en partie transférables aux réservoirs à plus grande échelle. Finalement, cette thèse identifie les failles dans les connaissances actuelles à combler pour améliorer les modèles et les grandes sources de variabilité et d'incertitude, guidant ainsi les recherches futures sur les GES dans les réservoirs.

Mots clés : dioxyde de carbone, méthane, gaz à effet de serre, réservoir, métabolisme, modélisation, flux.

ABSTRACT

Reservoirs are known to emit greenhouse gases (GHG) to the atmosphere, namely carbon dioxide (CO_2) and methane (CH_4), yet, the global extent of their emissions is still uncertain and currently debated. In reservoirs, GHG are emitted through various pathways (surface diffusion, ebullition, degassing, and downtream emissions), however, they are usually not all sampled in reservoirs carbon footprint assessments. GHG fluxes vary tremendously among reservoirs, but also within a system as a function of space, time, and flux pathway. This makes it challenging to predict ecosystem scale carbon emissions of current and future reservoirs, a task which requires a good understanding of the processes underlying CO_2 and CH_4 fluxes. Reservoir CO_2 and CH_4 fluxes are shaped as the sum of external horizontal inputs, sediment-water fluxes, vertical gas transport, and water column metabolism. These processes are rarely quantified in reservoirs, and are mostly studied seperately. Hence, current information on CO_2 and CH_4 regulation is fragmented, with no integrated picture of the relative importance of each process and how they vary and interact at an ecosystem scale. The general objective of this thesis is to build a complete portrait of CO_2 and CH_4 fluxes and the processes underlying them in the case study of Batang Ai, a tropical reservoir located on the Borneo Island. This goal was addressed using a combination of field sampling, experimental incubations, and modeling approaches.

Results showed that the reservoir had low to moderate diffusive and ebullitive GHG fluxes, and that its carbon footprint was mainly due to degassing and downstream emissions, especially of CH_4 (Chapter I). Measured flux data contrasted with current predictive models, which overestimated surface diffusion and ebullition and underestimated emissions below the dam. Soil composition, sedimentation patterns, net CO_2 metabolism, and deep water GHG dynamics, were identified as key elements to investigate in order to improve modeling of reservoir GHG emissions. The relative contribution of sources sustaining surface diffusion changed along the hydrological continuum, with a decreasing influence of horizonral inputs, and differed among the two gases, with higher inputs from sediments for CH_4 versus the bottom layer for CO_2 (Chapter II). Water column metabolism played a major role for both CO_2 and CH_4, although it was also the most variable and uncertain component of the epilimnetic gas budgets. Modeling of CO_2 and CH_4 in the deep layer, fueling downstream emissions, suggested that the accumulation of gases had stabilized around 10 years after impoundment (Chapter III). Comparing modeled results to empirical data revealed that anaerobic CO_2 production and water column methanogenesis, despite being poorly known processes, likely play an important role in deep GHG dynamics. Deep CO_2 and CH_4 patterns were tightly linked to oxygen (O_2) concentration, which had a large impact on aerobic respiration and on CH_4 oxidation. Among all model parameters, vertical gas diffusivity had an overarching role via its direct effect on CO_2 and CH_4 transport, and its impact on the O_2 profile, indirectly modulating metabolic processes.

Combining the results of the three chapters provides a comprehensive picture allowing a better understanding of the role and interplay between each flux pathway, process, and factor in shaping CO_2 and CH_4 dynamics at the ecosystem scale. Through an extensive spatial and temporal sampling, the study grasps the variability of measured components, and reveals how transitioning from a river to a reservoir system impacts them. Overall this research provides lacking information on reservoir GHG cycling in a permenently stratified system, a common feature in the understudied tropical regions where reservoir construction is rapidely expanding. Insights derived here, especially from the mechanistic modeling framework, are also partly transferable to reservoirs at large. Finally, the thesis identifies knwoledge gaps to address for improving the modeling framework and tackling the large sources of variability and uncertainty, thus guiding future research on GHG in reservoirs.

Keywords : carbon dioxide, methane, greenhouse gases, reservoir, metabolism, modeling, flux.

INTRODUCTION

0.1 Le contexte actuel de l'empreinte carbone des réservoirs

La construction de réservoirs d'eau douce date de 3000 avant J.-C. et a plusieurs utilités : l'irrigation, l'approvisionnement en eau, le contrôle des inondations, la navigation, et la production d'hydroélectricité. Il y a présentement plus de 58 000 grands barrages (plus de 15 m de haut) recensés à travers le monde, dont 20 % produisent de l'hydroélectricité qui fournit 24 % de la demande globale en électricité (ICOLD, 2019). Le secteur hydroélectrique est en expansion rapide, avec une croissance attendue de 50 à 100 % d'ici 2050 (International Hydropower Association (IHA), 2015). L'hydroélectricité a longtemps été considérée comme une énergie verte, ne produisant pas de gaz à effet de serre (GES). Cependant, au début des années 90, Rudd et al. (1993) suggèrent que la décomposition biologique de la matière organique inondée lors de la construction de réservoirs peut être une source importante de dioxyde de carbone (CO_2) et de méthane (CH_4) vers l'atmosphère. Cette affirmation a déclenché un débat au sein de la communauté scientifique (dos Santos *et al.*, 2006 ; Fearnside et Pueyo, 2012 ; Fearnside, 2006 ; Rosa *et al.*, 2004), et a mené à la collecte de données sur des réservoirs à travers le monde et à la publication de nombreuses études sur le sujet. Après deux décennies de recherche, la contribution des réservoirs aux émissions de GES fait consensus, mais l'amplitude de ces émissions à l'échelle globale reste incertaine (Deemer *et al.*, 2016). Cette incertitude est due d'une part à un manque de données sur certaines voies d'émissions (ex. émissions en aval) et dans certaines régions (ex. Afrique et Asie du Sud-Est), et d'autre part à une compréhension limitée des mécanismes régulant les émissions. Étant au croisement entre la crise climatique et la demande croissante en eau et en énergie, le sujet de l'empreinte carbone (C) des réservoirs reçoit présentement beaucoup d'attention, non seulement des chercheurs, mais aussi des acteurs du milieu et des médias. Dans ce contexte, il y a actuellement un intérêt marqué à combler le manque d'information concernant la dynamique des GES dans les réservoirs, afin de pouvoir mieux estimer et prédire leur impact sur climat actuel et futur.

0.2 Les sources de CO_2 et CH_4 dans les réservoirs

0.2.1 Le métabolisme aérobique

La production et la consommation de CO_2 dans la colonne d'eau se font principalement à travers le métabolisme aérobique de respiration et production primaire. La respiration aérobique est la transformation de la matière organique en CO_2 via la consommation d'oxygène (O_2). Dans les lacs, les taux de respiration aérobique varient grandement, allant de 0.029 à 4800 $mmolO_2.m^{-3}.d^{-1}$ (Pace et Prairie, 2005 ; Pollard, 2013). La respiration dépend de la disponibilité et de la labilité de son substrat : la matière organique (Amon et Benner, 1996 ; Cammack *et al.*, 2004). En effet, les taux de respiration aquatiques varient selon un gradient de statut trophique et de concentration en C organique dissout; des indicateurs de la productivité interne et des apports externes de matière organique (Pace et Prairie, 2005). La labilité de la matière organique peut être influencée par le ratio de ces deux sources et par la photooxydation, processus par lequel les radiations solaires dégradent la matière organique en molécules plus labiles et faciles à respirer (Cory et Kling, 2018). La respiration est sensible à la température (Carignan *et al.*, 2000), avec des taux généralement plus élevés dans les climats chauds (Lewis, 2010). Dans les réservoirs, la respiration est un processus majeur de décomposition de la matière inondée surtout dans les premiers temps après la construction des barrages (Abril *et al.*, 2005 ; Teodoru *et al.*, 2012 ; Thérien et Morrison, 2005). La consommation d'O_2 par la respiration est aussi responsable de la création de conditions hypoxiques et anoxiques surtout dans les eaux profondes des lacs et réservoirs.

À l’inverse, la production primaire (principalement la photosynthèse) produit de l’O_2 et de la matière organique, et constitue un puit de CO_2 majeur dans les systèmes aquatiques. La photosynthèse dépend de la lumière, de la température, et de la disponibilité des nutriments (surtout l’azote et le phosphore). Ainsi, les eaux tropicales ont en moyenne des taux de productivité primaire plus élevés (Amarasinghe et Vijverberg, 2002 ; Lemoalle, 1981 ; Likens, 1975). Bien que les facteurs contrôlant la production primaire soient les mêmes dans les lacs et les réservoirs, des différences ont été notées entre ces deux types de systèmes (Jones et Knowlton, 1993 ; Lind *et al.*, 1993 ; Walker, 1984). Les réservoirs sont généralement caractérisés par une forte influence des apports riverains et par des zones de transition hydrologiques d’un système lotique à lentique (Kimmel et Groeger, 1984). Cette configuration crée un gradient horizontal de nutriments, de turbidité, et d’atténuation de la lumière qui favorise une grande hétérogénéité spatiale de la productivité primaire dans les réservoirs comparés aux lacs (Kimmel, Bruce L. *et al.*, 1990 ; Knoll *et al.*, 2003).

0.2.2 La production et consommation de CH_4

La production de CH_4 se fait par méthanogenèse, une forme de respiration anaérobique performée par des microorganismes méthanogènes du domaine des archées. Deux types de méthanogenèse existent : la fermentation des acétates qui produit du CO_2 en plus du CH_4, et l’oxydation du CO_2 qui le consomme (Demirel et Scherer, 2008). Bien qu’il n’y a pas de consensus sur le sujet, la fermentation des acétates semble être la voie de méthanogenèse dominante dans les eaux douces (Conrad, 2005). La méthanogenèse est une réaction très couteuse en énergie, elle est donc principalement active dans des conditions biochimiques réduites, où d’autres accepteurs d’électrons comme l'O_2 ne sont pas disponibles (Ferry, 2012). La méthanogenèse se produit donc surtout dans les couches anoxiques des lacs et réservoirs, majoritairement dans les sédiments, mais a aussi été observé dans les eaux profondes (Iversen *et al.*, 1987 ; Lliros *et al.*, 2010 ; Musenze *et al.*, 2016). Cependant, il y a de plus en plus de preuves que la méthanogenèse se produit aussi dans les eaux oxygénées (dans des niches micro-anoxiques), mais son importance à l'échelle écosystémique reste peu connue (Bogard *et al.*, 2014 ; Donis *et al.*, 2017 ; Grossart *et al.*, 2011 ; Tang *et al.*, 2014). Le taux de méthanogenèse augmente avec la quantité et la labilité de la matière organique (Kelly et Chynoweth, 1981 ; West *et al.*, 2012), la production de CH_4 est donc très active dans les réservoirs nouvellement inondés (Matthews *et al.*, 2005). La méthanogenèse est aussi très sensible à la température (Yvon-Durocher *et al.*, 2014), ce qui en fait un processus particulièrement important dans les réservoirs tropicaux (Marotta *et al.*, 2014).

L'oxydation du CH_4 est un processus microbien qui consomme le CH_4 en tant que source de C et relâche du CO_2. Cette réaction est particulièrement importante en termes de GES car elle transforme le CH_4, un GES puissant, en CO_2 qui a un potentiel de réchauffement atmosphérique 32 fois moins élevé sur un horizon de 100 ans (Ciais *et al.*, 2013). L'oxydation du CH_4 se produit en grande majorité dans les environnements oxiques et hypoxiques, mais peut dans une moindre mesure se produire dans les environnements anoxiques (Valentine, 2002). Les taux maximaux d'oxydation du CH_4 sont retrouvés dans les zones hypoxiques et riches en CH_4, comme à l'interface eau-sédiment ou dans la zone metalimnétique (Bastviken *et al.*, 2002 ; Kankaala *et al.*, 2006 ; Thottathil *et al.*, 2019 ; Zigah *et al.*, 2015). Cependant, ce n'est pas clair si les organismes méthanotrophes préfèrent les zones hypoxiques à cause de l'effet direct de l'O_2 sur leur métabolisme (Rudd et Hamilton, 1978) ou dû à l'abondance de CH_4 dans ces zones (Borrel *et al.*, 2011). L'oxydation du CH_4 est optimale à 25 °C mais est active dans une large gamme de températures (Chowdhury et Dick, 2013). L'oxydation du CH_4 est moins active dans les environnements photiques dus à un effet d'inhibition de la lumière (Murase et Sugimoto, 2005 ; Shelley *et al.*, 2017). La proportion de CH_4 oxydé diffère d'un système à l'autre, dépendamment de l'interaction entre les facteurs, dont la communauté méthanotrophique (Reis *et al.*, 2020b) et la structure physicochimique de la colonne d'eau en termes de luminosité, stratification thermale et profile d'oxygène (Thottathil *et al.*, 2018 ; Vachon *et al.*, 2019).

0.2.3 Le bilan à l'échelle de l'écosystème

Les concentration de CO_2 et CH_4 dans l'eau sont déterminées par la balance entre les processus métaboliques internes, et par les apports externes. Dans le cas du CO_2, la balance entre la respiration aérobique et la production primaire détermine si un système est autotrophe ou hétérotrophe (net consommateur ou producteur de CO_2). La tendance globale suggère que l'hétérotrophie est plus fréquente dans les systèmes moins productifs (oligotrophes) (Duarte et Agustí, 1998) et plus riches en matière organique dissoute (Bogard *et al.*, 2020), notamment d'origine externe, qui favorisent la respiration bactérienne tout en limitant la disponibilité de la lumière et des nutriments pour la production primaire (Giorgio *et al.*, 1999). À l'inverse, la production primaire excède généralement la respiration dans les systèmes très productifs, où les bactéries sont plus sujettes à la prédation et à la lyse (Cotner et Biddanda, 2002 ; Roberts et Howarth, 2006). Bien que les systèmes autotrophes consomment du CO_2, leur haute productivité a tendance à promouvoir la sédimentation de C organique (Evans *et al.*, 1997) favorisant la production de CH_4 dans les zones benthiques (Adams, 2005 ; Almeida *et al.*, 2016 ; Beaulieu *et al.*, 2019 ; Sobek *et al.*, 2012). Le CH_4 produit peut être oxydé en CO_2 avant d'être émis vers l'atmosphère. La balance entre la production et la consommation du CH_4, bien que très peu étudiée (DelSontro *et al.*, 2018b), dépend d'une part de l'O_2 qui est fortement associé au métabolisme du CO_2, et d'autre part de facteurs physiques comme la lumière (Thottathil *et al.*, 2018) et la stratification thermale (Vachon *et al.*, 2019). Ainsi, les dynamiques du CO_2, du CH_4, et de l'O_2 sont étroitement liées, et sont modulées par des les traits physiques des lacs et réservoirs.

Les flux de CO_2 et CH_4 des systèmes aquatiques vers l'atmosphère ne reflètent pas seulement le métabolisme interne du C, mais aussi les apports externes de gaz. L'amplitude de ces apports dépend de la biogéochimie et de l'hydrologie du bassin versant, soit de la quantité de C présente dans les sols et de sa capacité à être lixiviée vers les systèmes aquatiques. La contribution des apports externes aux émissions aquatiques de CO_2 et CH_4 varie de négligeable à majeure (Bogard *et al.*, 2019 ; Rasilo *et al.*, 2017 ; Wilkinson *et al.*, 2016), et a tendance à augmenter avec la connectivité sol - eau, donc a diminué avec la taille du système (Hotchkiss *et al.*, 2015 ; Humborg *et al.*, 2010 ; Lapierre et del Giorgio, 2012). Les apports externes de CO_2 et de CH_4 sont souvent liés, non seulement dû à leur source commune, mais aussi dû au fait que l'oxydation du CH_4 à l'interface sol - eau peut alimenter les émissions de CO_2 dans systèmes aquatiques (Lupon *et al.*, 2019 ; Rasilo *et al.*, 2014).

Les sources de CO_2 et CH_4 dans les réservoirs, tout comme dans les lacs, sont régulées par l'interaction entre les propriétés physiques, chimiques, et biologiques du système et de son bassin versant. À l'échelle de l'écosystème, ces interactions restent mal connues dans les lacs, et encore moins dans les réservoirs. En ce sens, l'impact de la construction de réservoirs sur la dynamique aquatique des GES est encore un sujet de recherche actif (Maavara *et al.*, 2017).

0.3 Les émissions de GES des réservoirs

0.3.1 Les voies d'émissions

Les réservoirs émettent des GES vers l'atmosphère à travers plusieurs voies: la diffusion de surface, l'ébullition, le dégazage, et l'émission en aval. La diffusion de surface est l'échange de gaz entre l'air et l'eau à la surface du réservoir. Ce flux dépend d'une part du gradient de concentration entre les deux fluides (air et eau) qui détermine la direction et l'amplitude du flux de gaz, et d'autre part de la turbulence à l'interface air-eau qui détermine la vitesse de l'échange gazeux. La diffusion de surface est donc influencée par les sources et puits des GES dans la couche d'eau de surface. Cette voie d'émission est la plus documentée dans les réservoirs (et dans les lacs naturels) car elle est relativement facile à mesurer.

L'émission de GES par ébullition résulte de la formation de bulles de gaz dans les sédiments. Ces bulles sont composées principalement de CH_4, un gaz beaucoup plus enclin à former des bulles comparativement au CO_2 et à l'oxyde nitreux (N_2O) dû à sa faible solubilité dans l'eau. La formation et l'ascension de bulles de GES des sédiments vers l'atmosphère sont contrôlées par la quantité de gaz produite et par la pression hydrostatique. L'ébullition est donc généralement restreinte aux zones littorales où la température est plus élevée (plus grande production) et où la pression hydrostatique est plus faible (DelSontro *et al.*, 2016a ; Wik *et al.*, 2014). L'ébullition est particulièrement importante en termes de GES car elle permet au CH_4 d'atteindre directement l'atmosphère sans être oxydé en CO_2 dans la colonne d'eau (ce qui réduirait son potentiel de réchauffement climatique). L'ébullition est connue pour son extrême hétérogénéité spatiale et temporelle (Grinham *et al.*, 2011), ce qui rend le flux ebullitif de GES difficile à estimer à l'échelle d'un écosystème. Néanmoins, vu son importance dans les bilans aquatiques de GES (Deemer *et al.*, 2016), l'ébullition est de plus en plus mesurée dans les réservoirs.

Le dégazage représente le flux de gaz vers l'atmosphère dû au relâchement de pression lors de la décharge d'eaux profondes vers la surface. Ce cas se retrouve particulièrement dans les réservoirs hydroélectriques où les turbines sont alimentées par des eaux profondes souvent riches en CO_2 et CH_4. A cause de à sa faible solubilité, le CH_4 est particulièrement propice au dégazage. L'accumulation de GES dans les eaux profondes est surtout liée à la présence d'une stratification thermale, qui limite les échanges entre la couche profonde et la surface du réservoir. Le dégazage est principalement associé à la dynamique des GES dans les eaux profondes. C'est aussi le cas pour les émissions de GES en aval du réservoir. En effet, les GES produits à l'intérieur du réservoir (souvent dans les eaux profondes) peuvent être émis à la surface de la rivière effluente sur plusieurs dizaines de kilomètres en aval du barrage (Abril *et al.*, 2005). Les émissions de CH_4 en aval peuvent être atténuées par l'oxydation en CO_2 (DelSontro *et al.*, 2016b ; Guérin et Abril, 2007 ; Kemenes *et al.*, 2007). Les processus en aval du barrage (dégazage, émission de la rivière, et oxydation du CH_4) sont beaucoup moins documentés que les émissions par diffusion en surface et par ébullition (Deemer *et al.*, 2016). Pourtant, le dégazage et les émissions en aval sont dans plusieurs cas des sources majeures d'émission de GES des réservoirs (Galy-Lacaux *et al.*, 1997 ; Kemenes *et al.*, 2007).

0.3.2 La variabilité temporelle

À l'échelle journalière, la concentration et les flux de GES des réservoirs varient principalement en fonction de la lumière, de la température, et de la vitesse du vent. Ces facteurs physiques ont un impact direct sur l'échange gazeux diffusif et ebullitif (Grinham *et al.*, 2011 ; Keller et Stallard, 1994 ; Sellers *et al.*, 1995), et indirect sur la balance métabolique, ce qui cause des variations à court terme de CO_2 et d'O_2 particulièrement dans les systèmes productifs (Demarty *et al.*, 2009 ; Maberly, 2008). Des variations journalières de CH_4 ont aussi été observées dû à l'apport d'O_2 de la photosynthèse stimulant la méthanotrophie durant le jour (Bergier *et al.*, 2011).

Les variations saisonnières des flux de GES des réservoirs sont influencées par la température, la stabilité de la colonne d'eau, et l'hydrologie. Dans les réservoirs tropicaux, la température est relativement stable dans le temps, mais les précipitations peuvent induire une forte augmentation du ruissèlement et du niveau des eaux durant la saison des pluies. Cette saison est généralement associée à des émissions moins élevées de CO_2 et CH_4 des réservoirs dû à un temps de résidence plus court (Abril *et al.*, 2005 ; Bastien et Demarty, 2013 ; Galy-Lacaux *et al.*, 1999 ; Kemenes *et al.*, 2007 ; Roland *et al.*, 2010). Cependant, Pacheco *et al.*, (2015) a rapporté des émissions plus élevées lors de périodes de rétention courtes dues à l'augmentation des apports riverains et du mélange des eaux. Ceci souligne l'importance des patrons hydrologiques spécifiques à chaque système et de leur interaction avec les facteurs biochimiques. Dans les régions tempérées et boréales, l'été est caractérisé par la stratification thermale des eaux, qui tend à réduire les flux diffusifs de GES en empêchant le CO_2 et le CH_4 de l'hypolimnion d'atteindre la surface (Encinas Fernández *et al.*, 2014). D'un autre côté, les hautes températures estivales stimulent la production de CH_4 dans les sédiments littoraux (DelSontro *et al.*, 2010) et changent la balance métabolique souvent vers une diminution ou même une absorption du CO_2 (Adamczyk et Shurin, 2015 ; Wang *et al.*, 2011). Lors du mélange des eaux, au printemps et en automne, les GES stockés sous la glace ou dans l'hypolimnion sont relâchés produisant un pic d'émission de CO_2 et CH_4 vers l'atmosphère (Encinas Fernández *et al.*, 2014 ; Huotari *et al.*, 2009 ; Riera *et al.*, 1999 ; Rudd et Hamilton, 1978). Dans les réservoirs, la stratification saisonnière influence la concentration de GES dans la colonne d'eau, ce qui affecte le dégazage et les émissions en aval (Kemenes *et al.*, 2007).

Sur le long terme, les émissions de CO_2 des réservoirs suivent une tendance généralisée avec des émissions maximales durant les premières années du réservoir dû à la décomposition de la matière nouvellement inondée, suivie d'une décroissance exponentiellement des flux avec le temps (Abril *et al.*, 2005 ; Barros *et al.*, 2011 ; Ometto *et al.*, 2013 ; St. Louis *et al.*, 2000 ; Teodoru *et al.*, 2012). Les émissions de

CO_2 se stabilisent généralement dix an après l'inondation, devenant comparables aux émissions lacustres dans certains cas, mais restant plus élevées dans d'autres (Åberg *et al.*, 2004 ; Abril *et al.*, 2005 ; St. Louis *et al.*, 2000 ; Teodoru *et al.*, 2012 ; Tremblay *et al.*, 2005). L'évolution temporelle des émissions de CH_4 est plus variable étant parfois très élevée dans des réservoirs âgés (DelSontro *et al.*, 2010 ; Demarty *et al.*, 2011 ; Rosa *et al.*, 2003 ; Teodoru *et al.*, 2012).

Indépendamment de l'âge, les émissions des réservoirs varient aussi d'une année à l'autre selon les conditions climatiques (Lima, 2005 ; Musenze *et al.*, 2014). Globalement, les données de suivi à long terme sont rares dans les réservoirs, ce qui limite la compréhension de la dynamique des GES sur de longues échelles temporelles dans ces systèmes.

0.3.3 La variabilité spatiale

Les profils verticaux de GES dans les lacs et réservoirs sont le résultat de l'interaction entre les processus biologiques et physiques dans la colonne d'eau. La concentration du CO_2 dépend de la balance métabolique entre la respiration et la photosynthèse (Giorgio *et al.*, 1999). Cependant, ces deux processus peuvent être découplés dans l'espace, la photosynthèse étant contrainte à la zone phototique (couche de surface) et la respiration étant stimulée par l'abondance de matière organique dans les eaux profondes et les sédiments (Pace et Prairie, 2005). Ce patron est typiquement observé dans les réservoirs stratifiés, où l'hypolimnion est hautement concentré en CO_2 et CH_4 provenant de la décomposition de la matière organique inondée (Abril *et al.*, 2005 ; Chanudet *et al.*, 2011 ; Kemenes *et al.*, 2007). La présence d'une stratification des eaux restreint les échanges entre la couche profonde et celle de surface, ce qui amplifie les gradients verticaux d'O_2 et de GES. Le métalimnion est une couche de transition où les concentrations intermédiaires d'O_2 sont propices à l'oxydation du CH_4. Cette couche agit donc comme un filtre qui empêche le CH_4 d'atteindre la couche de surface (Abril *et al.*, 2005 ; Chanudet *et al.*, 2011 ; Galy-Lacaux *et al.*, 1997 ; Rudd et Hamilton, 1978). La stratification thermique module les échanges gazeux, ce qui influence l'oxydation du CH_4 (Vachon *et al.*, 2019), et les profils verticaux de CH_4 et CO_2.

Dans les réservoirs, les concentrations et flux de GES à la surface présentent une grande hétérogénéité spatiale, surtout dans le cas du CH_4 (Grinham *et al.*, 2011). Les concentrations et émissions de CH_4 sont généralement plus élevées en zone littorale due à la présence de sédiments plus chauds et moins profonds, ce qui stimule la production et l'ébullition de CH_4 (Hofmann *et al.*, 2010 ; Joyce, 2003 ; Sherman et Ford, 2011). Les zones riches en matière organique, comme les embouchures d'affluents, les rejets d'égouts, les aquacultures, et les zones fertiles nouvellement inondées, sont souvent associées à une forte production et émission de CH_4 et de CO_2 (Chen *et al.*, 2011 ; da Silva *et al.*, 2018 ; DelSontro *et al.*, 2011 ; Musenze *et al.*, 2014 ; Roland *et al.*, 2010 ; Sherman et Ford, 2011 ; Teodoru *et al.*, 2011 ; Zhao *et al.*, 2013). La variabilité spatiale du CO_2 en surface est aussi dépendante du métabolisme interne du système, ainsi, les zones de forte production primaire coïncident souvent avec des flux de CO_2 bas voir négatifs (Abril *et al.*, 2005 ; Chanudet *et al.*, 2011 ; Demarty *et al.*, 2009 ; Pacheco *et al.*, 2015 ; Rudorff *et al.*, 2011).

0.3.4 Les patrons à l'échelle globale

Les flux de GES mesurés dans les réservoirs varient globalement entre -623 et 7206 $mgC.m^{-2}.d^{-1}$, allant de l'absorption de C à des émissions comparables à celles des énergies fossiles (Demarty *et al.*, 2009 ; Giles, 2006 ; Tamooh *et al.*, 2013). Cette variabilité est causée par des facteurs agissant à différentes échelles, locales à globales. La disponibilité de la matière organique est un facteur central dans ce contexte, étant le substrat pour la production de CO_2 et CH_4. Ainsi, plusieurs études rapportent une corrélation directe entre la concentration en matière organique et les émissions de C à larges échelles (Barros *et al.*, 2011 ; Bastien et Demarty, 2013 ; Bergström *et al.*, 2004).

D’autres études ont identifié l’effet de variables comme l’âge du réservoir, la topographie du bassin versant, et l’utilisation du territoire comme modulateurs des flux de surface à travers leur effet indirect sur la quantité et la qualité de la matière organique dans les réservoirs (Adamczyk et Shurin, 2015 ; Barros *et al.*, 2011 ; Bastien et Demarty, 2013 ; Bergström *et al.*, 2004 ; Demarty *et al.*, 2009, 2011 ; Musenze *et al.*, 2014 ; Ometto *et al.*, 2013 ; Roland *et al.*, 2010 ; St. Louis *et al.*, 2000). La température est un autre facteur régional influençant la production et les flux de GES, ce qui se traduit par des émissions en moyenne plus élevée dans les réservoirs tropicaux par rapport aux régions tempérées et boréales (Barros *et al.*, 2011 ; Bastien et Demarty, 2013 ; Musenze *et al.*, 2014 ; St. Louis *et al.*, 2000 ; Tremblay *et al.*, 2005). À l’échelle locale, la morphométrie joue un rôle particulièrement important, avec de plus fortes émissions de CH_4 dans les systèmes de petite taille et peu profonds, une configuration qui favorise l’ébullition et restreint le potentiel d’oxydation du CH_4 (Barros *et al.*, 2011 ; Kankaala *et al.*, 2013a ; Lima, 2005). Une analyse globale a montré que 40 et 54 % de la variabilité des flux diffusifs de CO_2 et CH_4 respectivement était expliquée par la latitude, la concentration en matière organique, l’âge, et la profondeur des réservoirs (Barros *et al.*, 2011). Un modèle empirique a récemment été construit incluant l’effet du climat, de la morphométrie, et des caractéristiques du bassin versant, et prédisant les flux ebullitifs et le dégazage du CH_4 en plus des flux diffusifs (CO_2 et CH_4) (UNESCO/IHA, 2017). Cependant, les données et connaissances actuelles ne sont pas suffisantes pour intégrer toutes les émissions en aval des barrages, et pour tester et réduire l’incertitude des modèles. Ainsi, les estimés globaux d’émissions de C des réservoirs varient entre 0.5 et 2.3 $PgCO_2eq.yr^{-1}$ (Barros *et al.*, 2011 ; Bastviken *et al.*, 2011 ; Deemer *et al.*, 2016 ; St. Louis *et al.*, 2000).

0.4 Les objectifs de la thèse

L'objectif général de cette thèse est d'approfondir les connaissances sur la dynamique du CO_2 et du CH_4 dans les réservoirs tropicaux. La recherche présentée vise à établir un portrait exhaustif des flux de C vers l'atmosphère et des sources et processus qui les sous-tendent. La thèse cherche aussi à comprendre comment évoluent ces dynamiques à travers le continuum aquatique en étudiant les patrons spatiaux du CO_2, du CH_4, et de leurs sources le long de la transition d'une rivière vers un réservoir. L'accent est mis sur la compréhension de l'interaction entre les différentes composantes du cycle du C à l'échelle de l'écosystème. Plus spécifiquement, la thèse est divisée en trois chapitres (Figure 0.1) qui répondent aux objectifs suivants :

- Chapitre 1 : Évaluer l'empreinte C d'un réservoir tropical en prenant en compte toutes les voies d'émission, et comparer les données mesurées aux prédictions des modèles actuels afin de tester leur performance et guider leur amélioration.

- Chapitre 2 : Quantifier et établir un bilan des sources de CO_2 et CH_4 dans l'épilimnion afin d'évaluer la contribution de chaque source aux flux diffusifs de surface le long d'un gradient hydrologique.

- Chapitre 3 : Examiner l'évolution spatiale et temporelle du CO_2 et CH_4 dans la couche profonde, et modéliser leurs concentrations selon un profil vertical en aval du barrage pour comprendre l'influence et l'interaction des facteurs qui façonnent les émissions en aval.

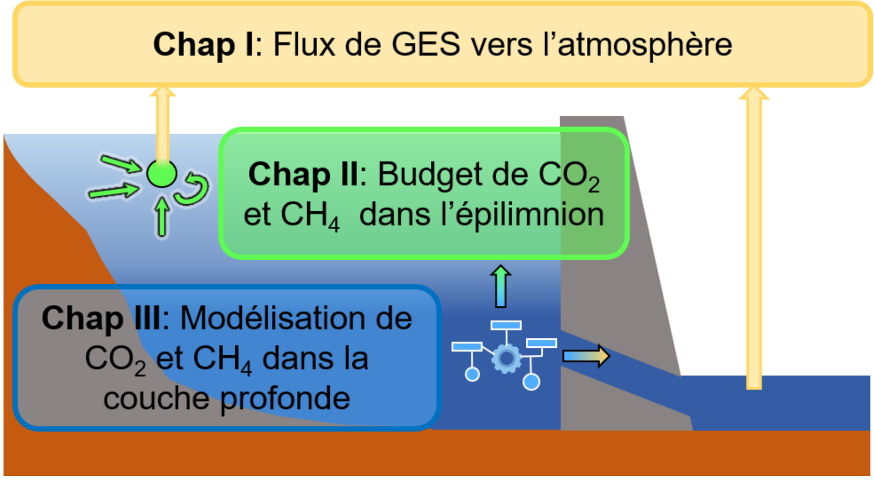

Figure 0.1: Schéma de la structure de la thèse illustrant les trois chapitres et les liens entre eux.

0.5 L'approche générale

Pour répondre aux questions énoncées, une étude de cas a été entreprise dans le réservoir Batang Ai situé sur l'ile de Bornéo dans la province de Sarawak en Malaisie. Le réservoir est géré par la compagnie hydroélectrique malaisienne Sarawak Energy Berhad avec laquelle une étroite collaboration a été établie pour rendre le projet possible. Le réservoir Batang Ai (68.4 km^2) a été inondé en 1985 suite à la construction d'un barrage de 85 m pour la production d'hydroélectricité. Il est situé dans le parc national Batang Ai, le bassin versant est donc principalement constitué de forêt tropicale (forêt mixte de diptérocarpes et forêt secondaire), avec peu d'activités humaines (quelques habitations, sites d'aquacultures, et plantation à petite échelle). Les sols du bassin versant sont acides et pauvres en nutriments, formés de roche sédimentaire dominée par du schiste argileux et du grès à gros grains (Wasli *et al.*, 2011). Le réservoir est oligotrophe dû au type de sol et au territoire forestier du bassin versant. L’eau du réservoir a un temps de résidence de 0.9 an, et est alimentée principalement par deux rivières en amont (Batang Ai et Engkari) qui se déversent dans les deux branches du réservoir, qui se croisent pour former le bassin principal du réservoir. Le bassin principal présente une stratification thermique permanente due au climat qui reste chaud toute l’année.

L’échantillonnage a été effectué durant 4 campagnes de terrain (durée d’environ 3 semaines), au cours de différentes années et mois : 1) novembre-décembre 2016, 2) avril-mai 2017, 3) février-mars 2018, 4) aout 2018. Durant les 4 campagnes d’échantillonnage, le climat était relativement similaire en termes de température et précipitations, mais le débit affluent était plus bas à la première et dernière campagne (Figure S3.1). Ainsi, l’échantillonnage couvre une variabilité temporelle et aussi spatiale vu qu’à chaque campagne, environ 39 sites ont été échantillonnés. Ces sites sont distribués à travers un gradient hydrologique allant des rivières affluentes, aux branches du réservoir, jusqu’au bassin principal, et à l’effluent plusieurs kilomètres en aval du barrage. Cette distribution spatiale a permis d’évaluer les changements dans la dynamique du CO_2 et du CH_4 lors de la transition d’un système hydrologique riverain à lacustre, reflétant l’impact de la construction d’un barrage.

Les conditions physicochimiques générales de l’eau (température, pH, concentrations en azote, phosphore, et matière organique dissoute) ont été mesurées dans tous les sites. L’étude des flux de GES vers l’atmosphère (Chapitre I) est basée principalement sur des mesures de gaz prises en surface (concentration, signature isotopique, flux). Afin d’examiner la dynamique du CO_2 et du CH_4 dans l’épilimnion (Chapitre II) et la couche profonde (Chapitre III), un échantillonnage plus approfondi a été effectué sur un sous-ensemble de 9 sites comprenant un profil vertical des gaz dans la colonne d’eau et dans les sédiments, ainsi que des mesures de métabolisme via des senseurs autonomes à haute fréquence et des incubations *in situ*. Les données collectées sur le terrain ont permis de construire un budget à l’échelle de l’écosystème des émissions vers l'atmosphère (Chapitre I) et des sources de CO_2 et CH_4 dans l'épilimnion, qui sous-tendent les flux diffusifs de surface (Chapitre II). Aussi, ces données ont servi à paramétriser la modélisation du CO_2 et CH_4 dans la couche profonde (Chapitre III) en lien avec les émissions en aval.

CHAPITRE I

THE CARBON FOOTPRINT OF A MALAYSIAN TROPICAL RESERVOIR: MEASURED VERSUS MODELED ESTIMATES HIGHLIGHT THE UNDERESTIMATED KEY ROLE OF DOWNSTREAM PROCESSES

Cynthia Soued[1], Yves T. Prairie[1]

[1]Groupe de Recherche Interuniversitaire en Limnologie et en Environnement Aquatique (GRIL), Département des Sciences Biologiques, Université du Québec à Montréal, Montréal, H2X 3X8, Canada.

Published in *Biogeosciences* (2020) DOI : 10.5194/bg-17-515-2020

N.B. References cited in this chapter are presented at the end of the thesis.

1.1 Abstract

Reservoirs are important sources of greenhouse gases (GHGs) to the atmosphere and their number is rapidly increasing, especially in tropical regions. Accurately predicting their current and future emissions is essential but hindered by fragmented data on the subject, which often fail to include all emission pathways (surface diffusion, ebullition, degassing, and downstream emissions) and the high spatial and temporal flux variability. Here we conducted a comprehensive sampling of Batang Ai reservoir (Malaysia), and compared field-based versus modeled estimates of its annual carbon footprint for each emission pathway. Carbon dioxide (CO_2) and methane (CH_4) surface diffusion were higher in upstream reaches. Reducing spatial and temporal sampling resolution resulted in up to 64 and 33 % change in flux estimate, respectively. Most GHGs present in discharged water were degassed at the turbines, and the remainder were gradually emitted along the outflow river, leaving time for CH_4 to be partly oxidized to CO_2. Overall, the reservoir emitted 2475 $gCO_2eq\ m^{-2}\ yr^{-1}$, with 89 % occurring downstream of the dam, mostly in the form of CH_4. These emissions, largely underestimated by predictions, are mitigated by CH_4 oxidation upstream and downstream of the dam, but could have been drastically reduced by slightly raising the water intake elevation depth. CO_2 surface diffusion and CH_4 ebullition were lower than predicted, whereas modeled CH_4 surface diffusion was accurate. Investigating latter discrepancies, we conclude that exploring morphometry, soil type, and stratification patterns as predictors can improve modeling of reservoir GHG emissions at local and global scales.

1.2 Introduction

Reservoirs provide a variety of services to humans (water supply, navigation, flood control, hydropower) and cover an estimated area exceeding 0.3 million km^2 globally (Lehner *et al.*, 2011). This area is increasing, with an expected rapid growth of the hydroelectric sector in the next two decades (International Hydropower Association (IHA), 2015), mainly in tropical and subtropical regions (Zarfl *et al.*, 2015). The flooding of terrestrial landscapes can transform them into significant greenhouse gas (GHG) sources to the atmosphere (Prairie *et al.*, 2018 ; Rudd *et al.*, 1993 ; Teodoru *et al.*, 2012). While part of reservoir GHG emissions would occur naturally (not legitimately attributable to damming), the remainder results from newly created environments favoring carbon (C) mineralization, particularly methane (CH_4) production (flooded organic-rich anoxic soils) (Prairie *et al.*, 2018). Field studies have revealed a wide range in measured fluxes, with spatial and temporal variability sometime spanning several orders of magnitude within a single reservoir (Paranaíba *et al.*, 2018 ; Sherman et Ford, 2011). Moreover, reservoirs can emit GHG through several pathways: diffusion of gas at the air-water interface (surface diffusion), release of gas bubbles formed in the sediments (ebullition), and for some reservoirs (mostly hydroelectric) through gas release following pressure drop upon water discharge (degassing), and through evasion of the remaining excess gas in the outflow river (downstream emissions). The relative contribution of these flux pathways to total emissions is extremely variable. While surface diffusion is the most frequently sampled, it is often not the main emission pathway (Demarty et Bastien, 2011). Indeed, measured ebullition, degassing, and downstream emissions range from negligible to several order of magnitude higher than surface diffusion in different reservoirs (Bastien et Demarty, 2013 ; DelSontro *et al.*, 2010 ; Galy-Lacaux *et al.*, 1997 ; Keller et Stallard, 1994 ; Kemenes *et al.*, 2007 ; Teodoru *et al.*, 2012 ; Venkiteswaran *et al.*, 2013), making it a challenge to model total reservoirs GHG emissions.

Literature syntheses over the past 20 years have yielded highly variable global estimates of reservoirs GHG footprint, ranging from 0.5 to 2.3 $PgCO_2eq\ yr^{-1}$ (Barros *et al.*, 2011 ; Bastviken *et al.*, 2011 ; Deemer *et al.*, 2016 ; St. Louis *et al.*, 2000). These estimates are based on global extrapolations of averages of sampled systems, representing an uneven spatial distribution biased toward North America and Europe, and an uneven mixture of emission pathways. Recent studies have highlighted the lack of spatial and temporal resolution as well as the frequent absence of some flux pathways (especially degassing, downstream, and N_2O emissions) in most reservoir GHG assessments (Beaulieu *et al.*, 2016 ; Deemer *et al.*, 2016). More recently, studies have focused on identifying drivers of reservoir GHG flux variability. Using global empirical data, Barros et al. (2011) proposed the first quantitative models for reservoir carbon dioxide (CO_2) and CH_4 surface diffusion as a negative function of reservoir age, latitude, and mean depth (for CO_2 only), and a positive function of dissolved organic carbon (DOC) inputs (Barros *et al.*, 2011). An online tool (G-res) for predicting reservoir CO_2 and CH_4 emissions was later developed on the basis of a similar empirical modeling approach of measured reservoir fluxes with globally available environmental data (UNESCO/IHA, 2017). Modeling frameworks to predict GHG emissions from existing and future reservoirs are essential tools for reservoir management. However, their accuracy is directly related to available information and inherently affected by gaps and biases of the published literature. For example, while the G-res model predicts reservoir CO_2 and CH_4 surface diffusion as well as CH_4 ebullition and degassing on the basis of temperature, age, % littoral zone and soil organic C, it does not consider N_2O emissions, CO_2 degassing, and downstream emissions due to scarcity of data. Overall, the paucity of comprehensive empirical studies limits our knowledge of reservoir GHG dynamics at a local scale, introducing uncertainties in large scale estimates and hindering model development.

The research reported here focuses on building a comprehensive assessment of GHG fluxes of Batang Ai, a tropical reservoir in South-east Asia (Malaysia), over four sampling campaigns spanning two years with an extensive spatial coverage. The main objective of this study is to provide a comprehensive account of CO_2, CH_4 and N_2O fluxes from surface diffusion, ebullition, degassing, and downstream emissions (accounting for riverine CH_4 oxidation) to better understand what shapes their relative contributions and their potential mitigation. The second objective is to compare our measured values with modeled estimates from each pathway and gas species to locate where the largest discrepancies are, and thereby identify research avenues for improving the current modeling framework.

1.3 Materials and methods

1.3.1 Study site and sampling campaigns

Batang Ai is a hydroelectric reservoir located on the Borneo Island in the Sarawak province of Malaysia (latitude 1.16º and longitude 111.9º). The regional climate is tropical equatorial with a relatively constant temperature throughout the year, on average 23ºC in the morning to 32ºC during the day. Annual rainfall varies between 3300 and 4600 mm with two monsoon seasons: November to February (northeast monsoon), and June to October (southwest) (Sarawak Government, 2019). Batang Ai reservoir was impounded in 1985 with no prior clearing of the vegetation, and has a dam wall of 85 m in height, a mean depth of 34 m, and a total area of 68.4 km^2. The reservoir catchment consists of 1149 km^2 of mostly forested land where human activities are limited to a few traditional habitations and associated croplands, and localized aquaculture sites within the reservoir main basin. The reservoir has two major inflows: the Batang Ai and Engkari rivers, which flow into two reservoir branches merging upstream of the main reservoir basin (Figure 1). Four sampling campaigns were conducted: 1) November 14th to December 5th 2016 (Nov-Dec 2016), 2) April 19th to May 3th 2017 (Apr-May 2017), 3) February 28th to March 13th 2018 (Feb-Mar 2018), and 4) August 12th to 29th 2018 (Aug 2018).

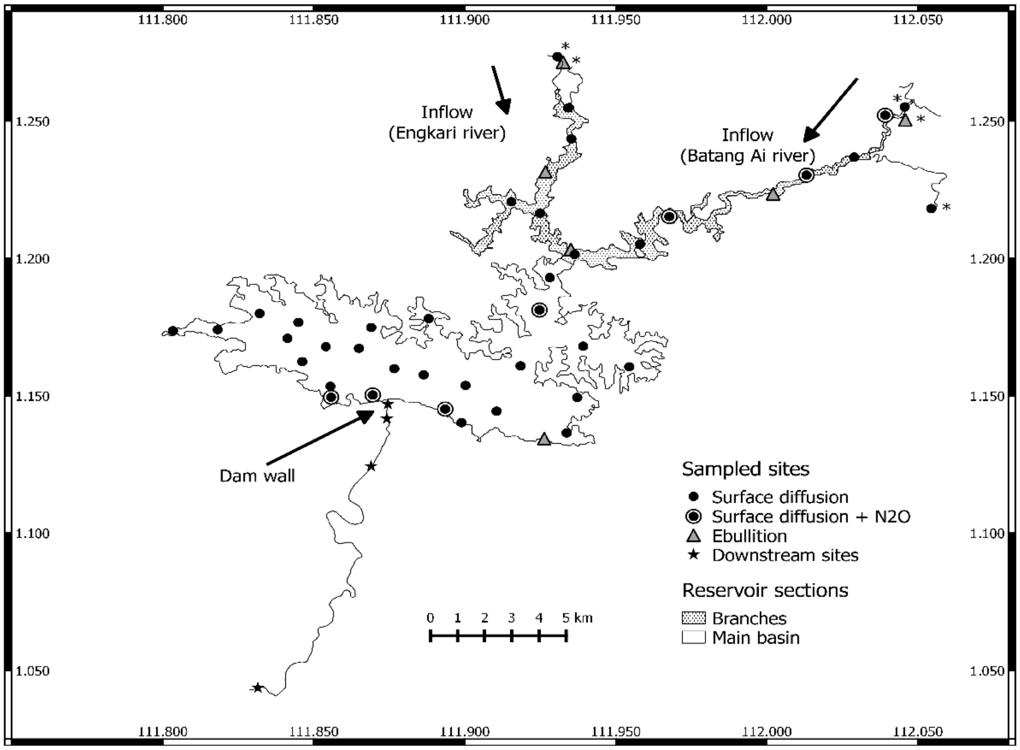

Figure 1.1: Map of Batang Ai showing the location of sampled sites and reservoir sections. * Represents the reservoir inflow sites.

1.3.2 Water chemistry

Samples for DOC, total phosphorus (TP), total nitrogen (TN), and chlorophyll a (Chla) analyses were collected from the water surface (<0.5 m) at all surface diffusion sampling sites shown in Figure 1 and during each campaign. For TP and TN, we collected non-filtered water in acid-washed glass vials stored at 4°C until analysis. TP was measured by spectrophotometry using the standard molybdenum blue method after persulphate digestion at 121ºC for 20 min, and a calibration with standard solutions from 10 to 100 µg L^{-1} with a 5 % precision (Wetzel et Likens, 2000). TN analyses were performed by alkaline persulphate digestion to NO_3, subsequently measured on a flow

Alpkem analyzer (OI Analytical Flow Solution 3100) calibrated with standard solutions from 0.05 to 2 mg L^{-1} with a 5 % precision (Patton et Kryskalla, 2003). Water filtered at 0.45 µm was used for DOC analysis with a Total Organic Carbon analyser 1010-OI following sodium persulphate digestion, and calibrated with standard solutions from 1 to 20 mg L^{-1} with a 5 % precision (detection limit of 0.1 mg L^{-1}). Chla was analysed through spectrophotometry following filtration on Whatman (GF/F) filters and extraction by hot 90 % ethanol solution (Sartory et Grobbelaar, 1984).

1.3.3 Surface diffusion

Surface diffusion is the flux of gas between the water surface and the air driven by a gradient in gas partial pressure. Surface diffusion of CO_2 and CH_4 to the atmosphere were measured at 36 sites in the reservoir and 3 sites in the inflow rivers (Figure 1.1), and sampling of the same sites was repeated each campaign (with a few exceptions). Fluxes were measured using a static air tight floating chamber connected in a closed loop to an Ultraportable gas Analyser (UGGA from LGR). Surface diffusion rates (F_{gas}) were derived from the linear change in CO_2 and CH_4 partial pressures (continuously monitored at 1 Hz for a minimum of 5 min) through time inside the chamber using the following Eq. (1.1):

$$F_{\text{gas}} = \frac{s\,V}{m\,A} \tag{1.1}$$

where s is the gas accumulation rate in the chamber, V = 25 L the chamber volume, A = 0.184 m^2 the chamber surface area, and m the gas molar volume at current atmospheric pressure.

N_2O surface diffusion was estimated at 7 of the sampled sites (Figure 1.1) using the following Eq. (1.2) (Lide, 2005):

$$F_{\text{gas}} = k_{\text{gas}} \left(C_{\text{gas}} - C_{\text{eq}} \right) \quad (1.2)$$

where k_{gas} is the gas exchange coefficient, C_{gas} is the gas concentration in the water and C_{eq} is the theoretical gas concentration at equilibrium given measured water temperature, atmospheric pressure and ambient gas concentration. C_{N2O} was measured using the headspace technique, with a 1.12 L sealed glass serum bottle containing surface water and a 0.12 L headspace of ambient air. After shaking the bottle for two minutes to achieve air-water equilibrium, the headspace gas was extracted from the bottle with an airtight syringe and injected in previously evacuated 9 mL glass vial capped with an air tight butyl stopper and aluminium seal. Three analytical replicates and a local sample of ambient air were taken at each site and analysed by gas chromatography using a Shimadzu GC-2040, with a Poropaq Q column to separate gases and an ECD detector calibrated with 0.3, 1, and 3 ppm of N_2O certified standard gas. After analysis the original N_2O concentration of the water was back-calculated based on the water temperature before and after shaking (for gas solubility), the ambient atmospheric pressure, the ratio of water to air in the sampling bottle, and the headspace N_2O concentration before shaking. k_{N2O} was derived from measured k_{CH4} values obtained by rearranging Eq. (1.2) for CH_4, with known values of F_{gas}, C_{gas}, and C_{eq}. The k_{CH4} to k_{N2O} transformation was done using the following Eq. (1.3) (Cole et Caraco, 1998 ; Ledwell, 1984):

$$k_{\text{N2O}} = \left(\frac{Sc_{\text{N2O}}}{Sc_{\text{CH4}}} \right)^{-0.67} k_{\text{CH4}} \quad (1.3)$$

where Sc is the gas Schmidt number (Wanninkhof, 1992).

CH_4 and CO_2 concentrations in the water were measured using the headspace technique. Surface water was collected in a 60 mL gas-tight plastic syringe in which a 30 mL headspace was created (using either ambient air or carbon free air). The syringe was shaken for 2 min to achieve air-water gas equilibrium. The gas phase was then injected in a 12 mL air-tight pre-evacuated vial and subsequently analysed through manual injection on a Shimadzu GC-8A Gas chromatograph with flame ionization detector following a calibration curve with certified gas standards (0-10000 ppm for CO_2 and 0-50000 ppm for CH_4). The samples were also analyzed for isotopic $\delta^{13}CO_2$ and $\delta^{13}CH_4$ signatures by manually injecting 18 mL of gas in a Cavity Ring Down Spectrometer (CRDS) equipped with a Small Sample Isotopic Module (SSIM A0314, Picarro G2201-*i* Analyzer) set in a non-continuous mode with a three point calibration curve based on certified gas standards (-40 -3.9, and 25.3 ‰ for $\delta^{13}CO_2$, and -66.5, -38.3, -23.9 ‰ for $\delta^{13}CH_4$).

1.3.4 Ebullition

Ebullition is the process through which gas bubbles formed in the sediments rise through the water column and are released to the atmosphere. Sediment gas ebullition was measured at four sites in the reservoir and two sites in the inflows (Figure 1.1) by deploying 0.785 m^2 underwater inverted funnel traps at 2 to 3 m deep for approximately 20 days in the reservoir and 1h in the inflows. The top part of a closed plastic syringe was fixed to the narrow end of the funnel trap where the emerging bubbles accumulated. Upon recovery, bubble gas volume was measured, collected from the syringe, and injected in 12 mL pre-evacuated air tight vials for CO_2 and CH_4 concentration analyses (using the aforementioned method). Ebullition rate was calculated assuming the original bubble composition was similar to bubbles collected almost right after ascent in the inflows sites, which was 100 % CH_4. Hence we considered CO_2 and N_2O ebullition to be null.

In order to estimate the potential for sediment accumulation fueling ebullition in the littoral zone, we calculated the mud energy boundary depth (EBD in m, below which fine grained sediments accumulation occurs) using the reservoir surface area (E in km^2) as the exposure parameter in the following Eq. (1.4) (Rowan *et al.*, 1992):

$$EBD = 2.685\ E^{0.305} \tag{1.4}$$

1.3.5 Degassing, downstream emissions and CH_4 oxidation

Degassing of CO_2 and CH_4 right after water discharge (F_{deg}), and downstream emissions of the remaining reservoir-derived GHGs in the outflow river (F_{dwn}) were calculated using the following Eq. (1.5) and Eq. (1.6):

$$F_{\mathrm{deg}} = Q\ (C_{\mathrm{up}} - C_0) \tag{1.5}$$

$$F_{\mathrm{dwn}} = Q\ (C_0 - C_{19} + C_{\mathrm{ox}}) \tag{1.6}$$

where Q is the water discharge, and C_{up}, C_0 and C_{19} the measured gas concentrations upstream of the dam at the water withdrawal depth, at the powerhouse right after water discharge, and in the outflow 19 km downstream of the dam respectively. C_{ox} is the net change in gas concentration due to oxidation (loss for CH_4 and gain for CO_2). For downstream emissions, we considered that, after a river stretch of 19 km, all excess gas originating from the reservoir was evaded and gas concentration was representative of the outflow river baseline. This assumption potentially underestimates actual downstream emissions (in case of remaining excess gas after 19 km). However, given the observed exponential decrease of gas concentration along the outflow (Figure 1.3), emissions after 19 km are expected to be small compared to those in the 0 to 19 km river stretch, consistent with observations in other reservoirs (Guérin *et al.*, 2006 ; Kemenes *et al.*, 2007).

Gas concentrations upstream and downstream of the dam were obtained by measuring, in each campaign, CO_2 and CH_4 concentrations in a vertical profile right upstream of the dam at a 1 to 3 m interval from 0 to 32 m, and at four locations in the outflow: at 0 (power house), 0.6, 2.7, and 19 km downstream of the dam (Figure 1.1). Sampling was done using a multi-parameter probe equipped with depth, oxygen, and temperature sensors (Yellow Spring Instruments, YSI model 600XLM-M) attached to a 12 Volt submersible Tornado pump (Proactive Environmental Products) for water collection. Gas concentration and δ^{13}C were measured as described in section 1.3.3. Water withdrawal depth ranged from 20 to 23 m and was estimated based on known values of elevations of water intake and water level compared to sea level. Gas concentration in the water exiting the reservoir was defined as the average measured gas concentrations in the ± 1 m range of the withdrawal depth.

Estimates of downstream CH_4 oxidation were obtained, for each sampling campaign, by calculating the fraction of CH_4 oxidized (F_{ox}) using the following Eq. (1.7):

$$F_{\mathrm{ox}} = \frac{-\left(ln\left(\delta^{13}CH_{4\mathrm{resid}}+1000\right)-\ln\left(\delta^{13}CH_{4\mathrm{source}}+1000\right)\right)\left(1-\frac{[CH_4]_{\mathrm{resid}}}{[CH_4]_{\mathrm{source}}}\right)}{\left(1-\frac{1}{\alpha}\right)\ln\left(\frac{[CH_4]_{\mathrm{resid}}}{[CH_4]_{\mathrm{source}}}\right)} \qquad (1.7)$$

Eq. (1.7) is based on a non-steady state isotopic model developed considering evasion (emission to the atmosphere) and oxidation as the two loss processes for CH_4 in the outflow river, assuming negligible isotopic fractionation for evasion (Knox *et al.*, 1992) and a fractionation of $\alpha = 1.02$ for oxidation (Coleman *et al.*, 1981) (see derivation in Supplementary Information). $[CH_4]_{\mathrm{source}}$, $[CH_4]_{\mathrm{resid}}$, $\delta^{13}CH_{4\mathrm{source}}$, and $\delta^{13}CH_{4\mathrm{resid}}$ are the concentrations of CH_4 and their corresponding isotopic signatures at the beginning of the outflow (km 0) and 19 km downstream, representing the source and residual pools of CH_4 respectively. The amount of CH_4 oxidized to CO_2 along the 19 km of river stretch for each sampling campaign was calculated as the product of F_{ox} and $[CH_4]_{\mathrm{source}}$. The resulting loss of CH_4 and gain of CO_2 in the outflow were accounted for in downstream emissions (C_{ox} in Eq. (1.6)). Note that downstream N_2O emissions were considered null since N_2O concentrations measured in the deep reservoir layer were lower than concentrations in the outflow.

1.3.6 Ecosystem scale C footprint

Batang Ai annual C footprint was calculated as the sum of surface diffusion, ebullition, degassing, and downstream emissions of CO_2, CH_4, and N_2O considering a greenhouse warming potential of 1, 34, and 298 respectively over a 100 years lifetime period (Myhre *et al.*, 2013). For each flux pathway, annual flux was estimated as the average of the sampling campaigns. Ecosystem scale estimate of surface diffusion was calculated for each campaign as the average of measured flux rates applied to the reservoir area for N_2O, and for CO_2 and CH_4 it was obtained by spatial interpolation of measured fluxes over the reservoir area based on inverse distance weighting with a power of two (a power of one yields similar averages, CV < 11 %) using package gstat version 1.1-6 in the R version 3.4.1 software (Pebesma, 2004 ; R Core Team, 2017). Ebullition at the reservoir scale was calculated as the average of measured reservoir ebullition rates applied to the littoral area (< 3 m deep).

The estimated GHG emissions of Batang Ai based on measured data was compared to values derived from the G-res model (UNESCO/IHA, 2017) and the model presented in Barros et al. (2011). Both models predict surface CO_2 and CH_4 diffusion as a function of age and account for the effect of temperature using however different proxies: the G-res uses effective temperature while Barros et al. model uses latitude (an indirect proxy that integrates other spatial differences). In terms of CO_2 surface diffusion, the G-res uses reservoir area, soil C content, and TP to quantify the effect of C inputs fueling CO_2 production, while Barros et al. model uses directly DOC inputs (based on in situ DOC concentration). For CH_4 surface diffusion, both models account for morphometry using the fraction of littoral area (G-res) or the mean depth (Barros et al. model). Overall, both models predict surface diffusion based on the same conceptual framework but use different proxies. CH_4 ebullition and degassing are modeled only by the G-res, being the sole model available to this date. Details on models equations and input variables are presented in the Supplementary Information (Table S1.2 and S1.3).

1.4 Results and discussion

1.4.1 Water chemistry

The reservoir is stratified throughout the year with a thermocline at a depth around 13 m and mostly anoxic conditions in the hypolimnion of the main basin (Figure S1.1). The system is oligotrophic, with very low concentrations of DOC, TP, TN, and Chla averaging 0.9 (SD ± 0.2) mg L^{-1}, 5.9 (SD ± 2.4) μg L^{-1}, 0.11 (SD ± 0.04) mg L^{-1}, and 1.3 (SD ± 0.7) μg L^{-1} respectively (Table S1.1), and high water transparency (Secchi depth > 5 m). In the reservoir inflows, concentrations of measured chemical species are slightly higher but still in the oligotrophic range (Table S1.1), however the transparency is much lower due to turbidity (Secchi < 0.5 m). The oligotrophic status of the reservoir likely results from nutrient poor soils (Wasli *et al.*, 2011) and a largely undisturbed forested catchment in the protected Batang Ai National Park. The reservoir's low Chla concentrations are comparable to the neighboring Bakun reservoir (Ling *et al.*, 2017), and its DOC concentrations are on the low end of the wide range of measured values in nearby rivers (Martin *et al.*, 2018).

1.4.2 Surface diffusion

Measured CO_2 diffusion in the reservoir averaged 7.7 (SD ± 18.2) mmol m^{-2} d^{-1} (Table S1.1), which is on the low end compared to other reservoirs (Deemer *et al.*, 2016) and even to natural lakes (Sobek *et al.*, 2005), but similar to CO_2 fluxes measured in two reservoirs in Lao PDR (Chanudet *et al.*, 2011). CO_2 diffusion across all sites ranged from substantial uptake to high emissions (from -30.8 to 593.9 mmol m^{-2} d^{-1}, Table

S1.1) reflecting a large spatial and temporal variability. Spatially, CO_2 fluxes measured in the main basin and branches had similar averages of 7.9 and 7.3 mmol m^{-2} d^{-1} respectively (overall SD ± 18.2), contrasting with higher and more variable values in the inflows with a mean of 137.3 (SD ± 192.4) mmol.m^{-2}.d^{-1} (Figure 1.2). Within the reservoir, CO_2 fluxes varied (SD ± 18.2 mmol m^{-2} d^{-1}) but did not follow a consistent pattern, and might reflect pre-flooding landscape heterogeneity (Teodoru *et al.*, 2011). Temporally, highest average reservoir CO_2 fluxes were measured in Apr-May 2017, when no CO_2 uptake was observed, contrary to other campaigns, especially Feb-Mar and Aug 2018, when CO_2 uptake was common (Figure S1.2) and average Chla concentrations were the highest. This reflects the important role of metabolism (namely CO_2 consumption by primary production) in modulating surface CO_2 fluxes in Batang Ai.

All CH_4 surface diffusion measurements were positive and ranged from 0.03 to 113.4 mmol m^{-2} d^{-1} (Table S1.1). Spatially, CH_4 fluxes were progressively higher moving further upstream (Figure 1.2 and S1.3) with decreasing water depth and increasing connection to the littoral. This gradient in morphometry induces an increasingly greater contact of the water with bottom and littoral sediments, where CH_4 is produced, explaining the spatial pattern of CH_4 fluxes. CH_4 surface diffusion also varied temporally, but to a lesser extent than CO_2, being on average highest in Aug 2018 in the reservoir and in Nov-Dec 2016 in the inflows.

Reservoir N_2O surface diffusion (measured with a limited spatial resolution) averaged -0.2 (SD ± 2.1) nmol m^{-2} d^{-1} (Table S1.1). The negative value indicates that the system acts as a slight net sink of N_2O, absorbing an estimated 2.1 gCO_2eq m^{-2} yr^{-1} (Table 1.2). Atmospheric N_2O uptake have previously been reported in aquatic systems and linked to low oxygen and nitrogen content conducive to complete denitrification which consumes N_2O (Soued *et al.*, 2016 ; Webb *et al.*, 2019). These environmental conditions match observations in Batang Ai, with a low average TN concentration of 0.11 (0.04) mg L^{-1} (Table S1.1) and anoxic deep waters (Figure S1.1).

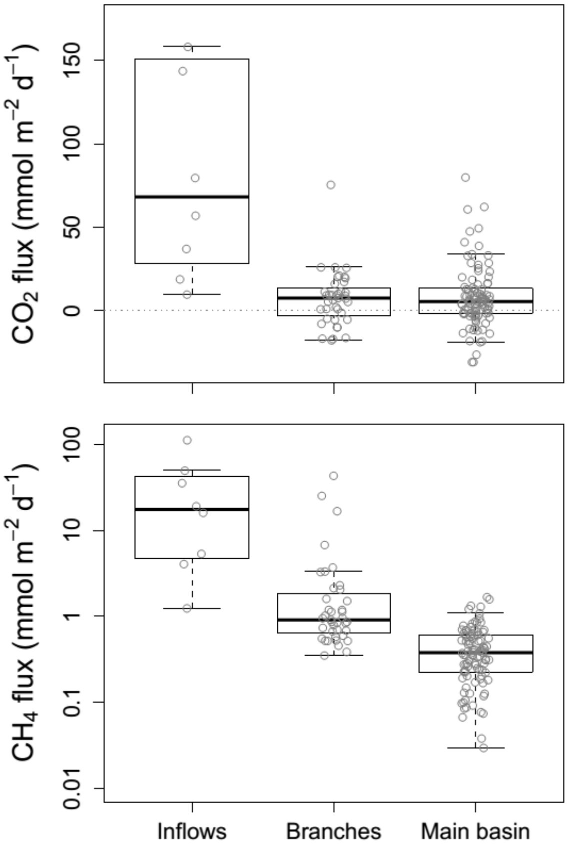

Figure 1.2: Boxplots of measured CH$_4$ (on a log axis) and CO$_2$ fluxes grouped according to spatial position. Boxes are bounded by the 25th and 75th percentile and show medians (solid lines), and whiskers show 10th and 90th percentiles. Gray circles show single data points.

1.4.3 Ebullution

We calculated that CH_4 ebullition rates in Batang Ai's littoral area ranged from 0.02 to 0.84 mmol m^{-2} d^{-1}, which contrasts with rates measured in its inflows that are several orders of magnitude higher (52 to 103 mmol m^{-2} d^{-1}). Similar patterns were observed in other reservoirs, where inflow arms where bubbling hot spots due to a higher organic C supply driven by terrestrial matter deposition (DelSontro *et al.*, 2011 ; Grinham *et al.*, 2018). Since ebullition rates are notoriously heterogeneous and were measured at only four sites in the reservoir, they may not reflect ecosystem-scale rates. However, our attempt to manually provoke ebullition at several other sites (by physically disturbing the sediments) did not result in any bubble release, confirming the low potential for ebullition in the reservoir littoral zone. Moreover, we calculated that fine grained sediment accumulation is unlikely at depths shallower than 9.7 m (estimated EBD) in Batang Ai. This, combined with the reservoir steep slope, prevents the sustained accumulation of organic material in littoral zones (Blais et Kalff, 1995), hence decreasing the potential for CH_4 production and bubbling there. Also, apparent littoral sediment composition in the reservoir; dense clay with low porosity, may further hinder bubble formation and emission (de Mello *et al.*, 2018).

1.4.4 Degassing and downstream emissions

Emissions downstream of the dam, expressed on a reservoir-wide areal basis, ranged from 19.3 to 30.0 mmol m^{-2} d^{-1} for CO_2 and from 5.9 to 13.8 mmol m^{-2} d^{-1} for CH_4 (Table 1.1). The amount of CO_2 exiting the reservoir varied little between sampling campaigns (CV = 3 %) contrary to CH_4 (CV = 28 %, Table 1.1 and Figure 1.3). Higher temporal variability of CH_4 concentration in discharged water is likely modulated by microbial CH_4 oxidation in the reservoir water column upstream of the dam. Evidence of high CH_4 oxidation are apparent in reservoir water column profiles, showing a sharp decline of CH_4 concentration and increase of $\delta^{13}CH_4$ right around the water withdrawal depth (Figure S1.1). This vertical pattern results from higher oxygen availability when moving up in the hypolimnion (Figure S1.1), promoting CH_4 oxidation at shallower depths.

Once GHGs have exited the reservoir, a large fraction (40 and 65 % for CO_2 and CH_4 respectively) is immediately lost to the atmosphere as degassing emissions (Table 1.1), which is in line with previous literature reports (Kemenes *et al.*, 2016). Along the outflow river, CO_2 and CH_4 concentrations gradually decreased, $\delta^{13}CO_2$ remained stable, whereas $\delta^{13}CH_4$ steadily increased (Figure 1.3). Given the very small isotopic fractionation (0.9992) of CH_4 during gas evasion (Knox *et al.*, 1992), the only process that can explain the observed $\delta^{13}CH_4$ increase is CH_4 oxidation (Bastviken *et al.*, 2002 ; Thottathil *et al.*, 2018). We estimated that riverine CH_4 oxidation ranged from 0.38 to 1.80 mmol m^{-2} d^{-1} (expressed per m^2 of reservoir area for comparison), transforming 18 to 32 % (depending on the sampling campaign) of the CH_4 to CO_2 within the first 19 km of the outflow. Riverine oxidation rates did not co-vary temporally with water temperature, oxygen availability, or CH_4 concentrations (known as typical drivers (Thottathil *et al.*, 2019)), hence they might be regulated by other factors like light and microbial assemblages (Murase et Sugimoto, 2005 ; Oswald *et al.*, 2015). Overall, riverine oxidation of CH_4 to CO_2 (which has a 34 times lower warming potential) reduced radiative forcing of downstream emissions (excluding degassing) by, on average, 21 %, and the total annual reservoir C footprint by 7 %. Despite having a measurable impact on reservoir GHG emissions, CH_4 oxidation downstream of dams was only considered in three other reservoirs to our knowledge (DelSontro *et al.*, 2016b ; Guérin et Abril, 2007 ; Kemenes *et al.*, 2007). Accounting for this process is particularly important in systems where downstream emissions are large, a common situation in tropical reservoirs (Demarty et Bastien, 2011). While additional data on the subject is needed, our results provide one of the first basis for understanding CH_4 oxidation downstream of dams, and eventually integrating this component to global models (from which it is currently absent).

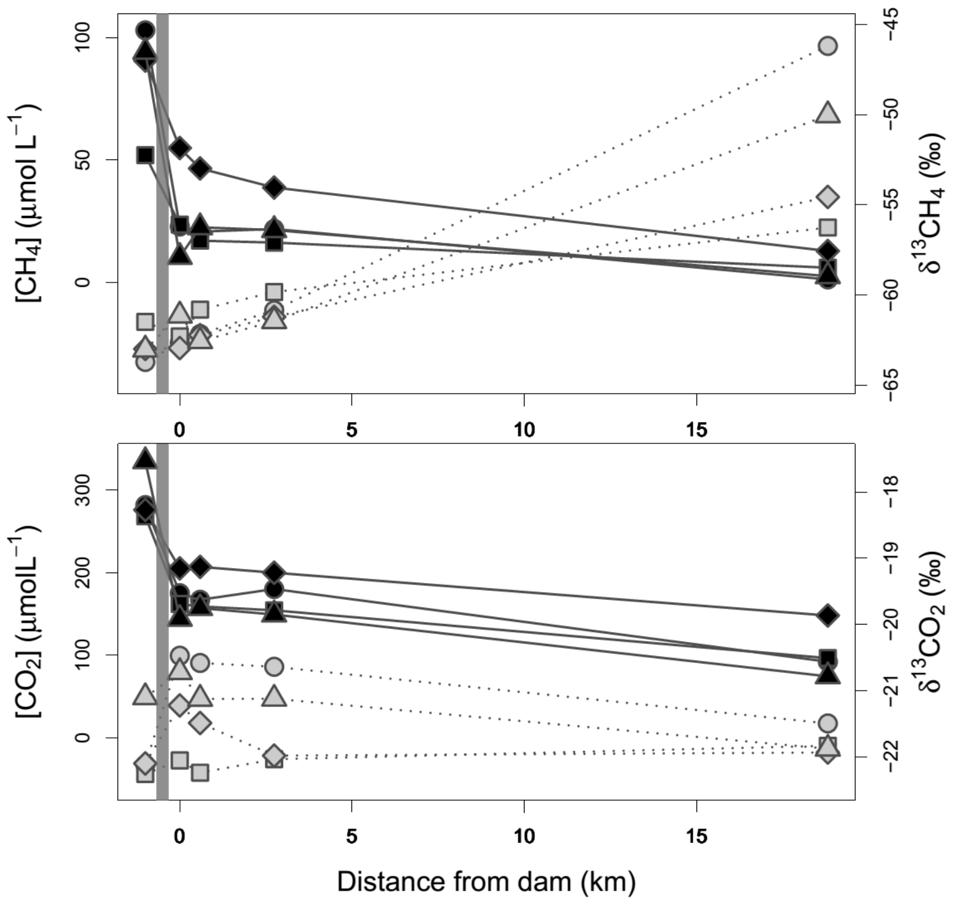

Figure 1.3: Concentrations (black symbols and solid line) and δ^{13}C (gray symbols and dotted lines) of CO_2 and CH_4 from right upstream of the dam (gray band) to 19 km downstream in the outflow river. Circles, squares, diamonds, and triangles represent values from Nov-Dec 2016, Apr-May 2017, Feb-Mar 2018, and Aug 2018 respectively.

Table 1.1: CO_2 and CH_4 dynamics downstream of the dam: gas export rate from upstream to downstream of the dam, degassing, result of CH_4 oxidation (CO_2 production and CH_4 consumption), downstream emissions, and total emissions to the atmosphere below the dam. Uncertainties based on variation coefficients are reported in parentheses. Units are in mmol m^{-2} d^{-1} of reservoir surface area.

	GHG downstream of the dam (mmol m^{-2} d^{-1})				
	Exported	Degassed	Gain / loss. by oxidation	Downstream emiss.	Total emiss.
CO_2					
Nov-Dec 2016	40.62 (±2.27)	15.26 (±0.85)	0.90 (±0.13)	12.67 (±0.71)	27.93 (±1.56)
Apr-May 2017	37.80 (±2.11)	14.91 (±0.83)	0.59 (±0.08)	9.83 (±0.55)	24.70 (±1.38)
Feb-Mar 2018	37.98 (±2.12)	9.58 (±0.54)	1.80 (±0.26)	9.70 (±0.54)	19.30 (±1.08)
Aug 2018	38.07 (±2.13)	21.67 (±1.21)	0.38 (±0.05)	8.31 (±0.46)	30.00 (±1.68)
CH_4					
Nov-Dec 2016	14.84 (±2.10)	11.56 (±1.64)	0.90 (±0.13)	2.19 (±0.31)	13.76 (±1.95)
Apr-May 2017	7.32 (±1.04)	4.00 (±0.57)	0.59 (±0.08)	1.90 (±0.27)	5.90 (±0.84)
Feb-Mar 2018	12.47 (±1.77)	4.92 (±0.70)	1.80 (±0.26)	3.99 (±0.57)	8.91 (±1.26)
Aug 2018	10.71 (±1.52)	9.54 (±1.35)	0.38 (±0.05)	0.51 (±0.07)	10.05 (±1.42)

1.4.5 Importance of sampling resolution

High spatial and temporal sampling resolution have been recently highlighted as an important but often lacking aspect of reservoir C footprint assessments (Deemer *et al.*, 2016 ; Paranaíba *et al.*, 2018). Reservoir scale fluxes are usually derived from applying an average of limited flux measurements to the entire reservoir area. For Batang Ai, this method overestimates by 14 % (130 gCO_2eq m^{-2} yr^{-1}) and 64 % (251 gCO_2eq m^{-2} yr^{-1}) CO_2 and CH_4 surface diffusion respectively compared to spatial interpolation. This is due to the effect of extreme values that are very constrained in space but have a disproportionate effect on the overall flux average. Also, reducing temporal sampling resolution to one campaign instead of four changes the reservoir C footprint estimate by up to 33 %. An additional source of uncertainty in reservoir flux estimates is the definition of a baseline value representing natural river emissions in order to calculate downstream emissions of excess gas in the outflow attributable to damming. In Batang Ai, downstream emission was estimated assuming the GHG concentration 19 km downstream of the dam is a representative baseline for the outflow, however, measured values in the pre-impounded river would have substantially reduced the estimate uncertainty. Results from Batang Ai reinforce the importance of pre and post-impoundment sampling resolution and upscaling methods in annual reservoir-scale GHG flux estimates.

1.4.6 Reservoir C footprint and potential mitigation

Most of Batang Ai emissions occur downstream of the dam through degassing (64.2 %) and downstream emissions (25.0 %), while surface diffusion contributed only 10.6 %, and ebullition 0.14 % (Table 1.2). In all pathways, radiative potential of CH_4 fluxes were higher than CO_2 and N_2O (especially for degassing), accounting for 79.0 % of Batang Ai CO_2eq emissions. This distribution of the flux can be attributed mostly to the accumulation of large quantities of CH_4 in the hypolimnion, combined with the fact that the withdrawal depth is located within this layer, allowing the accumulated gas to escape to the atmosphere. Previous studies on reservoirs with similar characteristics to Batang Ai (tropical climate with a permanent thermal stratification and deep water withdrawal) have also found degassing and downstream emissions to be the major emission pathways, especially for CH_4 (Galy-Lacaux *et al.*, 1997 ; Kemenes *et al.*, 2007).

Overall, we estimated that the reservoir emits on average 2475 (± 327) gCO_2eq m^{-2} yr^{-1} which corresponds to 0.169 TgCO_2eq yr^{-1} over the whole system. In comparison, the annual areal emission rate (diffusion and ebullition) of the inflows, based on a more limited sampling resolution, is estimated to range from 10.8 to 52.5 kgCO_2eq m^{-2} yr^{-1}, mainly due to extremely high ebullition. When applied to the approximated surface area of the river before impoundment (1.52 km^2), this rate translates to 0.016 – 0.080 TgCO_2eq (Table 1.2), assuming similar flux rates in the current inflows and pre-impoundment river. While the emission rate of the river per unit of area is an order of magnitude higher than for the reservoir, its estimated total flux remains 2.1 to 10.6 times lower due to a much smaller surface. Higher riverine emissions rates are probably due to a shallower depth and higher inputs of terrestrial organic matter, both conducive to CO_2 and CH_4 production and ebullition. Changing the landscape hydrology to a reservoir drastically reduced areal flux rates, especially ebullition, however, it widely expanded the volume of anoxic environments (sediments and hypolimnion), creating a vast new space for CH_4 production. The new hydrological regime also created an opportunity for the large quantities of gas produced in deep layers to easily escape to the atmosphere through the outflow and downstream river.

One way to reduce reservoir GHG emissions is to ensure low CO_2 and CH_4 concentrations at the water withdrawal depth. In Batang Ai, maximum CO_2 and CH_4 concentrations are found in the reservoir deep layers, and rapidly decrease from 20 to 10 m for CO_2 and from 25 to 15 m for CH_4 (Figure S1.1). This pattern is commonly found in lakes and reservoirs and results from thermal stratification and biological processes (aerobic respiration and CH_4 oxidation). Knowing this concentration profile, degassing and downstream emissions could have been reduced in Batang Ai by elevating the water withdrawal depth to avoid hypolimnetic gas release. We calculated that elevating the water withdrawal depth by 1, 3, and 5 m would result in a reduction of degassing and downstream emissions by 1, 11, and 22 % for CO_2 and by 28, 92, and 100 % for CH_4, respectively (Figure S1.4). Consequently, a minor change in the dam design could have drastically reduced Batang Ai's C footprint. This should be taken in consideration in future reservoir construction, especially in tropical regions.

1.4.7 Measured versus modeled fluxes

Based on measurements, Batang Ai emits on average 113 (± 22) $gCO_2eq\ m^{-2}\ yr^{-1}$ via surface CO_2 diffusion. This value is 41 times lower than predicted by Barros et al. model (4671 $gCO_2eq\ m^{-2}\ yr^{-1}$, Table 1.2) based on reservoir age, DOC inputs (derived from DOC water concentration), and latitude (Barros *et al.*, 2011). The high predicted value for Batang Ai, being a relatively old reservoir with very low DOC concentration, is mainly driven by its low latitude. While reservoirs in low latitudes globally have higher average CO_2 fluxes due to higher temperature and often dense flooded biomass (Barros *et al.*, 2011 ; St. Louis *et al.*, 2000), our results provide a clear example that not all tropical reservoirs have high CO_2 emissions by simple virtue of their geographical location. Despite high temperature, Batang Ai's very low water organic matter content (Table S1.1) offers little substrate for net heterotrophy, and its strong permanent stratification creates a physical barrier potentially retaining CO_2 derived from flooded biomass in the hypolimnion. The only three other sampled reservoirs in Southeast Asia (Nam Leuk and Nam Ngum in Lao PDR, and Palasari in Indonesia) also exhibited low organic C concentration (for reservoirs in Lao PDR) and low to negative average surface CO_2 diffusion despite their low latitude (Chanudet *et al.*, 2011 ; Macklin *et al.*, 2018). This suggests that, while additional data are needed, low CO_2 diffusion may be common in Southeast Asian reservoirs, and likely linked to the low organic C content.

In comparison, the G-res model predicts a CO_2 surface diffusion of 577 (509-655) $gCO_2eq\ m^{-2}\ yr^{-1}$, which includes the flux naturally sustained by catchment C inputs (397 $gCO_2eq\ m^{-2}\ yr^{-1}$, predicted flux 100 years after flooding) and the flux derived from organic matter flooding (180 $gCO_2eq\ m^{-2}\ yr^{-1}$). While the predicted G-res value is much closer than that predicted from the Barros et al. model, it still overestimates measured flux, mostly the natural baseline (catchment derived) part of it. The G-res predicts baseline CO_2 effluxes as a function of soil C content, a proxy for C input to the reservoir. While Batang Ai soil is rich in organic C (~50 g kg^{-1}), it also has a high clay content (> 40 %) (ISRIC - World Soil Information, 2019 ; Wasli *et al.*, 2011) which is known to bind with organic matter and reduce its leaching to the aquatic environment (Oades, 1988). This may explain the unusually low DOC concentration in the reservoir and its inflows (0.3 to 1.8 mg L^{-1}, Table S1.1) that are among the lowest reported in freshwaters globally (Sobek *et al.*, 2007). Clay-rich soils are ubiquitous in tropical landscapes (especially in Southeast Asia, Central America, and Central and Eastern Africa) (ISRIC - World Soil Information, 2019), however, their impact on global-scale patterns of aquatic DOC remains unknown. This may be due to a lack of aquatic DOC data, with the most recently published global study on the subject featuring only one tropical system and a heavy bias towards North America and Europe (Sobek *et al.*, 2007). Exploring the global-scale picture of aquatic DOC and its link to watershed soils characteristics would be a significant step forward in the modeling of reservoir CO_2 diffusion. Indeed, had the G-res model been able to capture the baseline emissions more correctly in Batang Ai (close to zero given the very low DOC inputs), predictions would have nearly matched observations. Finally, note that the G-res model is not suitable to predict CO_2 uptake, which was observed in 32 % of flux measurements in Batang Ai due to an occasionally net autotrophic surface metabolism favored under low C inputs (Bogard et del Giorgio, 2016). Improving this aspect of the model depends on the capacity to predict internal metabolism of aquatic systems at a global scale, which is currently lacking. Overall, reservoir CO_2 diffusion models may be less performant in certain regions, like Southeast Asia, due to an uneven spatial sampling distribution and a general lack of knowledge and data on C cycling in some parts of the world.

Our field-based estimate of Batang Ai CH_4 surface diffusion is 153 (± 22) $gCO_2eq\ m^{-2}\ yr^{-1}$, which differs by only 5 % and 15 % from the G-res and Barros et al. modeled predictions of 161 (132-197) and 176 $gCO_2eq\ m^{-2}\ yr^{-1}$ respectively (Table 1.2). Both models use as predictors age, a proxy for water temperature (air temperature or latitude), and an indicator of reservoir morphometry (% littoral area or mean depth), and Barros et al. also uses DOC input (Table S1.3). Similar predictors were identified in a recent global literature analysis, which also pointed out the role of trophic state in CH_4 diffusion, with Batang Ai falling well in the range of flux reported in other oligotrophic reservoirs (Deemer *et al.*, 2016). Overall, our results show that global modeling frameworks for CH_4 surface diffusion capture reasonably well the reality of Batang Ai.

Measured estimate of reservoir-scale CH_4 ebullition averaged 3.4 (± 1.9) $gCO_2eq\ m^{-2}\ yr^{-1}$ (Table 1.2), which is one of the lowest reported globally in reservoirs (Deemer *et al.*, 2016), and is an order of magnitude lower than the 52 (32 - 83) $gCO_2eq\ m^{-2}\ yr^{-1}$ predicted by the G-res model (the only available model for reservoir ebullition). This contrasts with the perception that tropical reservoirs consistently have high ebullitive emissions, and support the idea that the supply of sediment organic matter, rather than temperature, is the primary driver of ebullition (Grinham *et al.*, 2018). Batang Ai sediment properties and focusing patterns mentioned earlier could explain the model overestimation of CH_4 ebullition. The G-res model considers the fraction of littoral area and horizontal radiance (a proxy for heat input) as predictors of ebullition rate, but does not integrate other catchment properties. Building a stronger mechanistic understanding of the effect of sediment composition and accumulation patterns on CH_4 bubbling may improve our ability to more accurately predict reservoir ebullition flux.

Our empirical estimate shows that 409 (± 23) and 1798 (± 255) $gCO_2eq\ m^{-2}\ yr^{-1}$ are emitted as CO_2 and CH_4 respectively downstream of the dam (including degassing), accounting for 89 % of Batang Ai GHG emissions (Table 1.2). Currently there are no available model predicting downstream GHG emissions from reservoirs, except the G-res model which is able to predict only the CH_4 degassing part of this flux. Modeled CH_4 degassing in Batang Ai is 468 (266-832) $gCO_2eq\ m^{-2}\ yr^{-1}$ compared to an estimated 1342 (± 190) $gCO_2eq\ m^{-2}\ yr^{-1}$ based on our measurements. Predictive variables used to model CH_4 degassing are modeled CH_4 surface diffusion (based on % littoral area and temperature) and water retention time (Table S1.3). In Batang Ai main basin, the strong and permanent stratification favors oxygen depletion in the hypolimnion which promotes deep CH_4 accumulation combined with a decoupling between surface and deep water layers. The model relies strongly on surface CH_4 patterns to predict excess

CH_4 in the deep layer, which could explain why it underestimates CH_4 degassing in Batang Ai. Similar strong stratification patterns are ubiquitous in the tropics, with a recent study suggesting a large majority of tropical reservoirs are monomictic or oligomictic (Lehmusluoto *et al.*, 1997 ; Scott Winton *et al.*, 2019), hence more often stratified than temperate and boreal ones. This suggests that CH_4 degassing is potentially more frequently underestimated in low-latitude reservoirs. The G-res effort to predict CH_4 degassing is much needed given the importance of this pathway, and the next step would be to refine this model and develop predictions for other currently missing fluxes like CO_2 degassing and downstream emissions in the outflow. Our results suggest that improving latter aspects requires a better capacity to predict GHG accumulation in deep reservoirs layers across a wide range of stratification regimes.

Table 1.2: Estimated reservoir and inflow areal and total GHG fluxes to the atmosphere (± standard error for measured values, or 95 % confidence interval based on model standard error for G-res values) from different pathways based on measured and modeled approaches.

	Diffusion			**Ebullition**	**Degassing**		**Downstream river**		**Total**
	CO_2	CH_4	N_2O	CH_4	CO_2	CH_4	CO_2	CH_4	
				Flux rate ($gCO_2eq\ m^{-2}\ yr^{-1}$)					
Reservoir									
Measured	113 (± 22)	153 (± 22)	-2.1 (± 4)	3.4 (± 1.9)	247 (± 14)	1342 (± 190)	163 (± 9)	456 (± 65)	2475 (± 327)
G-res model	577 (509 - 655)	161 (132 - 197)	NA	52 (32 - 83)	NA	468 (266 - 832)	NA	NA	1258 (1041 - 1636)
Barros et al. model	4671	176	NA	NA	NA	NA	NA	NA	4847
Inflows									
Measured	156 - 9538	248 - 22510	NA	10377 - 20498	0	0	0	0	10781 - 52546
				Total flux ($TgCO_2eq\ yr^{-1}$)					
Reservoir (meas.)	0.008	0.010	-0.0001	0.0002	0.017	0.092	0.011	0.031	0.169
River*	0 - 0.014	0 - 0.034	NA	0.016 - 0.031	0.000	0.000	0.000	0.000	0.016 - 0.08

* Represents the estimated pre-impounded river fluxes assuming they were similar to current fluxes from the reservoir inflows.

1.5 Conclusions

The comprehensive GHG portrait of Batang Ai highlights the importance of spatial and temporal sampling resolution and the inclusion of all flux components in reservoir GHG assessments. Gas dynamics downstream of the dam (degassing, outflow emissions and CH_4 oxidation), commonly not assessed in reservoir GHG studies, are major elements in Batang Ai. We suggest that these emissions could have been greatly diminished with a minor change to the dam design (shallower water withdrawal). Mitigating GHG emissions from future reservoirs depends on the capacity to predict GHG fluxes from all pathways. In this regard, the comparison between Batang Ai measured and modeled GHG flux estimates allowed us to identify knowledge gaps based on which we propose the four following research avenues. 1) Refine the modeling of reservoir CO_2 diffusion by studying its link with metabolism and organic matter leaching from different soil types. 2) Examine the potential for CH_4 ebullition in littoral zones in relation to patterns of organic matter sedimentation linked to morphometry. 3) Improve the modeling of CH_4 degassing by better defining drivers of hypolimnetic CH_4 accumulation, namely thermal stratification. 4) Gather additional field data on GHG dynamics downstream of dams (degassing, river emissions, and river CH_4 oxidation) in order to incorporate all components of the flux to the modeling of reservoirs C footprint.

1.6 Acknowledgments

This work was funded by Sarawak Energy Berhad and the Natural Science and Engineering Research Council of Canada (Discovery grant to Y.T.P. and BES-D scholarship to C.S.). This is a contribution to the UNESCO chair in Global Environmental Change and the GRIL. We are grateful to Karen Lee Suan Ping and Jenny Choo Cheng Yi for their logistic support and participation in sampling campaigns. We also thank Jessica Fong Fung Yee, Amar Ma'aruf Bin Ismawi, Gerald Tawie Anak Thomas, Hilton Bin John, Paula Reis, Sara Mercier-Blais and Karelle Desrosiers for their help on the field, and Katherine Velghe and Marilyne Robidoux for their assistance during laboratory analyses.

1.7 Supplementary infomration

Table S1.1: Summary of the mean, standard deviation (SD), range (min and max), and number of observation (n) of physical and chemical variables measured at the surface of the reservoir and its inflows.

		Reservoir					**Inflows**				
Variables	**Units**	Mean	SD	Min	Max	n	Mean	SD	Min	Max	n
Water temperature	ºC	31	0.8	24	32	134	27	2.4	24	30	10
DOC	mg.L^{-1}	0.9	0.2	0.3	1.8	115	0.8	0.4	0.4	1.3	8
TP	µg.L^{-1}	5.9	2.4	2.8	23.3	114	20.7	7.6	11.7	36	8
TN	mg.L^{-1}	0.11	0.04	0.06	0.33	115	0.14	0.04	0.07	0.19	8
Chla	µg.L^{-1}	1.3	0.7	0.3	4.0	112	2.1	1.7	0.1	4.4	9
CO_2 diffusion	mmol.m^{-2}.d^{-1}	7.7	18.2	-30.8	80.0	129	137.3	192.4	9.7	593.9	8
CH_4 diffusion	mmol.m^{-2}.d^{-1}	0.6	0.6	0.03	3.7	129	30.7	37.4	1.2	113.4	8
N_2O diffusion	nmol.m^{-2}.d^{-1}	-0.2	2.1	-7.1	2.7	15					0
[CO_2]	µmol.L^{-1}	16.3	5.2	6.8	36.2	132	60.1	34.9	10.1	113.5	10
[CH_4]	µmol.L^{-1}	0.2	0.2	0.0	1.2	137	6.6	4.3	0.6	14.8	10
[N_2O]	nmol.L^{-1}	5.6	1.2	3.9	7.8	15	6.1		5.2	7.0	2

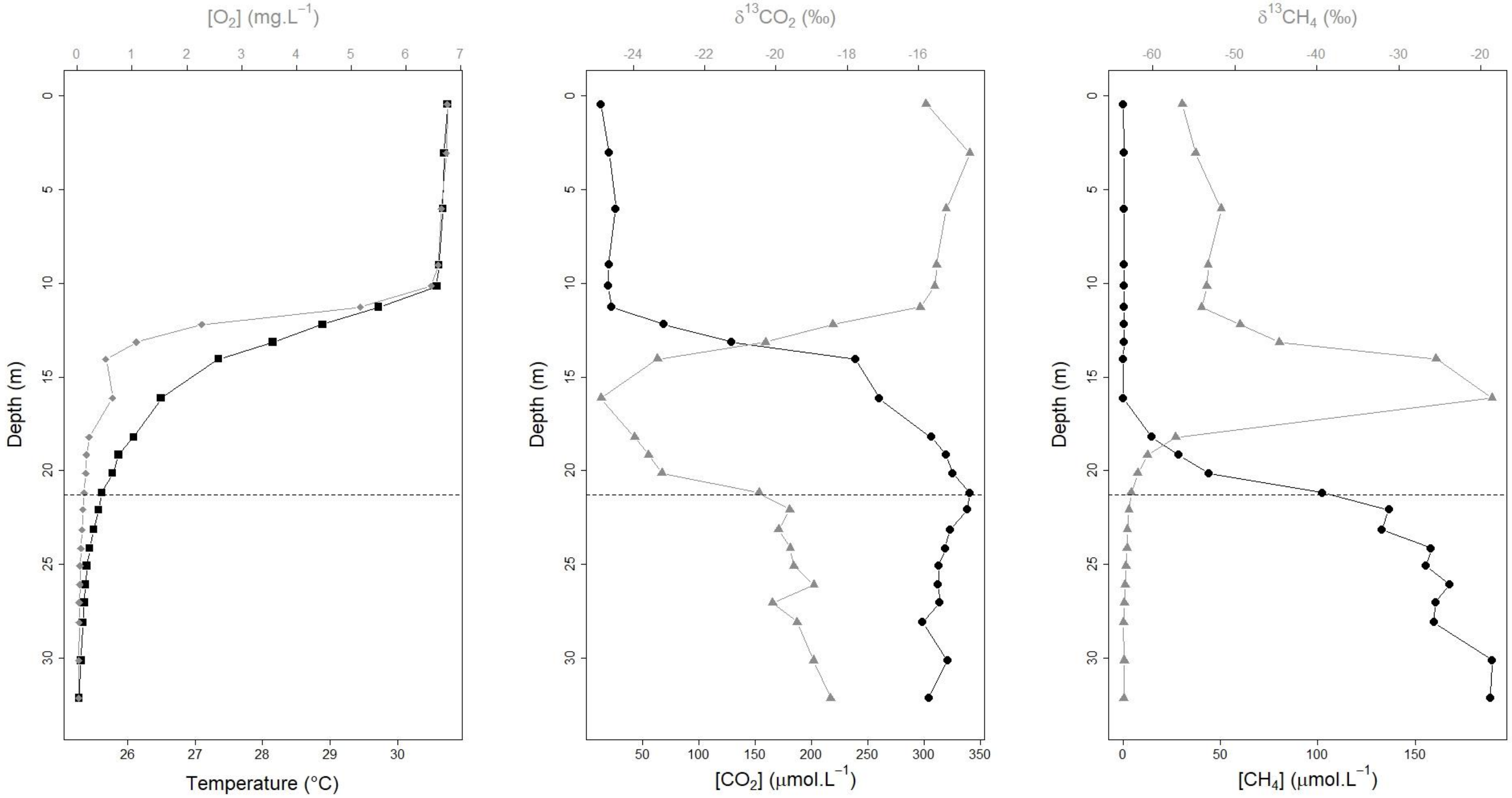

Figure S1.1: Profile example of water temperature (black squares), dissolved oxygen concentration (gray diamonds), CO_2 and CH_4 concentrations (black circles) and isotopic $\delta^{13}C$ signature (gray triangles) in the main basin of the reservoir right upstream of the dam in Aug 2018. The horizontal dashed line represent the water withdrawal depth.

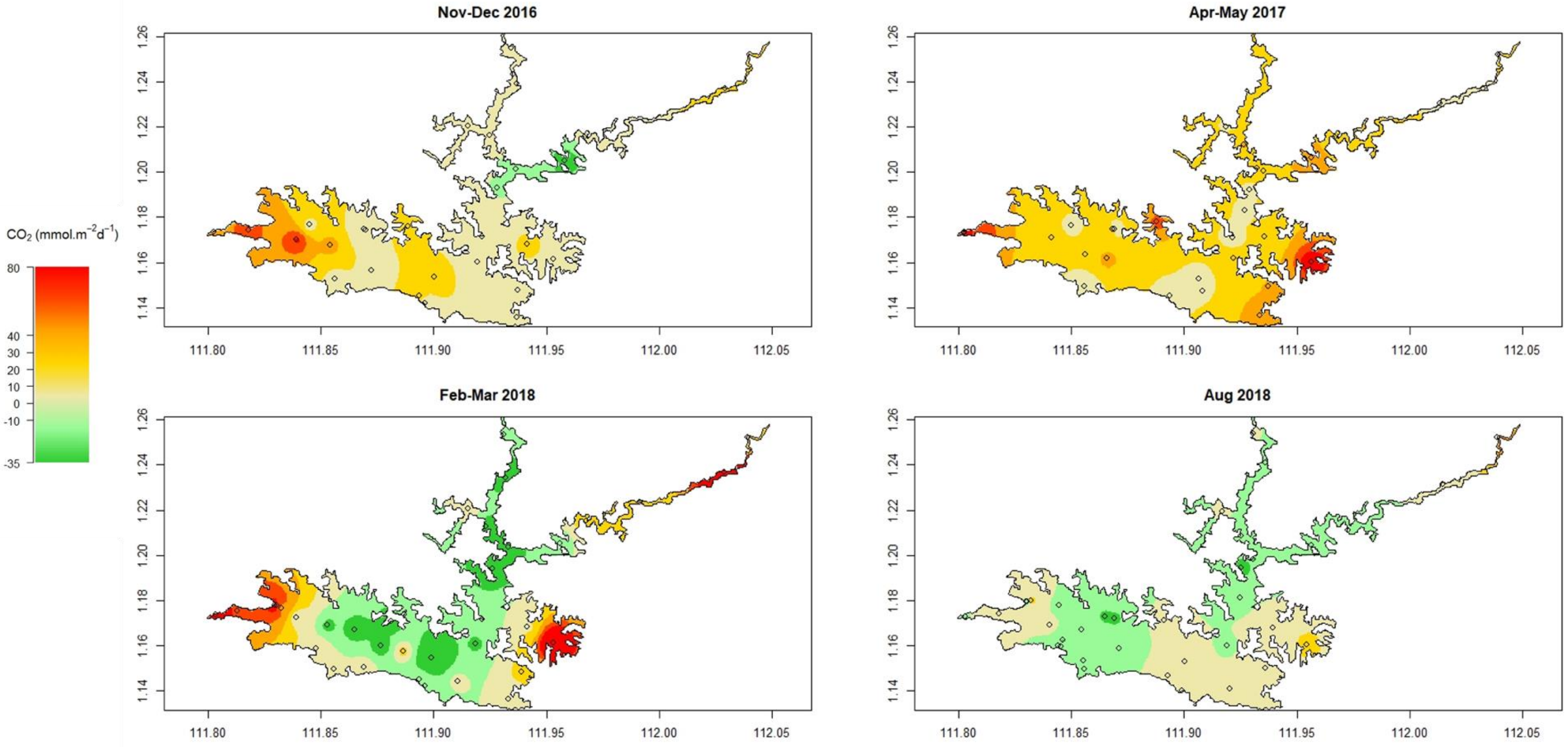

Figure S1.2: Maps of the spatially interpolated surface CO_2 diffusive flux in Batang Ai reservoir for each sampling campaign. Unit is in mmol.m^{-2}.d^{-1}. Graph axes are the spatial coordinates (latitude and longitude).

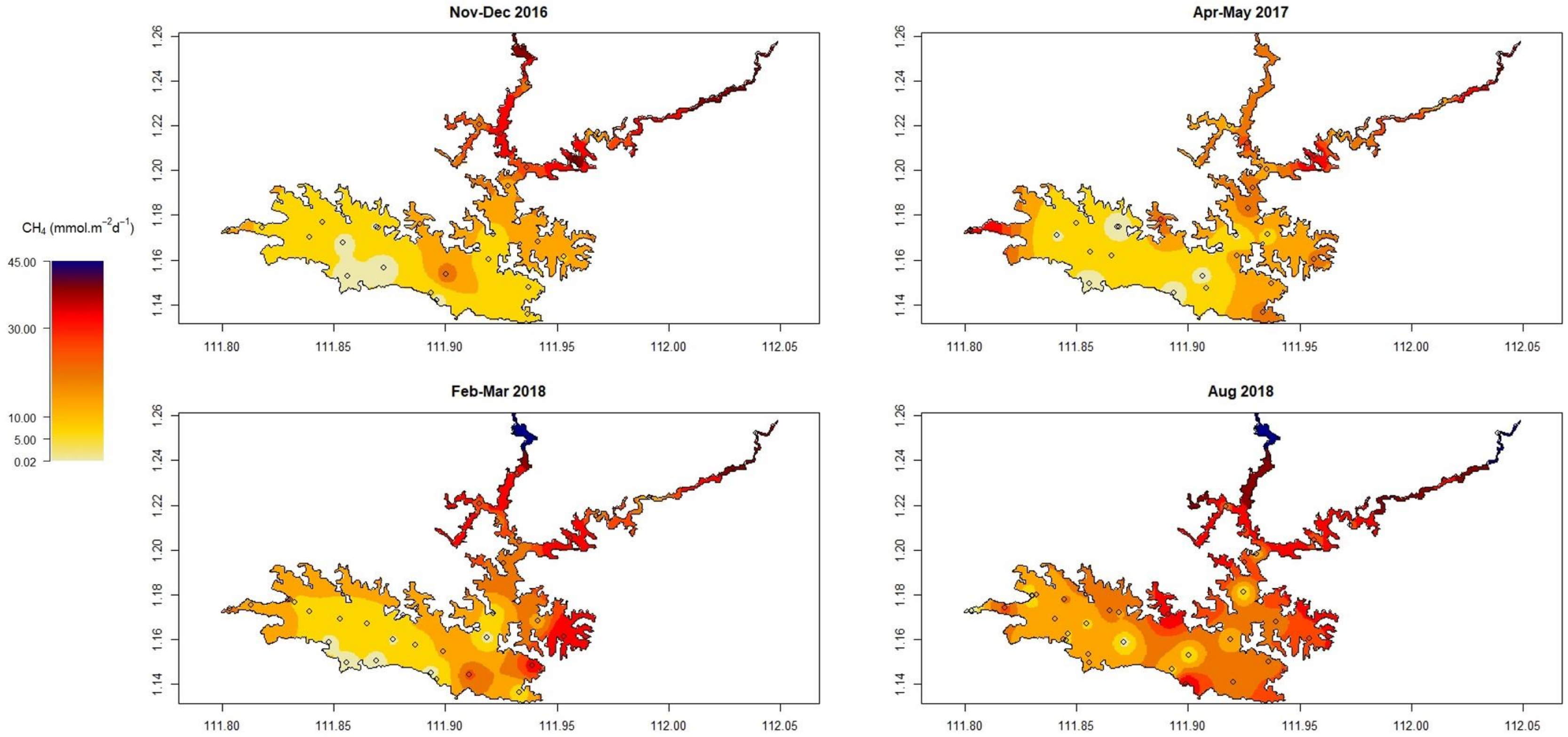

Figure S1.3: Maps of the spatially interpolated surface CH_4 diffusive flux in Batang Ai reservoir for each sampling campaign. Unit is in mmol.m^{-2}.d^{-1}. Graph axes are the spatial coordinates (latitude and longitude).

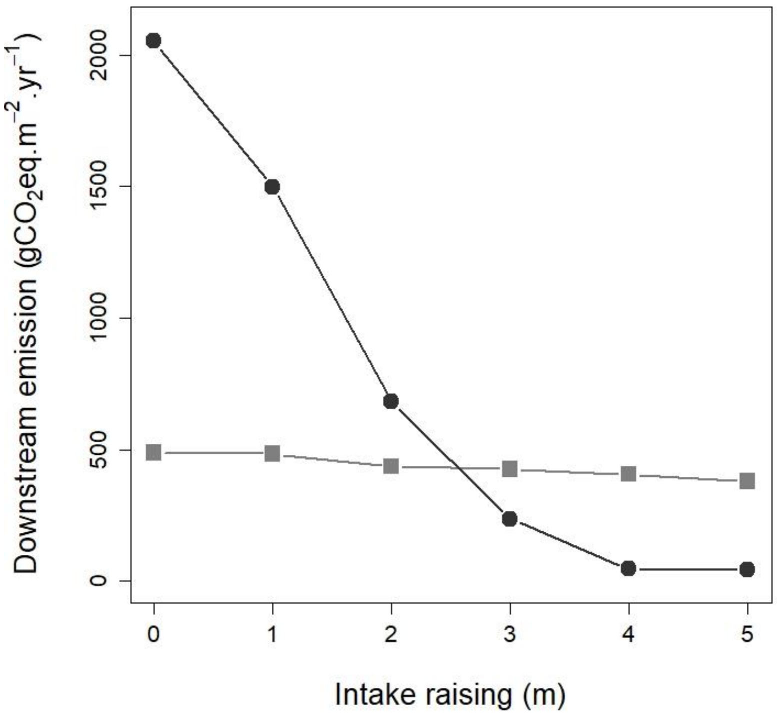

Figure S1.4: Simulated downstream emissions (including degassing) of CO_2 (gray squares) and CH_4 (dark circles) under different water withdrawal depth raise. Simulated emissions do not take into account CH_4 oxidation in the outflow river.

Table S1.2: Equations used to derive modeled CO_2 and CH_4 emissions based on the G-res and Barros et al. models. Input variables are described in Table S1.3.

	G-res model	**Barros et al. model**
$\log_{10}$ (CO_2 diffusion)	1.7892 - 0.3364 $\log_{10}$ (Age) + 0.0400 Effective temperature CO_2 + 0.06918 $\log_{10}$ (Reservoir area) + 0.0216 Soil C content + 0.1472 $\log_{10}$ (TP)	3.06 - 0.16 $\log_{10}$ (Age) - 0.01 Latitude + 0.41 $\log_{10}$ (DOC input) - $\log_{10}$ (400)
$\log_{10}$ (CH_4 diffusion)	0.8804 - 0.0116 Age + 0.6068 $\log_{10}$ (% littoral area / 100) + 0.04828 Effective temperature CH_4	1.33 - 0.36 $\log_{10}$ (Age) - 0.32 $\log_{10}$ (Mean depth) + 0.39 $\log_{10}$ (DOC input) - 0.01 Latitude
$\log_{10}$ (CH_4 ebullition)	-0.98574 + 1.0075 $\log_{10}$ (% littoral area / 100) + 0.04928 (Cumulative global horizontal radiance)	-
CH_4 degassing	$10^{(-5.5029 + 2.2857 \text{ log10 (Modeled CH4 diffusion) } + 0.9866 \text{ log10 (Water residence time)})}$ x Discharge / Reservoir area	-

Table S1.3: Input variables values, units, and source used in the modeling of Batang Ai CO_2 and CH_4 emissions.

Input variable	**Value**	**Unit**	**Source**
% Littoral area	5.15	%	$(1 - (1 - (3 / \text{Maximum depth}))^{((\text{Maximum depth} / \text{Mean depth}) - 1)}) \times 100$
Age	33	year	Mean reservoir age at sampling years (2016 - 2018)
Annual runoff	2219	$mm.yr^{-1}$	UNH/GRDC Composite Runoff Fields V1.0 (Fekete *et al.*, 2002)
Catchment area	1142	km^2	GranD database V1.3 (Lehner *et al.*, 2011)
Cumulative global horizontal radiance	56.4	$kWh.m^{-2}.yr^{-1}$	Surface meteorology and Solar Energy (NASA, 2008)
Discharge	106	$m^3.s^{-1}$	Average during the four sampling times (provided by Sarawak Energy)
DOC	0.8	$mg.L^{-1}$	Average of measured surface values in this study
DOC input	81.93	$mg.m^{-2}.d^{-1}$	(DOC x Volume) / (Reservoir area x Water residence time x 1000 x 365)
Effective temperature CH_4	26.37	℃	Mean annual temperature corrected for the effect on CH_4 from G-res tool (Prairie *et al.*, 2017)
Effective temperature CO_2	26.37	℃	Mean annual temperature corrected for the effect on CO_2 from G-res tool (Prairie *et al.*, 2017)
Latitude	1.16	Decimal degrees	Google earth
Maximum depth	85	m	GranD database V1.3 (Lehner *et al.*, 2011) – Height dam wall
Mean depth	34.4	m	GranD database V1.3 (Lehner *et al.*, 2011)
Modeled CH_4 diffusion	134	$gCO_2eq.m^{-2}.yr^{-1}$	Average over 100 years of CH_4 diffusion modeled based on the G-res equation (Table S2)
Reservoir area	68.4	km^2	GranD database V1.3 (Lehner *et al.*, 2011)
Soil C content	2.41	$kgC.m^{-2}$	Estimated based on Wasli et al. 2011
TP	6.77	$\mu g.L^{-1}$	Average of measured surface values in this study
Volume	2360×10^6	m^3	GranD database V1.3 (Lehner *et al.*, 2011)
Water residence time	0.93	year	(Mean depth x Reservoir area) / (catchment area x Annual runoff) x 1000

1.7.1 Modeling downstream river oxidation

The following section describes the conceptual framework underlying the isotopic model used to estimate CH_4 oxidation in the outflow of the reservoir. For that, we assume that the only source of water and CH_4 to the outflow (starting right downstream of the power house) is the reservoir discharge. We also assume oxidation and evasion to the atmosphere are the only two loss processes for CH_4 in the outflow, and that both reactions have a constant specific rate (they are a linear function of CH_4 concentration). When following a parcel of water travelling along the river, the change in CH_4 concentration can thus be described as:

$$\frac{d[CH_4]}{dt} = -k_{oxi}[CH_4] - k_{eva}[CH_4] \tag{S1.1}$$

with k_{oxi} and k_{eva} the rate coefficients of CH_4 oxidation and evasion respectively, and $[CH_4]$ the CH_4 concentration. Integration of Eq. (S1.1) yields the following generic time-depend solution:

$$[CH_4]_t = [CH_4]_0 \, e^{-(k_{oxi}+k_{eva})\,t} \tag{S1.2}$$

The instantaneous oxidation rate at a given time (t) or at a given point in the river is equal to:

$$oxidation\,rate = k_{oxi}\,[CH_4]_t \tag{S1.3}$$

Combining Eq. (S2) and Eq. (S1.3) yields the following equation:

$$oxidation\,rate = \; k_{oxi}\,[CH_4]_0 \, e^{-(k_{oxi}+k_{eva})\,t} \tag{S1.4}$$

Hence, the total amount of CH_4 oxidized between time 0 and time t (or between km 0 and t in the river) is derived from the integration of Eq. (S1.4):

$$amount\ oxidized = \; \int_0^t k_{oxi}\,[CH_4]_0 \, e^{-(k_{oxi}+k_{eva})\,t}\,dt \tag{S1.5}$$

Simplifying Eq. (S1.5) yields:

$$amount\ oxidized = [CH_4]_0 \left(\frac{k_{oxi}}{(k_{oxi}+k_{eva})}\right)\left(1 - e^{-(k_{oxi}+k_{eva})\ t}\right) \tag{S1.6}$$

The amount oxidized can also be calculated as the product of the original CH_4 concentration and the fraction of CH_4 oxidized (F_{ox}):

$$amount\ oxidized = [CH_4]_0\ F_{ox} \tag{S1.7}$$

According to Eq. (S1.6) and Eq. (S1.7), we can derive F_{ox} from the following equation:

$$F_{ox} = \left(\frac{k_{oxi}}{(k_{oxi}+k_{eva})}\right)\left(1 - e^{-(k_{oxi}+k_{eva})\ t}\right) \tag{S1.8}$$

In Eq. (S1.8), the second term of the product can be rearranged using Eq. (S1.2) to represent the remaining fraction of CH_4 concentration at time or km t:

$$F_{ox} = \left(\frac{k_{oxi}}{(k_{oxi}+k_{eva})}\right)\left(1 - \frac{[CH_4]_t}{[CH_4]_0}\right) \tag{S1.9}$$

Given a fractionation factor α for CH_4 oxidation, the behavior of the two CH_4 isotopes ($^{12}CH_4$ and $^{13}CH_4$) can be described based on Eq. (S1.2) as following:

$$[12CH_4]_t = [12CH_4]_0\ e^{-\left(k_{oxi}^{12}+k_{eva}\right)t} \tag{S1.10}$$

$$[13CH_4]_t = [13CH_4]_0\ e^{-\left(\frac{k_{oxi}^{12}}{\alpha}+k_{eva}\right)t} \tag{S1.11}$$

With $[12CH_4]$ and $[13CH_4]$ the concentrations of the two isotopes, and k_{oxi}^{12} the rate coefficient of oxidation for the $^{12}CH_4$ isotope. The isotopic ratio of CH_4 concentration at t (R_t) can be derived from Eq. (S1.10) and Eq. (S1.11) as following:

$$R_t = \frac{[13CH_4]_t}{[12CH_4]_t} = \frac{[13CH_4]_0\ e^{-(\frac{k_{oxi}}{\alpha}+k_{eva})\ t}}{[12CH_4]_0\ e^{-(k_{oxi}+k_{eva})\ t}} \tag{S1.12}$$

By simplifying Eq. (S1.12), R_t can be written as:

$$R_t = R_0\ e^{(1-\frac{1}{\alpha})\cdot k_{oxi}\ t} \tag{S1.13}$$

The term t can be isolated from Eq. (S1.13):

$$t = \frac{\ln({}^{R_t}/_{R_0})}{(1-\frac{1}{\alpha})\cdot k_{oxi}} \tag{S1.14}$$

Similarly, the term t can be isolated by rearranging Eq. (S1.2):

$$t = \frac{\ln({}^{[CH_4]_t}/_{[CH_4]_0})}{-(k_{oxi}+k_{eva})} \tag{S1.15}$$

Combining Eq. (S1.14) and Eq. (S1.15) results in:

$$\frac{\ln({}^{R_t}/_{R_0})}{(1-\frac{1}{\alpha})\cdot k_{oxi}} = \frac{\ln({}^{[CH_4]_t}/_{[CH_4]_0})}{-(k_{oxi}+k_{eva})} \tag{S1.16}$$

Rearranging E.S16 yields:

$$\frac{-\ln({}^{R_t}/_{R_0})}{(1-\frac{1}{\alpha})\cdot\ln({}^{[CH_4]_t}/_{[CH_4]_0})} = \frac{k_{oxi}}{(k_{oxi}+k_{eva})} \tag{S1.17}$$

Using Eq. (S1.9) and Eq. (S1.17), we can derive F_{ox} as:

$$F_{ox} = \frac{k_{oxi}}{(k_{oxi}+k_{eva})}\left(1-\frac{[CH_4]_t}{[CH_4]_0}\right) = \frac{-\ln({}^{R_t}/_{R_0})\cdot(1-{}^{[CH_4]_t}/_{[CH_4]_0})}{(1-\frac{1}{\alpha})\cdot\ln({}^{[CH_4]_t}/_{[CH_4]_0})} \tag{S1.18}$$

The isotopic ratios (R_t and R_0) can be converted to $\delta^{13}CH_4$ expressed in ‰ using the following standard isotopic equation calculation:

$$\delta^{13}\mathrm{CH_4} = \left(\frac{[\mathrm{13CH_4}]:[\mathrm{12CH_4}]}{[\mathrm{13CH_4}]_{\mathrm{std}}:[\mathrm{12CH_4}]_{\mathrm{std}}} - 1\right) \mathrm{x}\, 1000 \qquad \text{(S1.19)}$$

with $[13CH_4]_{std}$: $[12CH_4]_{std}$ the standard reference Pee Dee Belemite isotopic carbon ratio. The conversion of R_t and R_0 to $\delta^{13}CH_4$ in Eq. (S1.18) results in the following equation for F_{ox} calculation:

$$F_{ox} = \frac{-[\ln(\delta^{13}CH_{4_t}+1000)-\ln(\delta^{13}CH_{4_0}+1000)]\cdot(1-{}^{[CH_4]_t}/_{[CH_4]_0})}{(1-\frac{1}{\alpha})\cdot\ln({}^{[CH_4]_t}/_{[CH_4]_0})} \qquad \text{(S1.20)}$$

Eq. (S1.20) was used to determine F_{ox} and CH_4 oxidation (product of F_{ox} and $[CH_4]_0$) in Batang Ai river outflow using km 0 and 19 as a start and end points of the river stretch. Sampling of CH_4 concentration and isotopic signature was conducted at two other points within this river stretch (km 0.6 and 2.7). This additional sampling resolution can help test the adequacy of the model and its conceptual assumptions by recalculating CH_4 oxidation in individual segments (between 0-0.6 km, 0.6-2.7 km, and 2.7-19 km). If the model assumptions are correct (absence of other CH_4 source in the river, constant specific oxidation rate, and constant river velocity), the amount of CH_4 oxidized in the entire stretch (Ox_{total}) should equal the sum of the amount oxidized in each individual segment (Ox_{sum}). In two of the sampling campaigns (Apr-May 2017 and Feb-Mar 2018), the difference between Ox_{total} and Ox_{sum} was very small (CV < 5 %). In the two other campaigns, this difference was larger (CV of 12 and 35 % for Nov-Dec 2016 and Aug 2018 respectively), due to an additional CH_4 source causing occasional increases of CH_4 concentration along the stretch. Overall, model assumptions appear reasonable, however, to avoid overestimating the amount oxidized in cases of additional CH_4 sources, we considered Ox_{total} as the more suitable estimate, since it is less influenced by CH_4 addition in individual segments.

CHAPITRE II

QUANTIFYING SOURCES AND PROCESSES SUSTAINING SURFACE CO_2 AND CH_4 FLUXES IN A TROPICAL RESERVOIR

Cynthia Soued[1], Yves T. Prairie[1]

[1]Groupe de Recherche Interuniversitaire en Limnologie et en Environnement Aquatique (GRIL), Département des Sciences Biologiques, Université du Québec à Montréal, Montréal, H2X 3X8, Canada.

N.B. References cited in this chapter are presented at the end of the thesis.

2.1 Abstract

Freshwaters are important emitters of carbon dioxide (CO_2) and methane (CH_4) to the atmosphere, two potent greenhouse gases (GHG). While aquatic surface GHG fluxes have been extensively measured, there is much less information on their underlying sources. CO_2 and CH_4 air-water fluxes can originate from different sources in both lakes and reservoirs: horizontal riverine flow, vertical flux from the bottom layer, sediment inputs, and water column metabolism. These processes are generally studied separately, leading to a fragmented assessment of their relative role in sustaining CO_2 and CH_4 surface fluxes. In this study, we quantified sources / sinks of CO_2 and CH_4 in the epilimnetic layer of a permanently stratified tropical reservoir located on the Borneo Island. CO_2 and CH_4 concentrations, stable isotopes, and fluxes were measured at the sediment-water and air-water interfaces as well as within the water column in different locations and seasons. Results showed that horizontal inputs is an important source of both CO_2 and CH_4 (18 to 100 % of surface emissions) in the upstream reservoir branches. However, this contribution fades along the hydrological continuum, becoming negligible in the main basin of the reservoir, where CO_2 and CH_4 are uncoupled and driven by different processes. In the main basin, vertical CO_2 inputs and sediment CH_4 inputs contributed to on average 60 and 23 % respectively to the surface fluxes of the corresponding gas. Water column metabolism generally played a major role in the epilimnetic budget for CO_2 and CH_4. However, net metabolism was highly variable for both gases, shifting from positive to negative values, thus making it the most important but uncertain component of the epilimnetic gas budgets. Overall, our results highlight the importance of assessing all the components sustaining CO_2 and CH_4 surface fluxes and identify clear knowledge gaps hindering our predictive capacity of aquatic GHG fluxes.

2.2 Introduction

Surface inland waters are globally significant sources of greenhouse gases (GHG) to the atmosphere, namely carbon dioxide (CO_2) and methane (CH_4) (DelSontro *et al.*, 2018a). Freshwaters act as both transport vessels for terrestrial carbon (C) and as active biogeochemical processors, making them key sites of GHG exchange with the atmosphere (Tranvik *et al.*, 2018). The impoundment of rivers for hydropower generation, irrigation, flood control or other purposes, changes the landscape and its C cycling (Maavara *et al.*, 2017), often resulting in increased aquatic CO_2 and CH_4 emissions due to the decay of flooded organic matter (Prairie *et al.*, 2018 ; Venkiteswaran *et al.*, 2013). Globally, reservoirs are estimated to emit between 0.5 and 2.3 $PgCO_2eq.yr^{-1}$ (Barros *et al.*, 2011 ; Bastviken *et al.*, 2011 ; Deemer *et al.*, 2016 ; St. Louis *et al.*, 2000), and this number is predicted to increase with a rapid growth of the hydroelectric sector in the upcoming decades (Zarfl *et al.*, 2015). Several studies have focused on quantifying GHG surface diffusion from reservoirs around the world and have found extremely high variability temporally and spatially (Barros *et al.*, 2011 ; Deemer *et al.*, 2016), like it is the case in natural lakes (DelSontro *et al.*, 2018a ; Raymond *et al.*, 2013). However, less research exists on the sources and processes sustaining latter surface diffusive fluxes and their variability, especially in reservoirs.

GHG sources to surface waters can be both internal and external. The magnitude of allochthonous inputs, namely terrestrial organic and inorganic C, is known to increase with the soil-water connectivity (Hotchkiss *et al.*, 2015), and with soil C content and leaching capacity (Kindler *et al.*, 2011 ; Li *et al.*, 2017 ; Monteith *et al.*, 2007). Soil-derived gas inputs are also temporally variable, generally increasing with discharge, like during storm events (Vachon et del Giorgio, 2014) or during rainy seasons (Kim *et al.*, 2000 ; Zhang *et al.*, 2019). Terrestrial inputs in the form of organic C can indirectly sustain surface GHG emissions by fueling lake / reservoir in situ organic matter aerobic and anaerobic respiration (Karlsson *et al.*, 2007 ; Pace et Prairie, 2005 ;

Rasilo *et al.*, 2017). The metabolic balance between aerobic ecosystem respiration (ER) and gross primary production (GPP), and between methanogenesis and CH_4 oxidation, control the net internal production of CO_2 and CH_4 respectively, and in turn influence their surface fluxes. Respiration and primary production rates are highly variable in space and time, and generally a function of temperature, organic C content and nutrients (Hanson *et al.*, 2003 ; Pace et Prairie, 2005 ; Prairie *et al.*, 1989 ; Solomon *et al.*, 2013). Net heterotrophy (ER > GPP) is mainly associated with systems receiving high external inputs of organic C (Bogard *et al.*, 2020 ; Tank *et al.*, 2010 ; Wilkinson *et al.*, 2016), while net autotrophy (ER < GPP) has been associated to highly productive nutrient-rich systems (Hanson *et al.*, 2003 ; Sand-Jensen et Staehr, 2009). However, a large part of the variability in measured metabolic rates remains unexplained (Bogard *et al.*, 2020 ; Coloso *et al.*, 2011 ; Solomon *et al.*, 2013) and our ability to predict their net balance is still weak in part because the two processes are often studied separately. Additionally, anaerobic C degradation adds another level of complexity to the C metabolic balance by decoupling GPP and ER (Bogard et del Giorgio, 2016 ; Martinsen *et al.*, 2020 ; Vachon *et al.*, 2020). For instance, methanogenesis transforms organic C to CH_4 instead of CO_2, a gas product with a radiative forcing 34 times higher than CO_2 over a 100 years horizon. CH_4 is known to be mostly produced in both profundal and littoral sediments, and reach the water surface by vertical or lateral diffusive processes (Bastviken *et al.*, 2008 ; DelSontro *et al.*, 2018b ; Encinas Fernández *et al.*, 2014 ; Guérin *et al.*, 2016). However, there is increasing evidence that CH_4 production in the oxic water column contributes significantly to lakes CH_4 emissions (Bižić *et al.*, 2019 ; Bogard *et al.*, 2014 ; DelSontro *et al.*, 2018b ; Donis *et al.*, 2017 ; Tang *et al.*, 2014). Methanogenesis can be counter-balanced by the oxidation of CH_4 to CO_2 mainly in oxic and hypoxic environments (Conrad, 2009 ; Reis *et al.*, 2020b ; Thottathil *et al.*, 2019). While several studies have measured rates of CH_4 production and oxidation in lakes and reservoirs, few have quantified the net balance of these two processes at an ecosystem-scale (Bastviken *et al.*, 2008 ; Schmid *et al.*, 2007 ; Vachon *et al.*, 2019). According to Vachon et al. (2019), this balance is tightly controlled by physical processes within the water column. Physical mixing in lakes and reservoirs indirectly impacts C metabolic processes by shaping the O_2 profile, and directly affects GHG surface diffusion by controlling the transport of CO_2 and CH_4 from bottom to surface water layers (Barrette et Laprise, 2005 ; Kreling *et al.*, 2014 ; Pu *et al.*, 2020). Despite its potential importance (Kankaala *et al.*, 2013a), very few studies have focused on quantifying vertical gas transport and the role of this process in fueling surface GHG diffusion.

Understanding what regulates surface CO_2 and CH_4 concentrations and fluxes to the atmosphere requires knowledge of the interplay between all physical and biogeochemical processes involved. While a number of studies have assessed some processes individually or by difference, very few have measured all relevant components of the epilimnetic mass-balance simultaneously. Here we report on a field study in a tropical hydropower reservoir quantifying external inputs, sediments inputs, net CO_2 and CH_4 metabolism, vertical diffusion from deeper layers and gas exchange at the air-water interface. This allowed us to estimate the relative contribution of each process in shaping surface GHG emissions from a tropical East Asian reservoir, and to test whether the epilimnetic mass balance can be closed. The two major rivers feeding the Batang Ai reservoir flow into two elongated reservoir branches, acting as a transition zones, before reaching the reservoir main basin. This configuration, common in reservoirs, allowed us to quantify and compare epilimnetic CO_2 and CH_4 regulation in two morphometrically different areas of the reservoir (branches and main basin). Overall, the aim of this study is to provide ecosystem-scale portrait of the processes sustaining surface CO_2 and CH_4 emissions and examine how they change when transitioning from a river delta to the open basin.

2.3 Materials and methods

2.3.1 Site and sampling description

The study was conducted in Batang Ai hydroelectric reservoir in Sarawak Malaysia (latitude 1.16º and longitude 111.9º). The reservoir is located on the Borneo Island in a tropical equatorial climate with a constantly high temperature averaging 23ºC and 32ºC during nighttime and daytime respectively (Sarawak Government, 2019). The region experiences two weak monsoon seasons (November to February and June to October) with a yearly average rainfall of 3300 to 4600 mm (Sarawak Government, 2019). The reservoir was impounded in 1985 with a dam wall of 85 m, a surface area of ~68.4 km^2 and a watershed area of 1149 km^2 of mostly undisturbed forested land (limited rural habitations and small scale croplands). The reservoir water residence time is 0.9 year.

We distinguish between three sections of the study site: inflows, reservoir branches, and reservoir main basin shown in Figure 2.1. The inflows are the two main reservoir inlets: Batang Ai and Engkari rivers (3 to 10 m deep where sampled). The two rivers flow into two arms that we refer to as the reservoir branches (10.8 km^2, mean and max depths of 18 and 52 m respectively). The reservoir branches merge into the main basin of the reservoir (58.9 km^2, mean and max depths of 30 and 73 m respectively). Surface sampling was performed in 36 sites across the three study sections, and water column profile sampling (from 0 up to 32 m, each 0.5 to 3 m) was done in 9 sites in the reservoir branches and main basin (Figure 2.1). Sampling was repeated (with a few exceptions) during four campaigns: 1) November 14th to December 5th 2016 (Nov-Dec 2016), 2) April 19th to May 3th 2017 (Apr-May 2017), 3) February 28th to March 13th 2018 (Feb-Mar 2018), and 4) August 12th to 29th 2018 (Aug 2018).

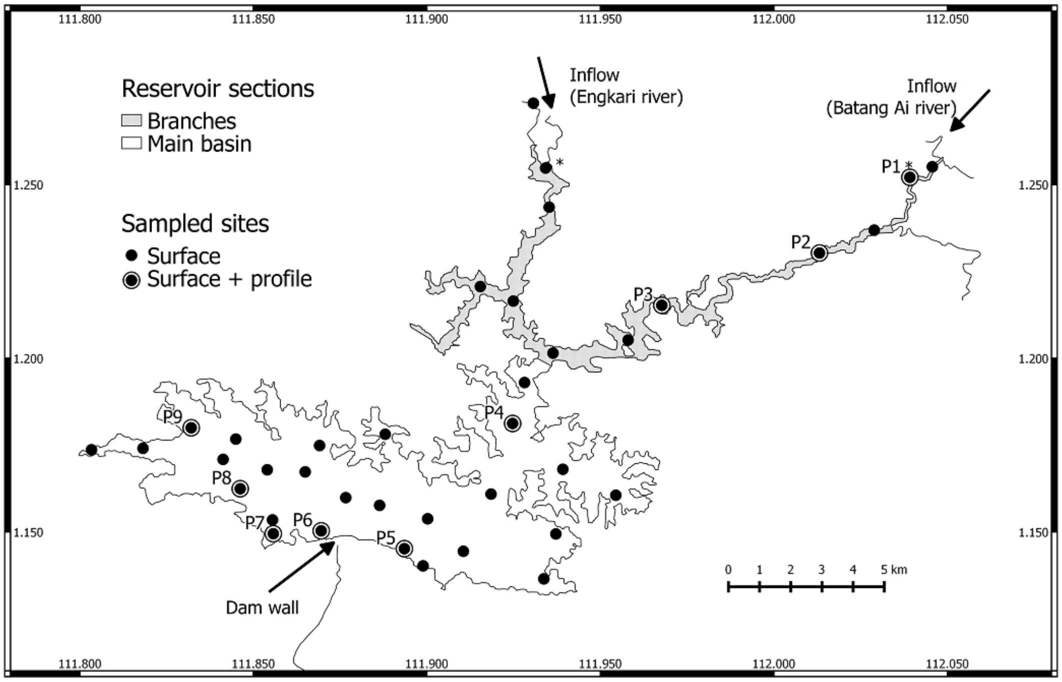

Figure 2.1: Map of Batang Ai reservoir with delimited sections (branches and main basin) and sampling points. * Represents sampling points at the branches extremities.

2.3.2 Physical and chemical analyses

Water temperature, dissolved oxygen, and pH were measured using a multi-parameter probe (YSI model 600XLM-M) equipped with a depth gauge and attached to a 12 Volt submersible pump (Proactive Environmental Products model Tornado) for water samples collection. Concentrations of dissolved organic carbon (DOC), total phosphorus (TP), total nitrogen (TN), and chlorophyll a (Chla) were measured during all campaigns in all surface sampling sites (Figure 2.1). Methods for latter analyses are described in detail in Soued et Prairie (2020). Briefly, TP and Chla (extracted with hot ethanol) were analyzed via spectrophotometry, and TN and DOC (filtered at 0.45 µm) were measured on an Alpkem Flow Solution IV autoanalyser and on a Total Organic Carbon analyser 1010-OI respectively.

For each site, we defined the depths of the thermocline and the top and bottom of the metalimnion based on measured temperature profiles using the R package rLakeAnalyzer (Winslow *et al.*, 2018). The epilimnion was defined from the surface to the top of the metalimnion, and was assumed to be a mixed layer.

2.3.3 Gas concentration, isotopic signature, and water-air fluxes

CO_2 and CH_4 gas concentrations and isotopic signatures ($\delta^{13}C$) were measured in duplicates at the surface in 36 sites and along vertical profiles in 9 sites (P1 to P9, Figure 2.1) using the headspace technique described in details in Soued et Prairie (2020). In brief, sampling was done by equilibrating the water sample with an air headspace inside a 60 mL syringe. The gas phase was then injected in a 12 mL pre-vacuumed air-tight vial, and analyzed on a gas chromatograph (Shimadzu GC-8A) for gas concentrations, and on a Cavity Ring Down Spectrometer (CRDS) equipped with a Small Sample Isotopic Module (SSIM, Picarro G2201 -i) for $\delta^{13}CO_2$ and $\delta^{13}CH_4$.

Surface diffusive fluxes of CO_2 and CH_4 were measured at all surface sampling sites during each campaigns. Flux rates were derived from linear changes in CO_2 and CH_4 concentrations in a static floating chamber connected in a closed loop to a gas analyzer (model UGGA, from Los Gatos Research). Measured gas concentrations, isotopic signature, and fluxes were spatially interpolated to the whole reservoir area using package gstat version 1.1-6 in the R version 3.4.1 software (Pebesma, 2004). Mean values were calculated for each campaign based on the interpolated maps (Soued et Prairie, 2020).

2.3.4 Horizontal GHG inputs

CO_2 and CH_4 inputs from the horizontal water flow (H) were estimated using Eq. (2.1):

$$H = C_{in}\, Q\, f_{epi} \tag{2.1}$$

With C_{in} the concentration of gas in the inflowing water, Q the reservoir water discharge, and f_{epi} the fraction of water flowing into the epilimnion. Q was taken as the mean of daily discharge during each campaign (considering minimal changes in inflow / outflow rates during campaigns). f_{epi} was estimated based on temperature profiles at the two ends of the right branch. To estimate gas inputs form the inflows to the branches, C_{in} was considered as the average of gas concentrations measured at the two upstream extremities of the branches (Figure 2.1). To estimate gas inputs form the branches to the main basin, C_{in} was considered as the gas concentrations measured at the confluence between the two branches (right upstream of the main basin).

2.3.5 Vertical GHG fluxes

We estimated CO_2 and CH_4 fluxes from the metalimnion to the epilimnion (F_v) based on the vertical gas diffusivity (K_z) and the gradient in gas concentration across the epilimnion-metalimnion interface using the Eq. (2.2) (Wüest et Lorke, 2009):

$$F_v = K_z\, (C_{meta} - C_{epi}) \tag{2.2}$$

where C_{meta} and C_{epi} are the gas concentrations at the top of the metalimnion and at the bottom of the epilimnion respectively, measured in profile sites (P1 to P9, Figure 2.1). K_z was derived from the following Eq. (2.3) (Osborn, 1980):

$$K_z = \Gamma \frac{\epsilon}{N^2} \tag{2.3}$$

where Γ is the mixing ratio set to 0.2 (Oakey, 1982), ϵ is the dissipation rate of turbulent kinetic energy, and N^2 is the buoyancy frequency. N^2 was calculated from measured temperature profiles (YSI probe) using function buoyancy.freq from the rLakeAnalyzer package (Winslow *et al.*, 2018) in the R software (R Core Team, 2017).

ϵ was derived from measured vertical shear microstructure profiles performed in the Aug 2018 campaign in all profile sites shown in Figure 2.1 (except P1 due to floating logs). Shear profiles were measured with a high frequency (512 Hz) MicroCTD profiler (Rockland Scientific) equipped with two velocity shear probes, two thermistors, tilt and vibration sensors, and a pressure sensor. At each site, the profiler was cast 10 times, 5 with an uprising configuration (from bottom to top of the water column) and 5 with a downward configuration (top to bottom), with a 4 min waiting time between profiles to allow water column disturbance to subside. Data quality check and ϵ calculation for each profile cast were performed with ODAS v4.3.03 Matlab library (by Rockland Scientific) based on Nasmyth shear spectrum (Oakey, 1982), with ϵ values averaged among the two shear probes and binned over 1-2 m segments along the profile. For each site, continuous ϵ profiles were interpolated by fitting a smooth spline through all ϵ values from replicate casts as a function of depth.

At the epilimnion-metalimnion interface (top of the metalimnion ± 2 m), calculated ϵ averaged 7.7 x10^{-9} (range from 3.4 x 10^{-9} to 1.6 x 10^{-8}) $m^2.s^{-3}$ across all sites sampled with the microCTD, with no significant difference between the main basin and branches sites. In order to estimate vertical gas diffusion, we applied the latter ϵ average to Eq. (2.2) and (2.3) for all measured gas profiles (except P1). The resulting F_v values for each gas were averaged across sites in the main basin and branches separately to derive estimates of F_v for each of these two reservoir sections.

2.3.6 Sediment GHG inputs

In order to estimate CO_2 and CH_4 inputs from the sediments to epilimnetic waters, we calculated sediment to water gas fluxes based on gas profiles in sediment cores collected in Apr-May 2017 and Feb-Mar 2018 at 7 sites (P1 to P3 in the reservoir branches and P4, P5, P7, and P9 in the main basin, Figure 2.1). Sediment cores were collected using a Glew gravity corer attached to a 6 cm wide plastic liner. The liner was pre-drilled with 1 cm holes covered with electric tape at each centimeter up to 40 cm. Upon recovery of the sediment core, 3 mL tip-less syringes were inserted into each hole to extract sediments from each centimeter. The sediment content of each syringe was emptied into a 25 mL glass vial prefilled with 6 mL nano-pure water and immediately air-tight sealed by a butyl rubber stopper crimped with an aluminum cap. Glass vials were pressurized with 40 mL of ambient air using a plastic syringe equipped with a needle to pierce the rubber cap. Glass vial were shaken for 2 min for equilibration before extracting the gas with a syringe and injecting it into a pre-evacuated air-tight vial for analysis CO_2 and CH_4 concentration and isotopic signature as described above. Additionally, samples of the water overlaying the sediments (~1 cm above) were collected for similar analyses of CO_2 and CH_4.

Sediment CO_2 and CH_4 flux rates to the overlaying water column were derived from the vertical gradient of gas concentration measured in the sediment cores and overlaying water (Berg *et al.*, 1998). The slope of CO_2 or CH_4 concentration as a function of depth (g, in $\mu mol.L^{-1}.m^{-1}$) was calculated for measured values in the first 5 cm of sediments and overlaying water. Most cores exhibited clear linear slopes (p-value < 0.05 and $R^2_{adj} > 0.5$). In the few cases where a linear slope was not evident, g was replaced by the gradient between the mean gas concentration in the first 3 cm and the overlaying water. The sediment gas flux rate (S_f in $mmol.m^{-2}.d^{-1}$) were calculated with Eq. (2.4):

$$S_f = \frac{g \times d}{p} \tag{2.4}$$

With *d* the diffusion coefficient set to 1.5×10^{-5} $cm^2.s^{-1}$ (Donis *et al.*, 2017), and *p* the sediment porosity assumed to be 2 % based on previous results in Batang Ai (Tan, 2015).

At an ecosystem scale, sediment CO_2 and CH_4 inputs to the water column (S) were estimated based on average and standard deviation values of sites located in each section of the reservoir (branches and main basin). For each section, mean sediment CO_2 and CH_4 flux rates were multiplied by the areal ratio of epilimnetic sediments (A_{epi}) versus total water area (A_0). The latter ratio was calculated based on the hypsometric model (Ferland *et al.*, 2014 ; Imboden, 1973) as shown in Eq. (2.5) to (2.7):

$$q = \left(\frac{z_{max}}{z_{mean}}\right) - 1 \tag{2.5}$$

$$A_{epi} = A_0\left(1 - \left(1 - \left(\frac{z_{epi}}{z_{max}}\right)\right)^q\right) \tag{2.6}$$

$$S = \frac{A_{epi}}{A_0}\, Sf \tag{2.7}$$

with q a parameter describing the general shape of the reservoir section, z_{max} and z_{mean} the maximum and mean depths respectively, and z_{epi} the mean depth of the epilimnion (8.0 and 10.5 m in the branches and main basin respectively).

2.3.7 Metabolic rates

Net metabolic rates of CO_2 and CH_4 production in the epilimnetic water column were estimated with *in situ* incubations. Incubations were performed in 5 sites (P2 and P3 in the branches and P4, P5 and P7 in the main basin, Figure 2.1). Water from 3 m deep was pumped into 5 L transparent glass jars with an air tight clamp lid. Before closing, jars were filled from the bottom and allowed to overflow, then sampled for initial CO_2 and CH_4 concentrations. Closed jars were fixed at 3 m to an anchored line in the reservoir sampling site, and incubated in *in situ* temperature and light conditions for 22.0 to 24.2 hours. Upon retrieval, samples of final CO_2 and CH_4 concentrations were collected form the jars. Volumetric daily rates of net CO_2 and CH_4 production were calculated based on the difference between final and initial gas concentrations rescaled to a 24 h period.

In addition to incubations, open water high frequency O_2 measurements were carried out to derive CO_2 metabolism on larger spatial and temporal scales. Rates of gross primary production (GPP), aerobic ecosystem respiration (ER), and net ecosystem production (NEP) were estimated in the reservoir surface layer by monitoring and inverse modeling diel O_2 changes in the epilimnion. O_2 was measured at a one minute interval using high frequency O_2 and temperature sensors (model miniDOT from Precision Measurement Engineering). Sensors were deployed in profile sites P1 to P3 in the branches and P4, P5, P7, and P9 in the main basin (Figure 2.1). Note that not all sites were sampled in all sampling campaigns. Sensors were attached to an anchored line at a depth of 0.7 to 3 m and deployment time varied between 4 days and two weeks. Upon retrieval of the sensors, a first data quality check and selection was made based on the sensor internal quality index and visual screening. Rates of ecosystem metabolism were then estimated based on an open system diel O_2 model (Odum, 1956), where change in O_2 concentration is a function of GPP, ER, and air-water gas exchange (K_{O2}) following Eq. (2.8) (Hall et Hotchkiss, 2017):

$$\frac{dO2}{dt} = \frac{GPP}{z_{epi}} + \frac{ER}{z_{epi}} + K_{O2}\left(O_{2_{sat}} - O_2\right) \tag{2.8}$$

with O_{2sat} the theoretical O_2 concentration at saturation considering the *in situ* temperature and atmospheric pressure, and O_2 is the actual measured O_2 concentration in the water. A detailed description of the model equations can be found in (Hall et Hotchkiss, 2017). Daily estimates of GPP, ER, and K_{O2} were derived by maximum likelihood fitting of the data to the model in Eq. (2.8) using the R package StreamMetabolizer (Appling *et al.*, 2018). In some cases, where the best K_{O2} was negative, the fitting process was rerun with a user defined positive K_{O2}, either equal to a value estimated for the previous or subsequent day at the same site (range of 0.03 – 0.96 d^{-1}) or fixed to 0.1 d^{-1} (if no other available estimate). A final selection of daily metabolic estimates was done based on the model goodness of fit assessed by calculating Pearson correlation coefficient between modeled and measured O_2 values and discarding days with a correlation lower than 0.9. Based on GPP and ER estimates, we calculated daily NEP as the balance between these two processes, and converted it to net CO_2 production rate by assuming a 1:1 metabolic quotient.

Average estimates of areal metabolic rates per campaign were obtained for the branches and main basin by first averaging data within each site and then across sites for each reservoir section. Note that one value derived from incubations was excluded from the calculation of the average net CH_4 production rate in the branches due to its high value of initial CH_4 concentration (an order of magnitude higher than in all other incubations and all epilimnetic data from this site). The high CH_4 concentration, unrepresentative of real conditions, was probably caused by CH_4 contamination during sampling, and triggered a high oxidation rate that would overestimate the real ecosystem average rate if included.

2.4 Results

2.4.1 Physical and chemical properties

Surface water temperature exhibited a marked increase from the inflows to the branches, averaging 27.1 and 30.7 ºC respectively (Table 2.1). There was no difference in surface water temperature between the branches and the main basin. The depth of the epilimnion tended to increase and become more stable along the water flow, going from 1.3 (± 1.6) m in the Batang Ai river delta, to 8.0 (± 2.3) m in its branch, and 10.6 (± 1.7) m in the main basin (Table 2.1). Light penetration exhibited the same spatial pattern, with an increasing Secchi depth along the water flow, from a mean of 1.3 in the inflows to 5.1 and 5.5 in the branches and main basin respectively (Table 2.1). All sections of the study system (reservoir inflows, branches, and main basin) exhibited oligotrophic water properties (Table 2.1).

Table 2.1: Mean (± SD) of physical and chemical variables measured at the surface of the three reservoir sections.

Variables	Units	Inflows	Branches	Main basin
z_{epi}	m	1.3 (± 1.6)	8 (± 2.3)	10.6 (± 1.7)
Secchi	m	1.2 (± 0.9)	5.1 (± 1.2)	5.5 (± 1.2)
Temp.	ºC	27.1 (± 2.5)	30.7 (± 0.5)	30.6 (± 0.5)
pH		6.5 (± 0.3)	7.2 (± 0.2)	7.2 (± 0.2)
O_2	%	94.9 (± 7.7)	102.7 (± 4.5)	99.3 (± 4.8)
DOC	mg $C.L^{-1}$	0.8 (± 0.4)	0.9 (± 0.2)	0.9 (± 0.2)
TP	µg $P.L^{-1}$	20.7 (± 7.6)	6.2 (± 1.7)	5.8 (± 2.6)
TN	mg $N.L^{-1}$	0.14 (± 0.04)	0.12 (± 0.04)	0.1 (± 0.03)
Chla	$\mu g.L^{-1}$	2.1 (± 1.7)	1.7 (± 1)	1.2 (± 0.5)

2.4.2 Surface GHG concentrations, fluxes, and isotopic signatures

Surface CO_2 and CH_4 patterns are summarized in Figure 2.2, presenting campaign averages of spatially interpolated gas concentration, flux, and isotopic signature along the different reservoir sections. Despite the temporal variability, the gas patterns along the water flow are robust, remaining similar throughout time (Figure 2.2).

Average CO_2 air-water flux and surface concentration were systematically higher in the inflows (mean [range]: 135.3 [18.9 – 368.8] $mmol.m^{-2}.d^{-1}$ and 58.0 [24.5 – 113.0] $\mu mol.L^{-1}$, respectively) compared to the branches (4.7 [-3.4 – 15.2] $mmol.m^{-2}.d^{-1}$ and 15.4 [12.2 – 19.3] $\mu mol.L^{-1}$) or the main basin (7.5 [0.3 – 15.1] $mmol.m^{-2}.d^{-1}$ and 16.0 [14.2 – 17.7] $\mu mol.L^{-1}$) (Figure 2.2). Surface CO_2 concentration in the reservoir (branches and main basin) was most strongly correlated inversely with water temperature ($R^2_{adj} = 0.22$, p-value < 0.001, Figure S2.1 and Table S2.1). Except for the

Apr-Mar 2017 campaign, there is a modest increase (2.2 to 3.3 ‰) of surface $\delta^{13}CO_2$ towards more enriched values from the inflows to the branches (Figure 2.2).

Similarly, surface CH_4 flux and concentration continually decreased along the water channel, being an order of magnitude higher in the inflows compared to the branches, and about twice as high in the branches compared to the main basin (Figure 2.2). Of all measured water properties, TN was the most strongly linked to reservoir surface CH_4 concentration ($R^2 = 0.14$, p-value < 0.001, Figure S2.1 and Table S2.1). In the main basin surface CH_4 concentration significantly decreased with distance to shore in Nov-Dec 2016 ($R^2_{adj} = 0.54$, p-value < 0.001), but this correlation was weaker ($R^2_{adj} \leq 0.13$, p-value ≥ 0.03) during other sampling campaigns (Figure 2.6). Surface $\delta^{13}CH_4$ values varied widely, between -83.3 and -47.6 ‰, but did not show a consistent spatial pattern (Figure 2.2) apart from a positive correlation with distance to shore in the main basin in Nov-Dec 2016 ($R^2_{adj} = 0.29$, p-value = 0.01, Figure 2.6).

The degree of coupling between CO_2 and CH_4 also followed a clear spatial pattern. While CO_2 and CH_4 surface concentrations were strongly linked in the inflows ($R^2_{adj} = 0.54$, p-value = 0.006), they became only weakly correlated in the branches ($R^2_{adj} = 0.17$, p=0.005) and not correlated at all in the main basin ($R^2_{adj} = 0.01$, p-value = 0.11) (Figure S2.2).

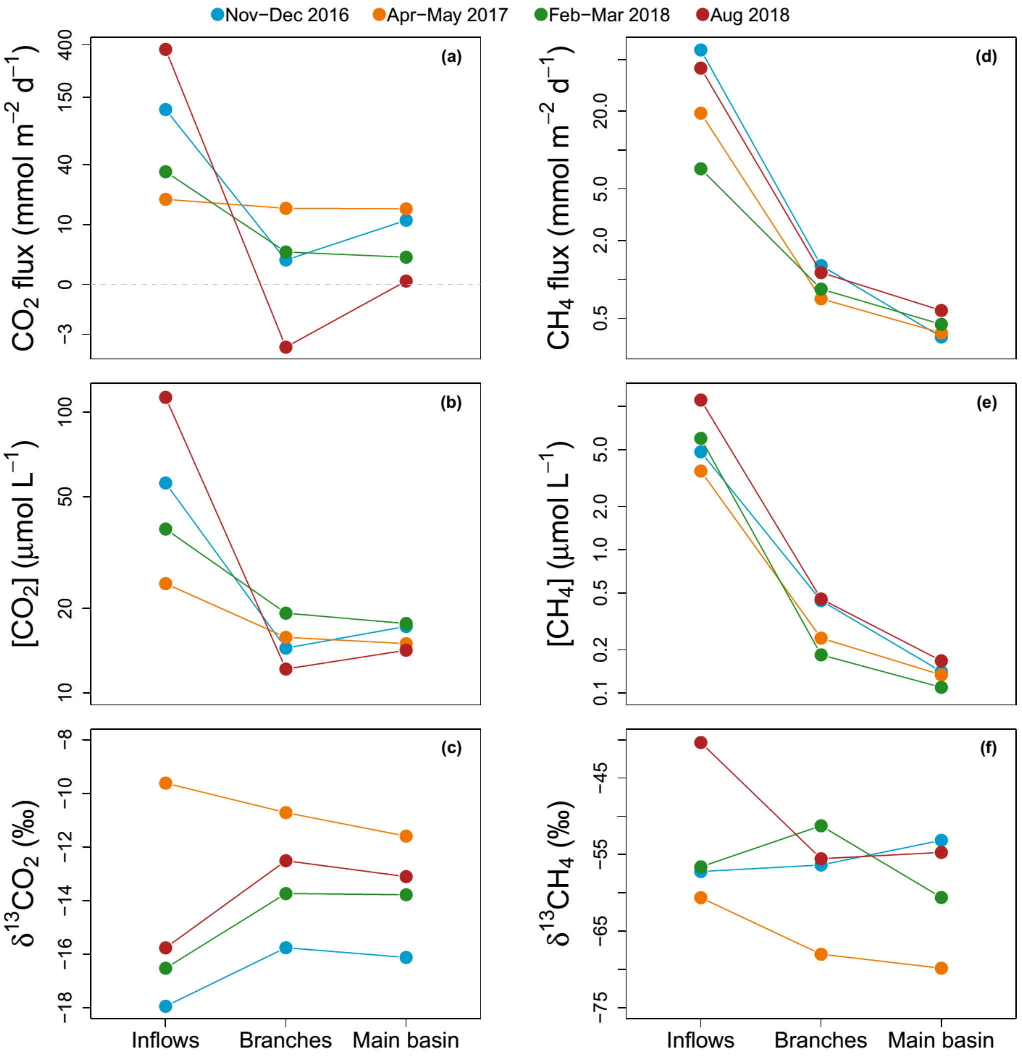

Figure 2.2: Average of spatially interpolated surface CO_2 and CH_4 fluxes, concentrations, and isotopic signatures along the hydrological continuum from the reservoir inflows to the main basin in all sampling campaigns (blue: Nov-Dec 2016, orange: Apr-May 2017, green: Feb-Mar 2018, red: Aug 2018).

2.4.3 Horizontal GHG flow

Horizontal inputs from the inflows to the surface layer of the branches were estimated to vary between 0.34 – 0.71 mol.s^{-1} for CO_2 and 0.02 – 0.25 mol.s^{-1} for CH_4. When expressed as rates over the branches surface area (to facilitate comparison with other components), this results in 2.7 – 5.7 and 0.16 – 1.97 mmol.m^{-2}.d^{-1} for CO_2 and CH_4 respectively (Table S2.2 and S2.3). These values are in the same order of magnitude as surface fluxes calculated in the branches (Figure 2.6 and Table S2.2 and S2.3). However, the effect of horizontal inputs faded spatially, with much lower inputs from the branches to the main reservoir basin, averaging 0.31 and 0.004 mmol.m^{-2}.d^{-1} for CO_2 and CH_4, respectively (Figure 2.6 and Table S2.2 and S2.3). For CH_4, this fits spatial and temporal surface flux measurements, being systematically higher in the branches, and maximal during the two sampling campaigns with the highest recorded horizontal inputs from the inflows (Table S2.3). In contrast, CO_2 surface flux was typically lower (sometimes negative) in the branches compared to the main basin, despite substantial riverine inputs to the branches (Table S2.2).

2.4.4 Vertical GHG fluxes

Vertical fluxes depend on the gas diffusivity and concentration gradient. Gas diffusivity is a function of the strength of stratification (N^2) and energy dissipation rate (ϵ). Measured values of N^2 and ϵ at the varied widely, from 5.9 x 10^{-5} to 2.3 x 10^{-3} s^{-2} and from 3.4 x10^{-9} to 1.6 x 10^{-8} m^2 s^{-3} respectively, yielding a median K_z value of 0.13 m^2.d^{-1} (range from 0.01 to 2.28 m^2.d^{-1}), but with no clear differences between the reservoir branches and main basin (Figure S2.3). Similarly, CO_2 and CH_4 concentration gradients varied substantially in both space and time (from -18.4 to 94.3 μmol L^{-1} m^{-1} for CO_2 and -0.19 to 0.4 μmol L^{-1} m^{-1} for CH_4). CO_2 concentration generally increased from the epilimnion to the metalimnion as a result of the respiratory CO_2 buildup in the deep layer. On rare occasions, an inverse gradient was observed, possibly due to autotrophic activity in the metalimnion. For CH_4, metalimnion to epilimnion concentration gradients were generally modest averaging 0.04 µmol L^{-1} m^{-1}, and even negative in one third of the profiles leading to the diffusion of epilimnetic CH_4 toward deeper layers instead of the reverse. The low to negative CH_4 vertical flux results from a highly active methanotrophic layer reducing CH_4 concentration in the metalimnion, as evidenced by the strong enrichment effect observed in $\delta^{13}CH_4$ profiles (Figure S2.4). The combination of vertical diffusivity and gas concentration gradients resulted in vertical fluxes averaging 3.4 (-1.8 to 20.5) mmol m^{-2} d^{-1} for CO_2, and 0.01 (-0.01 to 0.09) mmol m^{-2} d^{-1} for CH_4, with no significant differences between the reservoir branches and main basin (Figure S2.3).

2.4.5 GHG inputs from littoral sediments

Areal Gas fluxes from the sediments ranged from 1.2 to 4.0 and -0.29 to 1.10 mmol.m^{-2}.d^{-1} for CO_2 and CH_4, respectively (Figure S2.5). These fluxes are in the range of previously reported values in lakes and reservoirs (Adams, 2005 ; Algesten *et al.*, 2005 ; Gruca-Rokosz et Tomaszek, 2015 ; Huttunen *et al.*, 2006). Sediment GHG fluxes were not different in the branches versus the main basin for both CO_2 (mean of 2.2 vs 2.4 mmol.m^{-2}.d^{-1}) and CH_4 (mean of 0.17 vs 0.48 mmol.m^{-2}.d^{-1}) (Figure S2.5). Applying the measured averages to the area of epilimnetic sediments in each section yields estimates of sediment inputs to the epilimnion of 0.6 (± 0.03) and 0.5 (± 0.11) mmol.m^{-2}.d^{-1} for CO_2, and 0.04 (± 0.02) and 0.10 (± 0.06) mmol.m^{-2}.d^{-1} for CH_4 in the branches and main basin respectively (Figure 2.6 and Table S2.2 and S2.3). These inputs from littoral sediments likely represent an upper limit since they are based on deep pelagic sediment cores (littoral area were too compact for coring), where a higher organic matter accumulation and degradation is expected in the system (Blais et Kalff, 1995 ; Soued et Prairie, 2020). Even as upper estimates, the calculated rates of sediment GHG inputs remain a relatively modest fraction of the average emissions to the atmosphere for the branches and main basin both for CO_2 (13 % and 7 %, respectively) and CH_4 (4 % and 23 %, respectively) (Tables S2 and S3).

2.4.6 Metabolism

CO_2 metabolism. Estimates of GPP and ER based on diel O_2 monitoring collectively ranged from 3.6 to 34.5 µmol.L^{-1}.d^{-1} and from 5.8 to 29.5 µmol.L^{-1}.d^{-1}, respectively (Figure 2.4), which is well in range with reported rates for oligotrophic systems (Bogard et del Giorgio, 2016 ; Hanson *et al.*, 2003 ; Solomon *et al.*, 2013). As expected, rates of GPP and ER were correlated ($R^2_{adj} = 0.23$, p-value < 0.001, Figure 2.4), with photosynthetic production stimulating respiration of the produced organic matter. In most cases, GPP exceeded ER, and this was most pronounced in the branches and near aquaculture sites (Figure 2.4), where higher nutrients (TP and TN) and Chla concentrations were measured (Table 2.1).

In the reservoir branches, results from the diel O_2 monitoring method suggested systematic net CO_2 uptake ranging from -19.2 to -1.4 µmol.L^{-1}.d^{-1}, whereas results from two incubations were slightly above that range (-0.5 to 3.3 µmol.L^{-1}.d^{-1}) (Figure 2.4). In the main basin, incubation results ranged from -8.8 to 7.2 µmol L^{-1} d^{-1}, while the diel O_2 technique captured a wider variability in net CO_2 metabolic rates from -19.2 to 6.1 µmol L^{-1} d^{-1}, with an estimated CO_2 uptake in 39 out of 54 cases (Figure 4.2).

Areal net CO_2 metabolic rates, as the average of the two methods, yielded an ecosystem-scale estimate of -23.2 and -11.8 mmol.m^{-2}.d^{-1} in the reservoir branches and main basin respectively (Table S2.2).

CH_4 metabolism. Net metabolic CH_4 rates (obtained from incubations) ranged from -0.026 to 0.078 µmol.L^{-1}.d^{-1}, indicating that the CH_4 balance in the epilimnion of Batang Ai varied from net oxidation to net production (Table S2.3). CH_4 metabolic rates measured in Batang Ai are within the range of values observed in other systems for oxidation (Guérin et Abril, 2007 ; Thottathil *et al.*, 2019) and production (Bogard *et al.*, 2014 ; Donis *et al.*, 2017). No significant difference were detected between net metabolic CH_4 rates in the branches versus the main basin due to the high variability

and limited data points. Temporal patterns could not be assessed since the majority of the incubations were performed during the same sampling campaign (Nov-Dec 2016).

2.4.7 Ecosystem scale GHG budgets

Collectively, the fluxes estimated above can be summed to explore whether the epilimnetic GHG budgets can be closed within the uncertainty limits of each individual component. Concurrently, it can be used to identify the main processes sustaining GHG emissions in the different sections of the reservoir surface. Figure 2.3 depicts such reconstruction of the epilimnetic GHG budget of Batang Ai. While each process varied in time, their relative importance in driving surface fluxes was generally similar from one sampling campaign to another (Table S2.2 and S2.3).

CO_2 budget. For CO_2, epilimnetic sediment inputs had the smallest contribution, being typically an order of magnitude lower than measured surface fluxes in both sections of the reservoir (Table S2.2). Vertical CO_2 inputs from lower depths on the other hand contributed substantially to surface fluxes in both the branches and the main basin (mean of 0.7 and 4.5 $mmol.m^{-2}.d^{-1}$ respectively, Table S2.2), indicating that hypolimnetic processes impact surface emissions despite the permanent stratification. Horizontal inputs of CO_2 were in the same range as vertical inputs (mean of 4.3 $mmol.m^{-2}.d^{-1}$) in the branches, however, they decreased by an order of magnitude when reaching the main basin (mean of 0.3 $mmol.m^{-2}.d^{-1}$). Thus, direct CO_2 inputs from the inflows notably increase surface flux rates in the reservoir branches but only minimally in the main basin. Net CO_2 metabolism was surprisingly variable (switching from negative to positive NEP on a daily time scale), thus making it difficult to derive a sufficiently precise ecosystem-scale estimate to close the epilimnetic budget (Figure 2.3), despite high sampling resolution (n = 66 daily metabolic rates). Including the metabolism substantially shifts the mean of the CO_2 epilimnetic budget (sum of sources and sinks) to a negative value and drastically increases its uncertainty (Figure 2.3 and Table S2.2), reflecting a potentially important but poorly resolved role of metabolism

in the budget because of its variability. However, given that metabolism acts more likely as a CO_2 sink on average, our best assessment suggests that, vertical transport from deeper layers is the main source sustaining surface CO_2 out-flux in the main basin of Batang Ai.

CH_4 budget. In contrast with CO_2, vertical transport was the smallest source of CH_4 to the epilimnion, contributing to less than 2 % to surface fluxes in both reservoir sections (Table S2.3). In the branches, sediment inputs and net CH_4 metabolic rates were both relatively low (mean of 0.04 ± 0.02 and 0.04 ± 0.05 $mmol.m^{-2}.d^{-1}$) and had little impact on the budget, corresponding each to 4 % of surface fluxes in that section (Table S2.3). On the other hand, horizontal inputs was the dominant and most variable source sustaining CH_4 emissions in the branches, where the epilimnetic mass balance closed almost perfectly (Figure 2.6 and Table S2.3). Despite being the main CH_4 source in the branches, horizontal transport was a negligible component in the main basin (< 1 % of the flux, Table S2.3). Instead, sediment inputs played a larger role in that section, with a mean of 0.10 (± 0.06) $mmol.m^{-2}.d^{-1}$, fueling 23 % of surface emissions in the main basin. As with CO_2, the most variable CH_4 component of the mass balance in the main basin was the net metabolism within the epilimnion (mean of -0.16 ± 0.19 $mmol.m^{-2}.d^{-1}$). Considering all sources, the CH_4 budget indicates a deficit of 0.34 $mmol.m^{-2}.d^{-1}$ in order to explain measured surface emissions in the main basin (Figure 2.3 and Table S2.3).

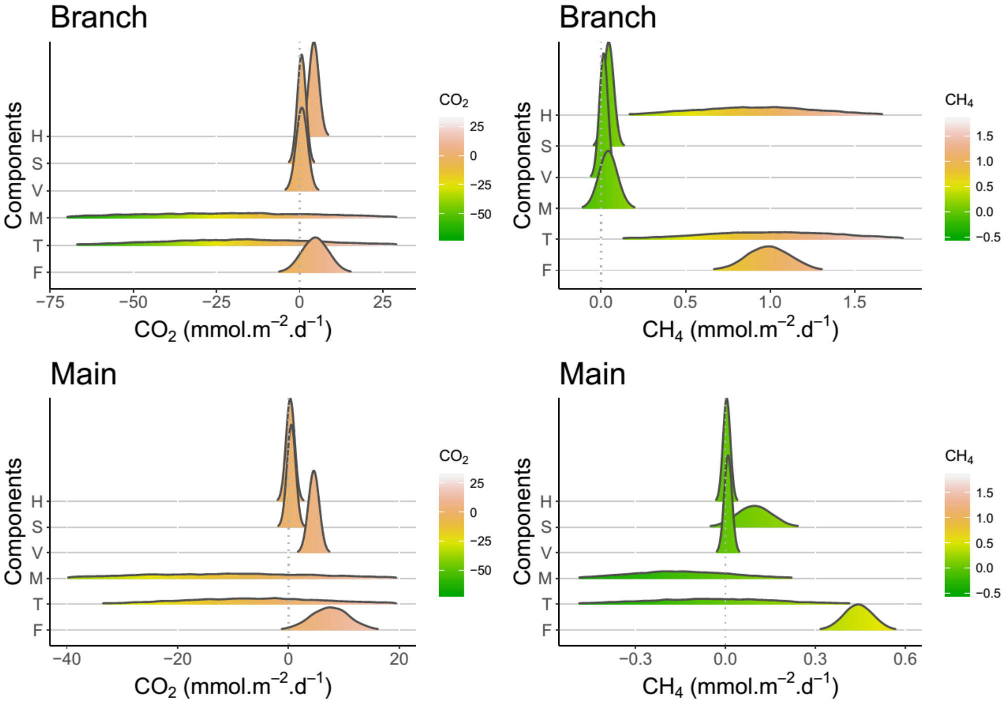

Figure 2.3: Density distributions of the different components of CO_2 and CH_4 surface budget in the reservoir branches and main basin (H = horizontal flow inputs, S = sediment inputs, V = vertical inputs, M = net metabolism, T = sum of all estimated sources and processes in the surface layer, and F = measured surface fluxes). Density curves are based on simulated normal distributions using the mean and standard error of each component.

2.5 Discussion

Our results have highlighted both the importance and the challenges associated with quantifying simultaneously all the components of the epilimnetic CO_2 and CH_4 budgets, particularly in a hydrologically complex reservoir system. While mass fluxes (hydrological, sedimentary and air-water fluxes) are relatively easy to constrain, internal C processing, namely the net metabolic balances between production and consumption of CO_2 and CH_4 are highly dynamic in both time and space, leading to significant uncertainties when extrapolated to the scale of whole ecosystem compartments (in our case, the epilimnion). In many studies, some components are only inferred by difference. While convenient from a mass-balance perspective, we argue that assessing all components together is necessary to clearly identify knowledge gaps as well as sources of uncertainty.

2.5.1 Spatial dynamics of CO_2 and CH_4

The decrease in gas concentration and air-water fluxes along the hydrological continuum observed across sampling campaigns and for both CH_4 and CO_2 reflects a robust spatial structure of the gases. Concurrently, estimates of the horizontal GHG inputs shows a clear and consistent spatial pattern, being high in the branches but negligible in the main basin. A temporal effect of riverine inputs was also observed as the two sampling campaigns with the highest horizontal CH_4 inputs coincided with the highest CH_4 emissions in the branches (Table S2.3). All these results concord with the progressively reduced influence of direct GHG catchment inputs and greater preponderance of internal processes along the hydrological flow (Hotchkiss *et al.*, 2015).

For CO_2, the sharpest change in surface metrics (concentration, flux, and isotopic signature) was observed between the inflows and the reservoir branches (Figure 2.2). Despite large riverine inputs (Table S2.2), the branches exhibited low CO_2 concentration and fluxes, as well as an increase in $\delta^{13}CO_2$ matching with high GPP values (Figure 2.2 and 2.4). This may reflect increased light availability for phytoplankton when transitioning from the turbid inflows to the reservoir branches (higher Secchi depth, Table 2.1), a pattern previously reported in other reservoirs (Kimmel et Groeger, 1984 ; Pacheco *et al.*, 2015 ; Thornton *et al.*, 1990). While the branch areas are often associated with high CO_2 out-flux due to riverine inputs (Beaulieu *et al.*, 2016 ; Paranaíba *et al.*, 2018 ; Pasche *et al.*, 2019 ; Roland *et al.*, 2010 ; Rudorff *et al.*, 2011), they are occasionally observed to have low air-water flux due to simultaneous nutrient inputs (Paranaíba *et al.*, 2018 ; Wilkinson *et al.*, 2016). In Batang Ai, inflows have a high nutrients (TP and TN) to DOC ratio compared to the reservoir branches (Table 2.1), providing higher inputs of nutrients relative to organic matter, and thus likely stimulating primary production more than respiration. This hypothesis is consistent with a higher GPP: ER ratio and mean Chla concentrations measured in the branches compared to the main basin (Figure 2.4 and Table 2.1). The fact that CO_2 concentration within the reservoir (branches and main basin) was negatively correlated to temperature (Figure S2.1), likely due to its effect on GPP (Bogard *et al.*, 2020), highlights the important role of primary production in modulating CO_2 dynamics throughout the reservoir, and particularly in the branches.

The correlation between surface CH_4 surface and TN in the reservoir suggests that primary production may also affect CH_4 dynamics. Nutrient content was shown in previous studies to enhance CH_4 production in the sediments (Beaulieu *et al.*, 2019 ; Gebert *et al.*, 2006 ; Isidorova *et al.*, 2019) and in the oxic water column (Bogard *et al.*, 2014), through its link with algal production and decomposition. However, CH_4 concentration and flux variability were strongly driven by a spatial / hydrological structure, gradually decreasing from the inflows to the main basin. This likely reflects the combined effect of terrestrial inputs and a decreasing contact of water with sediments along the water channel. Surface $\delta^{13}CH_4$ signatures varied substantially but without a consistent spatial pattern (Figure 2.2), indicating that the surface CH_4 pool is shaped by multiple sources / processes varying through space and time.

The changing relative contribution of sources and processes shaping surface CO_2 and CH_4 concentrations varies with the system hydro-morphology, from the inflows to the main reservoir basin, and lead to a progressive decoupling between the two gases along the continuum (Figure S2.2). The observed CO_2 and CH_4 coupling in the inflows and branches is associated to a common catchment source, as previously reported in other systems including soil-water (Lupon *et al.*, 2019), streams (Rasilo *et al.*, 2017), and lake and reservoir inflow areas (Loken *et al.*, 2019 ; Natchimuthu *et al.*, 2017 ; Paranaíba *et al.*, 2018). Indeed, horizontal inputs are the main source of both CO_2 and CH_4 in the upstream reaches of Batang Ai, accounting on average for 91 and 92 % of their respective surface out-flux in the branch section (Figure 2.3 and Tables S2.2 and S2.3). However, when reaching the main basin, driving sources diverge between the two gases, with vertical inputs from the bottom layer supporting on average 60 % of CO_2 compared to 2 % of CH_4 fluxes, while sediment inputs sustained 7 versus 23 % of CO_2 and CH_4 fluxes respectively in that section. This decoupling partly results from the two gases having distinct metabolic pathways: mainly aerobic for CO_2 and anaerobic for CH_4, leading to their sources and sinks being spatially disconnected in the main basin. Consequently, sediments being a mostly anaerobic environment are a more important source of CH_4 relative to CO_2, while the metalimnetic layer being oxic-hypoxic acts as a sink of CH_4 and source of CO_2 via aerobic CH_4 oxidation (Figure S2.4). Overall, the spatial patterns reported here highlight the hydrodynamic zonation common in reservoirs and its diverging effect on CO_2 versus CH_4 cycling.

2.5.2 CO_2 metabolism

Our observation that GPP often exceeded ER (Figure 2.4) was not unexpected given the low DOC concentration (< 1 $mg.L^{-1}$) throughout the study system. Previous work has reported that DOC > 4 $mg.L^{-1}$ is required to sustain persistent net heterotrophy and CO_2 evasion (Hanson *et al.*, 2003 ; Prairie *et al.*, 2002). Throughout the reservoir, we found high day-to-day variability in both ER and GPP, but with no apparent link to weather data, namely light and rain (unpublished). The absence of such a link at a daily time scale has been previously reported (Coloso *et al.*, 2011), while other studies associated daily variations in metabolism with changes in water inflows carrying nutrients (Pacheco *et al.*, 2015 ; Staehr et Sand-Jensen, 2007), or thermocline stability regulating hypolimnetic water incursions to the epilimnion. Such variations in thermocline depth are thought to be more common in warm tropical systems (Lewis, 2010), and were observed across sampling campaigns in Batang Ai, especially in the branches where the depth of the mixed layer varied considerably (SD = 2.3 m, Table 2.1). Hence, hydrological and physical factors may regulate spatial and daily patterns of GPP and ER rates in Batang Ai through their influence on nutrient dynamics.

The accuracy of rates derived from diel O_2 monitoring partly depends on the respiratory and photosynthetic quotients (RQ and PQ) assumed for the conversion of metabolic rates from O_2 to CO_2. A quotient differing from the assumed 1:1 ratio can lead to an apparent under or over-estimation of net CO_2 production. The fact that net CO_2 metabolic rates were on average higher in incubations, based on direct CO_2 measurements, compared to diel O_2 monitoring (Figure 2.4 and Table S2.2), hints towards a deviation of the metabolic quotients form unity in Batang Ai. Additionally, surface O_2 versus CO_2 concentrations shows that the departure of these gases from saturation varies widely around the expected 1:-1 line, with many surface samples oversaturated in both O_2 and CO_2, especially in the branches (Figure 2.5). This indicates an excess O_2 and / or CO_2 that can be due to a PQ and / or a RQ higher than 1, or to external CO_2 inputs to the epilimnion (Vachon *et al.*, 2020), for instance from the inflows or the bottom layer. While CO_2 horizontal inputs in the branches and vertical inputs in the main basin (Table S2.2) certainly play a role in surface O_2 / CO_2 decoupling, this pattern is also likely shaped by metabolic quotients. Metabolic quotients have been shown to be widely variable, depending on the type and magnitude of photochemical and biological reactions at play (Berggren *et al.*, 2012 ; Lefèvre et Merlivat, 2012 ; Vachon *et al.*, 2020 ; Williams et Robertson, 1991). The lack of direct measure of metabolic quotients in Batang Ai adds uncertainty to the net CO_2 metabolism estimates based on O_2 data. The observed decoupling of O_2 and CO_2 metabolism in Batang Ai highlights the need for a deeper understanding of the biochemical reactions occurring in the epilimnion, and their effect on metabolic quotients.

Overall, our results from Batang Ai reservoir point to water column metabolism as both a key process in the CO_2 epilimnetic budget and a challenging one to estimate at an ecosystem scale (Figure 2.3). Improving this requires a better mechanistic knowledge of the physical and biochemical processes at play and how they interact to shape NEP.

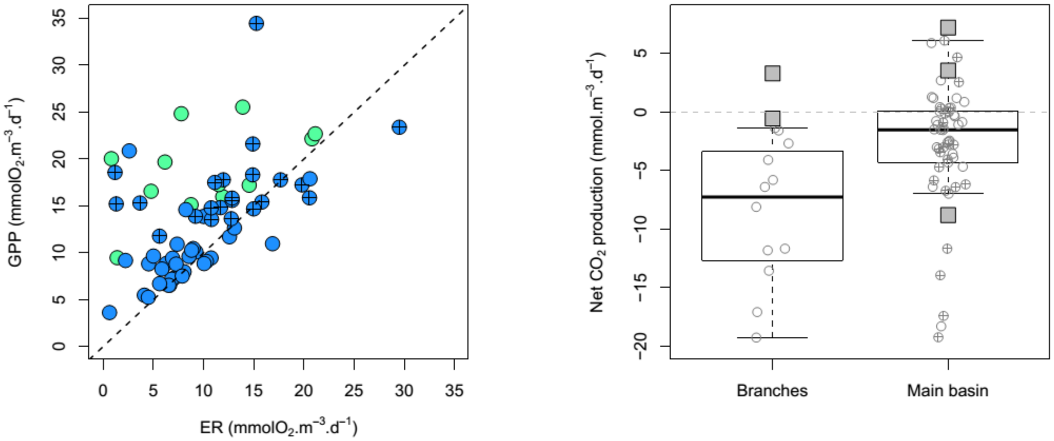

Figure 2.4: Epilimnetic daily GPP versus ER rates (left panel) derived from free water O_2 sensors deployed in the reservoir branches (green points) and main basin (blue points, cross symbol indicates proximity to aquaculture sites), with the 1:1 line (dotted). Boxplots of the corresponding rates of CO_2 NEP (right panel) in the branches and main basin, with boxes bounds, whiskers, solid line, and open circles representing the 25th and 75th percentiles, the 10th and 90th percentiles, the median, and single data points. Grey squares are values from incubations.

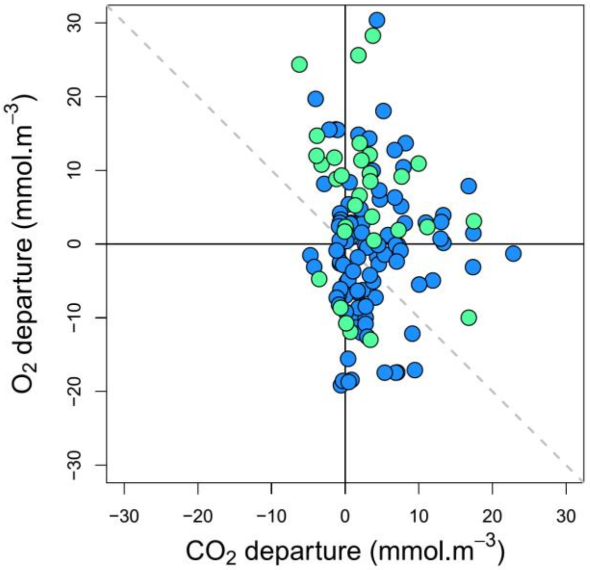

Figure 2.5: Surface O_2 versus CO_2 departure from saturation for all sampled surface sites in the reservoir main basin (blue points) and branches (green points) across all sampling campaigns.

2.5.3 CH_4 metabolism

Incubation results exhibited a wide range of net CH_4 metabolism: from net oxidation to net production, with rates within the range of values observed in other systems for both oxidation (Guérin et Abril, 2007 ; Thottathil *et al.*, 2019) and production (Bogard *et al.*, 2014 ; Donis *et al.*, 2017). CH_4 oxidation is known to be highly dependent on CH_4 availability and is optimal in low oxygen and low light conditions (Borrel *et al.*, 2011 ; Thottathil *et al.*, 2018, 2019), whereas CH_4 production in the oxic water is still poorly understood but have been frequently linked to phytoplankton growth (Berg *et al.*, 2014 ; Bogard *et al.*, 2014 ; Lenhart *et al.*, 2015 ; Wang *et al.*, 2017). A large variability in results exists among the studies that have assessed the net balance of CH_4 metabolism in the water column, with some studies reporting pelagic CH_4 production as a largely dominant process (Donis *et al.*, 2017) while others find no trace of it (Bastviken *et al.*, 2008). Based on spatial patterns of surface CH_4 concentration and isotopic signature with distance to shore, DelSontro et al. (2018b) showed that, in 30 % of their studied temperate lakes, CH_4 oxidation was dominant versus 70 % dominated by net pelagic production. In Batang Ai, surface $\delta^{13}CH_4$ values were highly variable (-82.5 to -47.7 ‰) but mostly uncorrelated with distance to shore, except a positive correlation indicative of oxidation in the Nov-Dec 2016 ($R^2_{adj} = 0.29$, p-value = 0.01) coinciding with a strong inverse pattern for CH_4 concentration ($R^2_{adj} = 0.54$, p-value < 0.001, Figure 2.6). This suggests a temporal shift in processes driving surface CH_4 patterns. Also, some measured surface $\delta^{13}CH_4$ values were lower than the mean $\delta^{13}CH_4$ form the sediments (-66.0 ‰, unpublished data), suggesting another highly depleted source of pelagic CH_4 in the system. This is in line with water incubation results often showing positive net CH_4 production (Table S2.3). When reported as mean areal rates, CH_4 metabolism ranged from net consumption to net production of CH_4 (-0.29 to 0.94 $mmol.m^{-2}.d^{-1}$), which reflects its potential in having a high impact, either positive or negative, on the epilimnetic CH_4 budget at the reservoir scale (Figure 2.3 and Table S2.3). Results in Batang Ai show that the net balance of CH_4 metabolic processes varies widely even within a single system. However, the factors regulating this balance remain largely unknown. Investigating such factors constitute a key step in resolving CH_4 budgets in lakes and reservoirs.

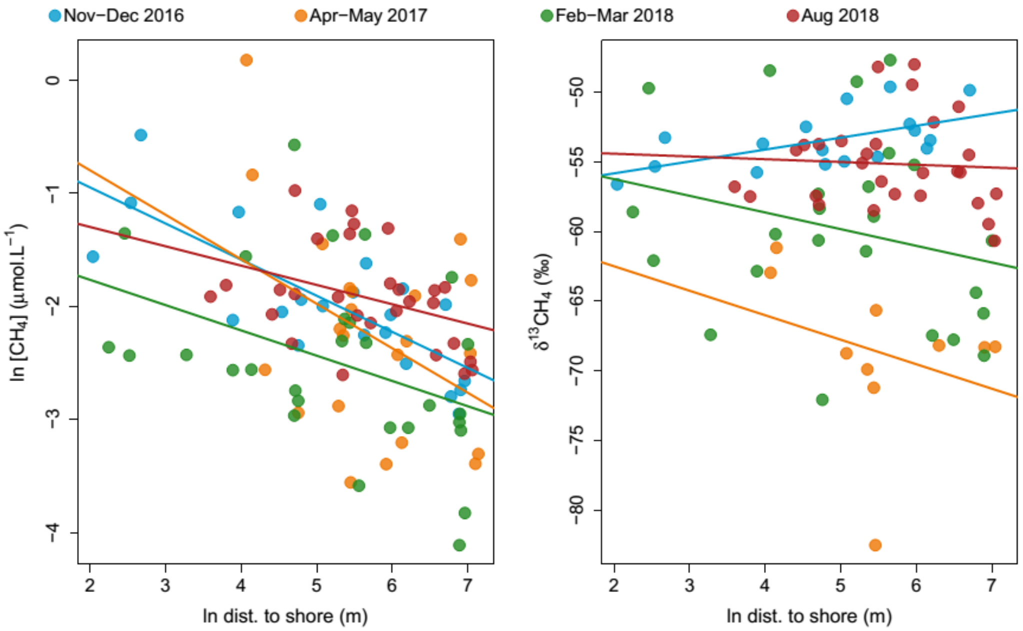

Figure 2.6: Regression of CH_4 concentration (left panel) and isotopic signature (right panel) as a function of distance to shore in each sampling campaign in the main reservoir basin. For CH_4 concentration, regressions lines have the following statistics in order of sampling: p-values: < 0.001, 0.06, 0.03, 0.05, and R^2_{adj}: 0.54, 0.13, 0.11. For $\delta^{13}CH_4$, all regressions had p-values > 0.2 except for the Nov-Dec 2016 campaign with p-value = 0.01 and $R^2_{adj} = 0.29$.

2.5.4 Epilimnetic GHG budgets

For CO_2, measured surface fluxes in both reservoir sections fall in the range of possible values estimated by the sum of epilimnetic processes and their uncertainties (Figure 2.6 and Table S2.2). However, the averages of those two terms differ substantially, due to negative values of metabolism shifting the mean of the mass balance towards net CO_2 consumption whereas, on average, surface out-flux was measured from the reservoir. This discrepancy indicates either a missing source of CO_2 in the budget or the underestimation of one of the processes. While lateral groundwater input is a potential source not explicitly considered, it is probably modest given the small ratio of littoral area to epilimnion volume, and is unlikely to account for the large CO_2 deficit in the budget. On the other hand, underestimation of the CO_2 metabolic balance is much more likely, given its large variability and uncertainty around its mean value. Additionally, a systematic underestimation of the CO_2 metabolic rates derived from the diel O_2 method is very possible in Batang Ai given the likely deviation of metabolic quotients around the 1:1 line. As an example, when setting the photosynthetic quotient to 1.2 instead of 1, which remains well within the literature range (Lefèvre et Merlivat, 2012 ; Williams et Robertson, 1991), the average epilimnetic CO_2 mass balance would increase from -17.7 to 4.3 mmol.m^{-2}.d^{-1} in the branches and from -6.5 to 6.2 mmol.m^{-2}.d^{-1} in the main basin, closely matching measured surface fluxes of 4.7 and 7.5 mmol.m^{-2}.d^{-1} in the respective sections. Thus, constraining the metabolic component, especially the O_2: CO_2 quotients, is key for closing the CO_2 epilimnetic budget.

In the case of CH_4, the epilimnetic mass balance in the branches is surprisingly close to the observed surface flux, largely fueled by horizontal inputs. Hence, CH_4 emissions from the branches reflect catchment CH_4 loads rather than internal processes. However, in the main basin, these inputs become negligible and the estimated budget does not match measured emissions, indicating a deficit of 0.49 mmolCH_4.m^{-2}.d^{-1}. This amount cannot be explained by a potential underestimation of horizontal or vertical inputs since they are two orders of magnitude lower. Similarly, sediment inputs would need to be six time higher than estimated to fulfill the budget deficit, which is unlikely given their much lower range of uncertainty. Thus, the most plausible source to close the mass balance in the main basin would be water column CH_4 production. Although the estimated CH_4 metabolism indicates an average net consumption rather than a net production (-0.16 mmol.m^{-2}.d^{-1}), this mean value is based on only 3 data points and has a high uncertainty associated to it (SE = 0.19 mmol.m^{-2}.d^{-1}, Table S2.3). Closing the mass balance would require a net volumetric CH_4 production of about 0.03 µmol.L^{-1}.d^{-1} in the water column of the main basin. This value seems plausible since an equal production rate was measured in one of the incubations, and it is at the low end of the range reported in other systems (Bogard *et al.*, 2014 ; DelSontro *et al.*, 2018b ; Donis *et al.*, 2017). The combination of our results point to water column metabolism as the main source of CH_4 in the main basin of Batang Ai, and could be sustaining up to 75 % of surface emissions in that section. However, this process seems highly dynamic and requires more intensive research into its controls at spatial and temporal scales, commensurate with CH_4 emissions.

2.6 Conclusion

The estimated epilimnetic CO_2 and CH_4 budgets in Batang Ai has helped define the role of different processes in shaping the reservoir surface GHG fluxes to the atmosphere. Results showed that horizontal riverine inputs are important sources of GHG in the reservoir branches (especially for CH_4). This creates a coupling between CO_2 and CH_4 close to the river deltas, which gradually fades along the water flow, until the surface concentrations of the two gases become completely uncoupled in the main basin being driven by different sources. For instance, vertical inputs from the bottom layer contributed significantly to surface CO_2 saturation, while being negligible in the case of CH_4 due to metalimnetic oxidation. Inversely, sediment inputs played a notably greater role in sustaining epilimnetic oversaturation of CH_4 compared to CO_2 in the main basin. Nonetheless, the epilimnetic budgets of both gases are highly sensitive to their respective water column metabolism. This result is likely representative of large systems with a high volume of water versus sediments, which is common for hydroelectric reservoirs. The metabolic balances of CO_2 and CH_4 were also extremely variable in space and time, switching from a net production to a net consumption of the gases, and leading to highly uncertain ecosystem-scale estimates, which emphasizes the key but unconstrained role of metabolism in the overall GHG budgets. Factors driving these metabolic changes are not well constrained based on current knowledge, highlighting the need for further research on the subject. Overall, this study gives an integrative portrait of the relative contribution of different sources to surface CO_2 and CH_4 fluxes in a permanently stratified reservoir including its transition zones (branches). Conclusions and insights derived from this work likely reflect C dynamics in other similar systems, and offer useful tools to guide future research.

2.7 Acknowledgments

This work was funded by Sarawak Energy Berhad and the Natural Science and Engineering Research Council of Canada (Discovery grant to Y.T.P. and BES-D scholarship to C.S.). We are grateful to Karen Lee Suan Ping and Jenny Choo Cheng Yi for their logistic support and participation in sampling campaigns. We also thank Jessica Fong Fung Yee, Amar Ma'aruf Bin Ismawi, Gerald Tawie Anak Thomas, Hilton Bin John, Paula Reis, Sara Mercier-Blais and Karelle Desrosiers for their help on the field, and Katherine Velghe and Marilyne Robidoux for their assistance during laboratory analyses.

2.8 Supplementary information

Table S2.1: Non-parametric Kendall correlation (cor) and their p-value between reservoir surface CO_2 and CH_4 concentrations with physical and chemical variables.

	$[CO_2]$		$[CH_4]$		
Variables	cor	p-value	cor	p-value	n
Water temperature	-0.36	< 0.001	0.07	0.223	131
% O_2	-0.01	0.933	0.15	0.013	130
Chla	0.12	0.056	0.18	0.005	110
DOC	0.01	0.939	0.17	0.008	113
TP	0.14	0.031	0.13	0.049	112
TN	0.1	0.112	0.27	< 0.001	113

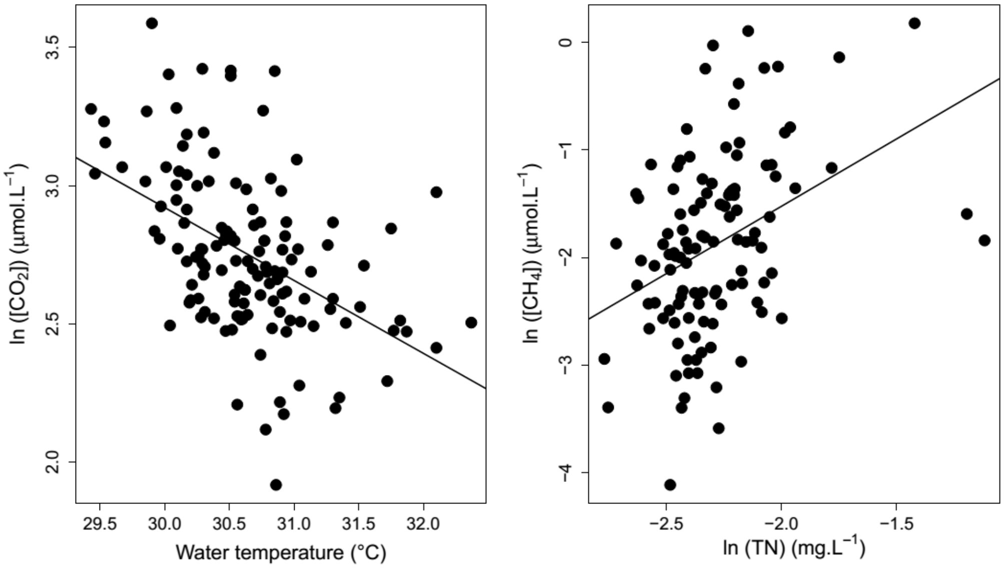

Figure S2.1: Linear regressions of natural logarithm of surface CO_2 and CH_4 concentrations with water temperature (left panel, p-value < 0.001, $R^2_{adj} = 0.22$) and TN (right panel, p-value < 0.001, $R^2_{adj} = 0.14$) respectively in the reservoir (branches and main basin).

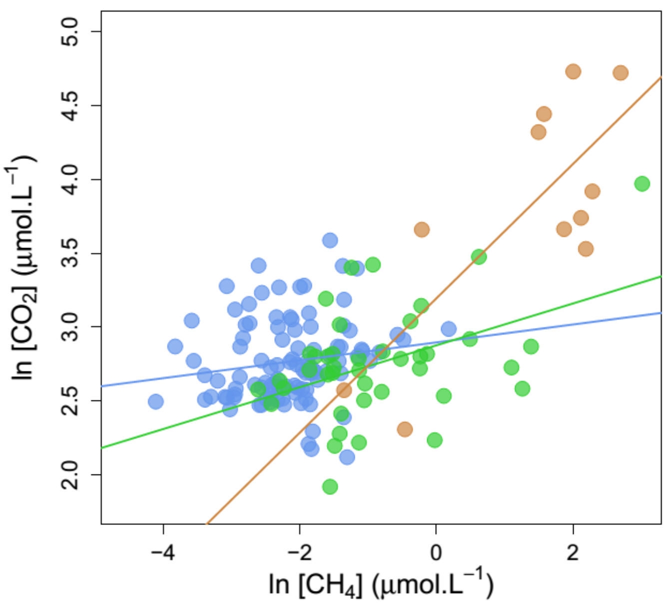

Figure S2.2: Linear regressions of natural logarithm of surface concentrations of CO_2 versus CH_4 in the reservoir inflows (brown, p-value = 0.006 and $R^2_{adj} = 0.54$), branches (green, p-value = 0.005 and $R^2_{adj} = .0.17$), and main basin (blue, p-value = 0.11 and $R^2_{adj} = 0.01$).

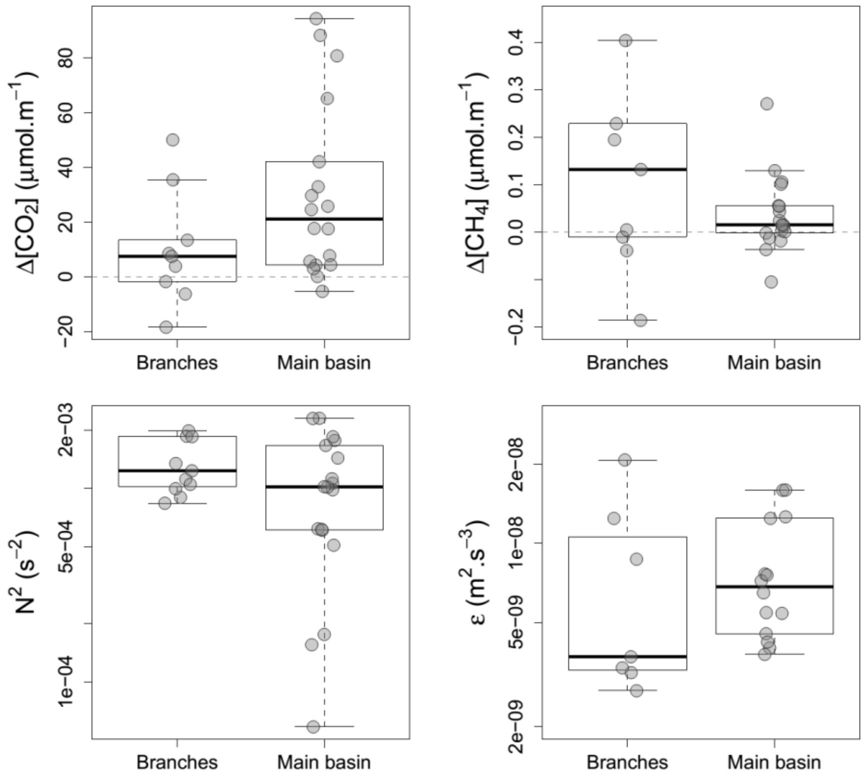

Figure S2.3: Boxplots of the buoyancy frequency (N^2, bottom left panel), dissipation rate (ϵ, bottom right panel), and CH_4 and CO_2 concentration gradients at the epilimnion-metalimnion interface (top panels) at epilimnion-metalimnion interface in the reservoir branches and main basin. Boxes bounds, whiskers, solid lines, and open circles represent the 25th and 75th percentiles, the 10th and 90th percentiles, the median, and single data points respectively.

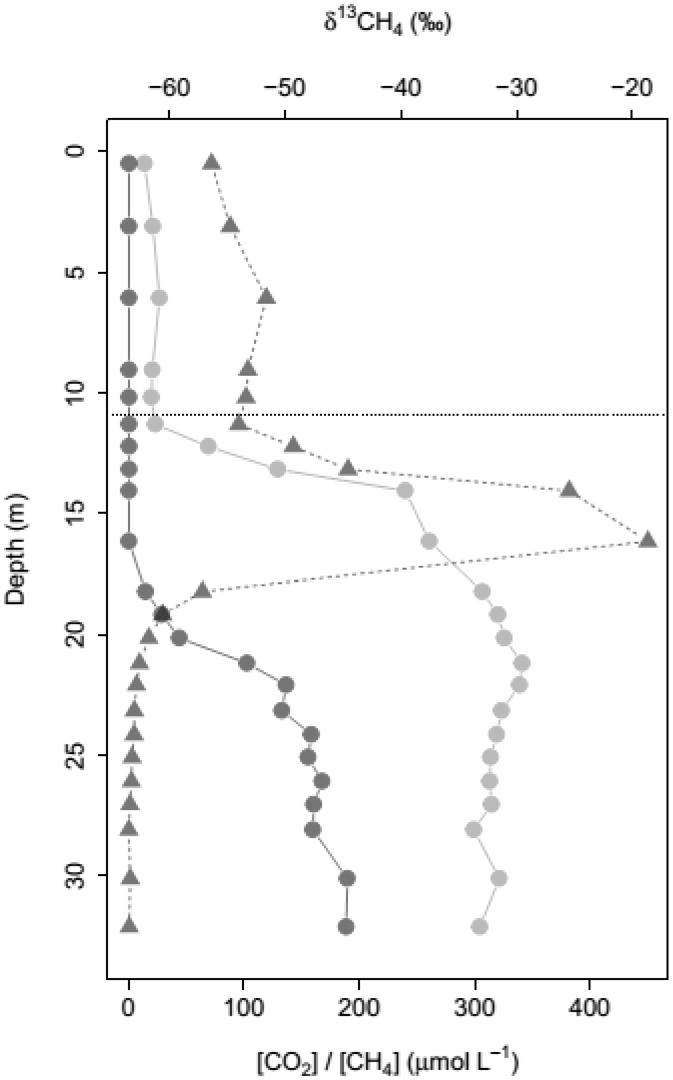

Figure S2.4: Example of a vertical profile (main reservoir, Aug 2018) of CO_2 (light gray points) and CH_4 (dark gray points) concentrations, as well as $\delta^{13}CH_4$ (dark grey triangles) as a function of depth. The dotted line represents the top of the metalimnion.

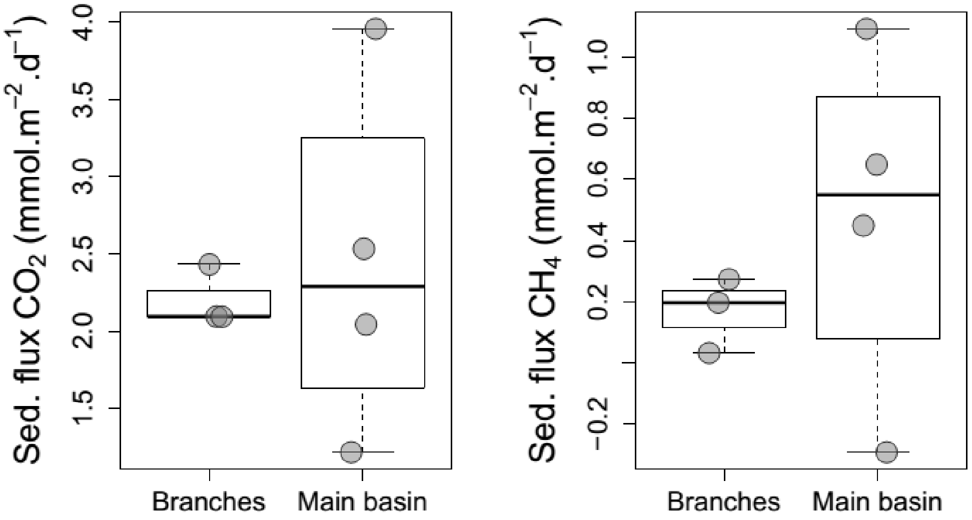

Figure S2.5: Boxplot of sediment CO_2 and CH_4 flux rates (per sediment area) across sampled sites in the reservoir branches and main basin. Boxes bounds, whiskers, solid lines, and open circles represent the 25th and 75th percentiles, the 10th and 90th percentiles, the median, and single data points respectively.

Table S2.2: Estimated averages (± SE) of rates of CO_2 inputs to the epilimnion from horizontal flow (H), sediments (S), vertical transport (V), and internal metabolism (M_inc and M_mod when derived from incubations and inverse O_2 modeling respectively), their sum (T, considering an average of M_inc and M_mdod) and surface flux to the atmosphere (F) in the branches and main basin for each sampling campaign and their mean. Units are mmol.m^{-2}.d^{-1} of water surface area. *Represents missing value, assumed to be equal to the mean of other campaigns.

		H	S	V	M_inc	M_mod	T	F
Branches	Nov-Dec 2016	5.7 (± 2.6)	_0.6 (± 0)_*	-1.8 (± NA)	1.4 (± 1.9)	-63.2 (± NA)	-26.5 (± 36.1)	2.8
	Apr-May 2017	2.7 (± 0.2)	_0.6 (± 0)_*	3.6 (± 2.3)	_1.4 (± 1.9)_*	-32.4 (± 20)	-8.6 (± 19.4)	15.2
	Feb-Mar 2018	3.2 (± 1.1)	_0.6 (± 0)_*	0.9 (± 0.5)	_1.4 (± 1.9)_*	_-47.8 (± 20)_*	-18.6 (± 26.2)	4.1
	Aug 2018	5.5 (± 3.3)	_0.6 (± 0)_*	0.1 (± 0.5)	_1.4 (± 1.9)_*	_-47.8 (± 20)_*	-17.1 (± 28.4)	-3.4
	Mean	4.3 (± 0.8)	0.6 (± 0)	0.7 (± 1.1)	1.4 (± 1.9)	-47.8 (± 15.4)	-17.7 (± 26.5)	4.7 (± 3.9)
Main basin	Nov-Dec 2016	0.2 (± NA)	_0.5 (± 0.1)_*	6 (± 2.2)	-2.6 (± 6.2)	-21.4 (± 5.6)	-5.3 (± 11.7)	11.3
	Apr-May 2017	0.4 (± NA)	_0.5 (± 0.1)_*	3.1 (± 1.3)	7.2 (± NA)	-49 (± 37.3)	-16.9 (± 29.5)	15.1
	Feb-Mar 2018	0.5 (± NA)	_0.5 (± 0.1)_*	4.7 (± 1)	_2.3 (± 6.2)_*	-17 (± 4.5)	-1.6 (± 10.8)	3.3
	Aug 2018	0.1 (± NA)	_0.5 (± 0.1)_*	4.3 (± 3.3)	_2.3 (± 6.2)_*	-16.2 (± 20.9)	-2 (± 12.6)	0.3
	Mean	0.3 (± 0.1)	0.5 (± 0.1)	4.5 (± 0.6)	2.3 (± 4.9)	-25.9 (± 7.8)	-6.5 (± 14.9)	7.5 (± 3.4)

Table S2.3: Estimated averages (± SE) of rates of CH_4 inputs to the epilimnion from horizontal flow (H), sediments (S), vertical transport (V), and internal metabolism (M_inc), their sum (T) and surface flux to the atmosphere (F) in the branches and main basin for each sampling campaign and their mean. Units are mmol.m^{-2}.d^{-1} of water surface area. *Represents missing value, assumed to be equal to the mean of other campaigns.

		H	S	V	M_inc	T	F
Branches	Nov-Dec 2016	0.94 (± 0.67)	*0.04 (± 0.02)**	-0.001 (± NA)	0.04 (± 0.05)	1.03 (± 0.74)	1.28
	Apr-May 2017	0.58 (± 0.08)	*0.04 (± 0.02)**	0.001 (± 0.008)	*0.04 (± 0.05)**	0.67 (± 0.16)	0.71
	Feb-Mar 2018	0.16 (± 0.08)	*0.04 (± 0.02)**	0.025 (± 0.016)	*0.04 (± 0.05)**	0.27 (± 0.17)	0.84
	Aug 2018	1.97 (± 1.39)	*0.04 (± 0.02)**	0.034 (± 0.029)	*0.04 (± 0.05)**	2.09 (± 1.49)	1.13
	Mean	0.91 (± 0.39)	0.04 (± 0.02)	0.015 (± 0.009)	0.04 (± 0.05)	1.01 (± 0.46)	0.99 (± 0.13)
Main basin	Nov-Dec 2016	0.005 (± NA)	0.1 (± 0.06)*	0.001 (± 0.004)	-0.35 (± 0.32)	-0.24 (± 0.38)	0.36
	Apr-May 2017	0.003 (± NA)	0.1 (± 0.06)*	0.013 (± 0.008)	0.03 (± NA)	0.14 (± 0.39)	0.39
	Feb-Mar 2018	0.003 (± NA)	0.1 (± 0.06)*	0.001 (± 0.003)	*-0.16 (± 0.32)**	-0.06 (± 0.38)	0.45
	Aug 2018	0.003 (± NA)	0.1 (± 0.06)*	0.018 (± 0.008)	*-0.16 (± 0.32)**	-0.04 (± 0.39)	0.58
	Mean	0.004 (± 0.001)	0.1 (± 0.06)	0.008 (± 0.004)	-0.16 (± 0.19)	-0.05 (± 0.25)	0.44 (± 0.05)

CHAPITRE III

CO_2 AND CH_4 DYNAMICS AND ITS DETERMINANTS IN THE DEEP LAYER OF A TROPICAL RESERVOIR

Cynthia Soued[1], Yves T. Prairie[1]

[1]Groupe de Recherche Interuniversitaire en Limnologie et en Environnement Aquatique (GRIL), Département des Sciences Biologiques, Université du Québec à Montréal, Montréal, H2X 3X8, Canada.

N.B. References cited in this chapter are presented at the end of the thesis.

3.1 Abstract

Deep layers of lakes and reservoirs are active sites of carbon dioxide (CO_2) and methane (CH_4) production and accumulation. These two potent greenhouse gases can be emitted to the atmosphere during water column mixing and, for hydropower reservoirs, from deep water discharge to the downstream river. Regulation of deep CO_2 and CH_4 concentrations depends on multiple factors including rates of sediment-water exchange, aerobic respiration, methanogenesis, CH_4 oxidation, and vertical diffusion. These drivers are interlinked but have mostly been studied separately, making their relative importance and interactions in a system difficult to disentangle. In this study, we use empirical observations combined with an integrative modeling approach to build a comprehensive picture of CO_2 and CH_4 dynamics in the deep layer of a permanently stratified reservoir located on the tropical Borneo Island (Malaysia). Results show that O_2 acts as a key modulator of deep CO_2 and CH_4 metabolism, and largely shapes their spatial and temporal patterns at the ecosystem scale. The availability of O_2 in the deep layer depended on vertical diffusion, which also controlled CO_2 and CH_4 movement. Our model reproduced well the shape of vertical profiles of concentration and isotopic signature, and highlighted the central role of gas diffusivity in hypolimnetic GHG dynamics through its direct effect on gas transport and its interaction with water column metabolism. Furthermore, it suggests that the GHG stocks are now in a steady-state between production and removal processes. The predictive framework developed here could be applied to better understand and predict hypolimnetic GHG storage and emissions in lakes and reservoirs.

3.2 Introduction

Inland waters are key elements of the carbon (C) cycle, emitting large amounts of greenhouse gases (GHG) to the atmosphere in the form of CO_2 and CH_4. These emissions are sustained by external inputs and internal processing of C in aquatic systems. While emissions occur at the air-water interface, a substantial portion of the C mineralization occurs below the thermocline, in the water column and sediments of the hypolimnion, where CO_2 and CH_4 tend to accumulate. The importance of hypolimnetic GHG storage is evident during lakes mixing, like at fall overturn, known to induce large peaks in GHG out-flux (Bastviken *et al.*, 2004 ; Ducharme-Riel *et al.*, 2015 ; Encinas Fernández *et al.*, 2014). Deep GHG storage is particularly important in permanently stratified systems (usually in the tropics), where rare mixing events can trigger alarming amounts of gas release (Schmid *et al.*, 2005, 2006). In natural lakes, a large fraction of the CH_4 produced is consumed by methanotrophic bacteria before reaching the atmosphere. In reservoirs however, deep water withdrawal often leads to a direct release of hypolimnetic GHG to the atmosphere through degassing upon discharge to the outflow river and subsequent diffusive emissions (Demarty et Bastien, 2011 ; Guérin *et al.*, 2006 ; Kemenes *et al.*, 2016). The contribution of degassing and downstream emissions to the overall reservoir C footprint is highly variable, ranging from near negligible to dominant (Galy-Lacaux *et al.*, 1997 ; Kemenes *et al.*, 2007 ; Soued et Prairie, 2020 ; Teodoru *et al.*, 2012). What distinguishes such divergent behaviors resides in the interplay between the physical and biogeochemical processes regulating the dynamics of CO_2 and CH_4 and their interaction in the hypolimnion of these systems. Therefore, predicting reservoir degassing and downstream GHG emissions is important but challenging, being constrained by the current knowledge on hypolimnetic GHG dynamics.

Dissolved oxygen (O_2) has been shown to play a key role in both CO_2 and CH_4 dynamics. Indeed, the production of CO_2 derives mostly from aerobic respiration which depends on O_2 availability as an electron acceptor. Dissolved O_2 also inhibits CH_4 production and strongly modulates its oxidation (Conrad, 2009 ; Thottathil *et al.*, 2019). The vertical penetration of O_2 from the well-oxygenated surface to the deep layers of aquatic systems is controlled by physical factors, namely gas diffusivity, which also controls both CO_2 and CH_4 transport throughout the water column (Barrette et Laprise, 2005 ; Kreling *et al.*, 2014 ; Pu *et al.*, 2020). The interplay between these physical processes and production and consumption rates of CO_2 and CH_4 in the water column and the sediments shapes the vertical profiles of the two gases and their temporal evolution.

The multiple processes regulating CO_2 and CH_4 dynamics in deep waters have often been examined separately, with studies focusing exclusively on aerobic respiration (Karlsson *et al.*, 2007 ; Solomon *et al.*, 2013), CH_4 oxidation (Bastviken *et al.*, 2002 ; Thottathil *et al.*, 2019), sediment C gas production (Cardoso *et al.*, 2013 ; Gruca-Rokosz et Tomaszek, 2015), or physical processes (Guérin *et al.*, 2016 ; Rimmer *et al.*, 2006). These studies have greatly improved our understanding of the magnitude and regulation of individual rates of processes involved in aquatic C cycling. However, integrative studies building a comprehensive picture of hypolimnetic CO_2 and CH_4 dynamics are rare and essentially limited to temperate lakes (Bastviken *et al.*, 2008 ; Vachon *et al.*, 2019). Such approaches yielded estimates of the relative proportion of CH_4 produced versus oxidized and emitted (Bastviken *et al.*, 2008), and also revealed the effect of internal gas diffusivity on this balance (Vachon *et al.*, 2019). However, the current understanding of C processes and how they interact at an ecosystem scale to shape deep C gas profiles is still limited, especially in tropical regions.

In this study, we investigate the hypolimnetic CO_2 and CH_4 dynamics in Batang Ai hydroelectric reservoir, located on the tropical Borneo Island (Malaysia). Deep GHG dynamics are particularly important in this system because its permanent stratification traps large quantities of CO_2 and CH_4 in the hypolimnion, and deep water withdrawal discharges this GHG rich waters directly downstream of the dam accounting for 89 % of the reservoir C footprint (Soued et Prairie, 2020). The research reported here has three main objectives. The first is to assess the spatial patterns of CO_2 and CH_4 concentrations in the deep reservoir layer along a hydrological gradient of distance from the inflowing river delta. This aims at understanding the effect of a changing flow and morphometry (common in reservoirs) on the spatial behaviour of deep CO_2 and CH_4. The second is to re-construct, through modeling, the temporal evolution of CO_2 and CH_4 accumulation in the deep layer since the construction of the dam until 35 years later. This is useful to estimate past reservoir emissions and to determine whether deep reservoir gas storage is still increasing or has reached a steady state. The third objective is to combine field measurements of C processes into a mechanistic model of hypolimnetic O_2, CO_2 and CH_4 concentrations along a vertical profile. This framework was used as a tool to test the relative impact of different factors on deep GHG vertical profiles. Addressing these objectives jointly leads to a comprehensive understanding of deep GHG dynamics in the study system, and provides useful general knowledge transferable to other lakes and reservoirs.

3.3 Materials and methods

3.3.1 Site and sampling description

Batang Ai is a hydroelectric reservoir impounded in 1985 on the Borneo Island (Sarawak, Malaysia). The region experiences a tropical equatorial climate with annual rainfall between 3300 and 4600 mm, being more abundant from October to March (Sarawak Government, 2019 ; Weather Spark, s. d.). Average monthly temperature varies very little throughout the year (≤ 2 ºC), changing mostly on a daily scale (day and night means of 32 vs 23 ºC respectively) (Sarawak Government, 2019 ; Weather Spark, s. d.). The reservoir is located in the Batang Ai National Park (with limited human activities), drains a mostly forested catchment of 1149 km^2 and has a total area of 68.4 km^2, a water residence time of 0.9 year, and a maximum and mean depths of 28 and 73 m respectively. The two main reservoir inlets are the Batang Ai and Engkari rivers (max depth ~10 m) that flow into two wider reservoir branches which converge into a main basin (Figure 3.1). Batang Ai is a clear water oligotrophic reservoir with very low mean concentrations of dissolved organic C (< 1 $mg.L^{-1}$), phosphorus (< 6 $\mu g.L^{-1}$), nitrogen (< 0.2 $mg.L^{-1}$), and chlorophyll a (< 1 $\mu g.L^{-1}$) as described in (Soued et Prairie, 2020).

Four sampling campaigns were conducted in Nov-Dec 2016, Apr-May 2017, Feb-Mar 2018, and Aug 2018, with the corresponding weather and flow conditions shown in Figure S3.1. During each campaign, 4 to 9 sites (P1 - P9) were sampled along a hydrological gradient from the Batang Ai river delta to the main basin (Figure 3.1). In each, site vertical water column profiles were performed from 0 up to 32 m (each 0.5 – 3 m), and one water sample was collected at 60 m. At each sampled depth, water temperature and dissolved O_2 were measured using a multi-parameter probe (Yellow Spring Instruments, model 600XLM-M) equipped with depth gauge. The probe was attached to a submersible pump and plastic tubing from which water was collected for gas analyses. For each sampled profile, temperature data were used to calculate the buoyancy frequency (N^2), the thermocline depth, and the top and bottom of the metalimnion with the package rLakeAnalyzer v1.11.4.1 (Winslow *et al.*, 2018) in the R software (R Core Team, 2017). In this study we use the term “deep layer” to refer to the layer below the epilimnion (the metalimnion and hypolimnion).

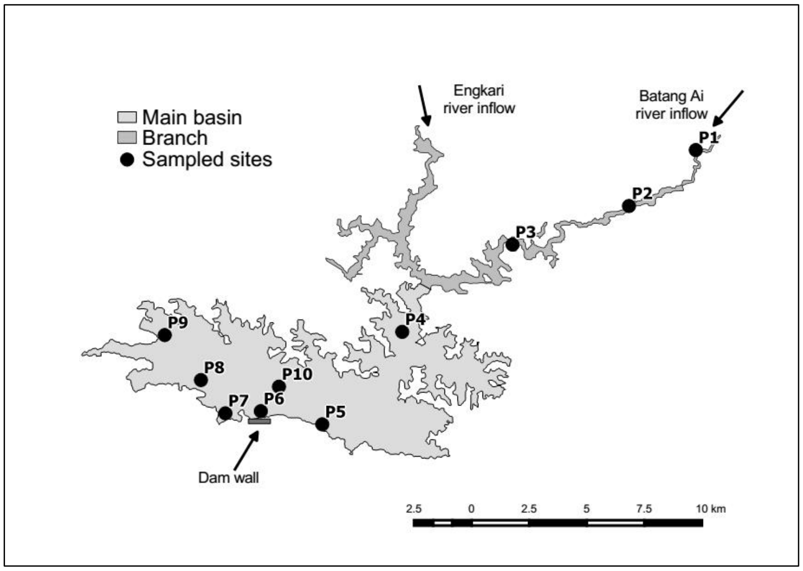

Figure 3.1: Map of Batang Ai reservoir sections and sampling sites.

3.3.2 Gas concentrations and isotopic signatures

CO_2 and CH_4 water concentrations and stable isotopic signatures ($\delta^{13}CO_2$ and $\delta^{13}CH_4$) were measured in all vertical profiles. Water was collected in 60 mL gas-tight syringes inside which a 30 mL ambient or C free air was created. The water and gas phases in the syringe were equilibrated by shaking, and then gas was injected in a 12 mL pre-evacuated air-tight glass vial. Sampled gas was analyzed for CO_2 and CH_4 concentrations on a Shimadzu GC-8A Gas chromatograph and for $\delta^{13}CO_2$ and $\delta^{13}CH_4$ on a Cavity Ring Down Spectrometer (CRDS) equipped with a Small Sample Isotopic Module (SSIM, Picarro G2201 -i). Original water gas concentrations and isotopic signatures were back-calculated accounting for temperature (gas solubility), atmospheric pressure, headspace ratio, and gas values (concentrations and stable isotopic signatures) before and after equilibration.

3.3.3 Sediment sampling

Sediment CO_2 and CH_4 concentrations, isotopic signatures, and fluxes to the overlaying water column were measured in 7 sites (P1-5, P7, and P9, Figure 3.1). Sediment cores were collected with a Glew gravity corer equipped with a plastic liner (6 cm diameter) pre-drilled with 1 cm holes at every centimeter up to 20 cm. During sampling, holes were covered with electric tape, and upon recovery the tape was removed and 3 mL tip-less syringes were inserted through the holes to extract sediments at different depths within the core. Extracted sediments were put in 25 mL glass vials, mixed with 6 mL nano-pure water, and sealed with an air-tight butyl rubber stopper crimped with an aluminum cap. Glass vials were pressurized by injecting 40 mL of ambient air using a syringe and needle. The water and sediment content was equilibrated with the gas phase in the vial by shaking, then the gas phase was collected and analyzed for CO_2 and CH_4 and water concentrations and isotopic signatures as described above (section 3.3.2).

Sediment to water fluxes of CO_2 and CH_4 were estimated based on the gradient in gas concentrations at the sediment-water interface (g, in μmol.L^{-1}.m^{-1}). In most cores, there was a clear positive linear slope between gas concentration and depth in the first 5 cm of sediments and overlaying water (p-value < 0.05 and $R^2_{adj} > 0.5$). In these cases, the latter slope was considered as the term g in Eq. (3.1) below. Otherwise, g was calculated as the gas concentration gradient between the mean of the first 3 cm of sediments and the overlaying water. The sediment to water gas flux rate (S_f in mmol.m^{-2}.d^{-1}) was calculated with following Eq. (3.1):

$$S_f = \frac{g \times d}{p} \tag{3.1}$$

with d is the diffusion coefficient set to 1.5×10^{-5} cm^2.s^{-1} (Donis *et al.*, 2017), and p the sediment porosity taken as 2 % based on previous results in Batang Ai reservoir (Tan, 2015).

3.3.4 Water column metabolic rates

Metabolic rates (aerobic respiration and net CH_4 oxidation) were measured at 5 sites (P2, P3, P4, P5, P7, Figure 3.1), during different sampling campaigns, and at different depths (3, 12, and 20 m) in the water column of Batang Ai. Rates were derived from in situ water incubations in 5 L glass jars with an air-tight clamp lid. Jars were filled and overflowed with water from specific depths, then closed, wrapped inside a black light-proof bag, and fixed to a rope at the corresponding sampling depth for a period of 22 to 24h. To monitor O_2 changes inside the incubations, high frequency O_2 and temperature sensors (model miniDOT from Precision Measurement Engineering) were fixed inside the jars. CH_4 concentrations and stable isotopic signatures were measured at the start and end of the incubations with the same technique as described above (section 3.3.2). Net rates of aerobic respiration and CH_4 oxidation were calculated as the difference between initial and final gas concentrations divided by the incubation time.

CH_4 oxidation was also assessed based on $\delta^{13}CH_4$ values measured in vertical profiles at all sampled sites. In this regard, the fraction of CH_4 oxidized (F_{ox}) was calculated with the following Eq. (3.2):

$$F_{ox} = -e^{(\ln(\delta 13C_{source}+1000)-\ln(\delta 13\mathrm{C}_{\mathrm{resid}}+1000))/(\alpha-1)} + 1) \tag{3.2}$$

with $\delta^{13}C_{source}$ the $\delta^{13}CH_4$ value in the top sediment layer at each site, considered as the only CH_4 source to the deep layer, and $\delta^{13}C_{resid}$ is the residual $\delta^{13}CH_4$ measured at each point in the profile.

3.3.5 Modeling framework and parameters

General framework. The concentrations of O_2, CO_2, CH_4 were modeled in the deep layer of the main basin of Batang Ai as a function of vertical depth (z, from 10 to 60 m) and time (from 0 to 100 years after impoundment). $\delta^{13}CH_4$ was also modeled based on the isotopic ratio of $^{12}CH_4$ and $^{13}CH_4$ predicted concentrations. The model framework is based on a system of coupled second degree partial differential equations described in Eq. (3.3) to (3.6):

$$\frac{d[O_2]z}{dt} = K_z \frac{\partial^2 [O_2]}{\partial z^2} + R_w + R_s \tag{3.3}$$

$$\frac{d[CO_2]z}{dt} = K_z \frac{\partial^2 [CO2]}{\partial z^2} + R_w + R_s + Sa_{CO2} \tag{3.4}$$

$$\frac{d[^{12}CH_4]z}{dt} = K_z \frac{\partial^2[^{12}CH_4]}{\partial z^2} + P_{CH4} - MOX_{sp}\left[^{12}CH_4\right] \tag{3.5}$$

$$\frac{d[^{13}CH_4]z}{dt} = K_z \frac{\partial^2[^{13}CH_4]}{\partial z^2} + S_{13:12} * P_{CH4} - \frac{MOX_{sp}[^{13}CH_4]}{\alpha} \tag{3.6}$$

where $[O_2]z$, $[CO_2]z$, $[^{12}CH_4]z$, and $[^{13}CH_4]z$ are the respective gas concentrations at depth z. K_z is the vertical water column gas diffusivity. R_w and R_s are the aerobic respiration rates in the water column and sediments, respectively. Sa_{CO2} is the CO_2 inputs to the water column derived from anoxic sediment processes. P_{CH4} is the CH_4 production rate, MOX_{sp} is the specific CH_4 oxidation rate with a fractionation factor of $\alpha = 1.02$ (Coleman *et al.*, 1981), and $S_{13:12} = 0.0104$ is the concentration ratio of $^{13}CH_4$ / $^{12}CH_4$ in the sediments (considered as the only CH_4 source, with a measured mean $\delta^{13}CH_4 = -66$ ‰). The estimation of each parameter is described in the subsequent paragraphs. In brief, the change in concentration of each gas at a given depth depends on the sum of processes consuming or producing the gas and on the movement of the gas along the vertical profile. Note that the model, being one-dimensional, does not consider horizontal advective transport, and thus ignores the effect of riverine inputs and hypolimnetic water withdrawal at the dam, which introduces uncertainty in the modeling framework. The system of equation was solved in the software Matlab R2018a using the function 'pdepe' function to solve initial boundary value problems (Skeel et Berzins, 1990). Initial values were set to the concentrations of each gas corresponding to its atmospheric partial pressure and water solubility at 30.2 ºC (the temperature at 10 m). Boundary conditions (Neumann) at the bottom (60 m) were set to 0, while at the top of the deep layer (10 m depth), Dirichlet boundary constant concentration values were set to 220, 21.2, and 0.07 $\mu mol.L^{-1}$ for O_2, CO_2, and CH_4 respectively (corresponding to measured means at the base of the mixed layer).

Gas diffusivity. K_z was estimated using two methods. The first one is based on the model of Hondzo and Stefan (1994) using N^2 and lake surface area (as a proxy for wind induced turbulence) following Eq. (3.7):

$$K_z = 8.17 * 10^{-4} * A_0 * N^{2^{-0.43}} * \frac{86400}{1000} \tag{3.7}$$

with A_0 = 58.9 km^2 the surface area of the reservoir main basin. The second method is based on the general equation of Osborn (1980) outlined in Eq. (3.8):

$$K_z = \Gamma \frac{\epsilon}{N^2} \tag{3.8}$$

with Γ = 0.2 the mixing ratio (Lee *et al.*, 2017 ; Oakey, 1982), and ϵ is the turbulent dissipation rate (W kg^{-1}). N^2 and ϵ were both estimated based on empirical measurements of temperature and shear microstructure profiles using a MicroCTD probe (Rockland Scientific). The high frequency probe (512 Hz) was equipped with a temperature and two velocity shear sensors as well as tilt, vibration, and depth sensors. Measurements were done at 3 sites in the main basin (P8, P9, P10, Figure 3.1) during the Aug 2018 sampling campaign. At each site, 10 replicates cast from 2 to 23 m were performed with the profiler launched half the time from top to bottom (downward configuration) and the other half from bottom to top (uprising configuration). Casts were separated by a minimum waiting time of 4 min to avoid measuring shear created by the previous cast. After a quality check, ϵ was calculated for each profile based on Nasmyth shear spectrum (Oakey, 1982), using ODAS v4.3.03 Matlab library (by Rockland Scientific), and values were binned over 1-2 m and averaged among the two shear probes. Deep layer ϵ values did not yield any clear pattern as a function of depth. Thus, the parameter ϵ in the model (Eq. (3.7) and (3.8)) was considered to be a constant of 1.5 $x10^{-8}$ $m^{-2}.s^{-3}$ representing the mean of all field data along the deep layer vertical profile (10 to 23 m). N^2 as a function of depth (Eq. (3.7) and (3.8)) was calculated as described in section 3.3.1 based on a single temperature profile (site P10, Figure 3.1) on which a smooth spline curve was fitted (function ‘smooth.spline’ in R software). The resulting N^2 profile was best fitted to a sigmoid curve (Figure 3.S2) with the following Eq. (3.9):

$$N_z^2 = \left(\frac{1}{1+e^{0.43\,(z-4.45)}}\right) 0.0025 + 3.8 * 10^{-5} \tag{3.9}$$

Combining Eq. (3.9) to Eq. (3.7) and (3.8) yields two predictive functions of K_z with depth in the deep reservoir layer. The mean of the two functions was used to calculate K_z as a function of depth in the general model framework (Eq. (3.3) to (3.6)).

Aerobic and anaerobic respiration. R_w represents water column O_2 consumption and CO_2 production (assuming a respiratory quotient of 1). R_w was modeled as a Michaelis-Menten function, with the advantage of considering O_2 consumption as a quasi zero-order reaction at high O_2 and approaching a first-order reaction at low O_2, as described by Eq. (3.10):

$$R_w = r_{wmax} * \frac{[O_2]}{Ox_{50} + [O_2]} \tag{3.10}$$

with r_{wmax} the maximum respiration rate, and Ox_{50} the O_2 concentration at which the respiration rate reaches 50 % of r_{wmax}. This form of equation ties R_w to O_2 when available O_2 becomes limiting. In Eq. (3.10), Ox_{50} was set to 50 $\mu mol.L^{-1}$, and r_{wmax} to 21.7 $\mu mol.L^{-1}.d^{-1}$, which corresponds to the mean of measured respiration rates in *in situ* deep water incubations (described in section 3.3.4) for which O_2 concentration was higher than Ox_{50}. The model described in Eq. (3.10) and measured R_w data are shown in Figure S3.3. Modeling R_s, the aerobic sediment respiration, was done using the same equation structure and replacing r_{wmax} by r_{smax} which is the maximal sediment respiration rate, calculated with Eq. (3.11):

$$r_{smax} = S_{CO2} * \left(\frac{q}{z_{max} - z}\right) \tag{3.11}$$

with S_{CO2} the mean sediment to water CO_2 flux measured in the main reservoir basin (as described in section 3.3.3) considered here as the upper limit for aerobic sediment respiration, and q the bathymetric shape index (Ferland *et al.*, 2014 ; Imboden, 1973) calculated based on the mean and max depths of the main basin (z_{mean} = 30 m, and z_{max} = 73 m respectively) following Eq. (3.12):

$$q = \left(\frac{z_{max}}{z_{mean}}\right) - 1 \tag{3.12}$$

This term allows the translation of areal sediment flux rates to volumetric sediment CO_2 inputs to a given water depth considering the changing ratio of water volume to sediment area along the vertical profile. Total O_2 consumption is the sum of R_w and R_s at each depth, however, CO_2 production can also occur under anaerobic conditions, mostly in the sediments. Some of the processes producing CO_2 without consuming O_2 include sulfate reduction and acetoclastic methanogenesis (Borrel *et al.*, 2011 ; Fahrner *et al.*, 2008 ; Gruca-Rokosz et Tomaszek, 2015 ; Holmer et Storkholm, 2001), the latter being observed in Batang Ai sediments (section 3.4.2). Anaerobic CO_2 production was included in the model as an additional term: Sa_{CO2} that was considered equal to 15 % of the maximum sediment respiration rate (r_{smax}), which occurs regardless of available O_2 (as opposed to the term R_s).

CH_4 production and consumption. Deep CH_4 production was assumed to occur exclusively in the sediments with a volumetric rate (P_{CH4}) that varies as a function of depth (water volume to sediment ratio) following Eq. (3.13):

$$P_{CH4} = S_{CH4} * \left(\frac{q}{z_{max} - z}\right) \tag{3.13}$$

with S_{CH4} the mean of measured areal sediment to water CH_4 flux (described in section 3.3.3). CH_4 consumption by oxidation was calculated by multiplying CH_4 concentration by MOX_{sp}, the specific CH_4 oxidation rate (Eq. (3.5) and (3.6)). MOX_{sp} was modeled as a function O_2 concentration using the model of Thottathil et al. (2019) in Eq. (3.14) (Figure S3.3):

$$MOX_{sp} = e^{\lambda\,[O_2]} - e^{(\lambda+\beta)\,[O_2]} \tag{3.14}$$

with $\lambda = 0.01$ and $\beta = 0.18$ (same values as in Thottathil et al. (2019)). This model was chosen because it is the only model describing MOX inhibition by O_2 and because our data showed strong evidence of MOX dependence on O_2 concentration (Figure S3.7 and section 3.4.4). Measured MOX rates derived from incubations in Batang Ai could not be used to parametrize the model due to the low number and large variability of data (Figure S3.7).

3.3.6 Model evaluation and sensitivity analyses

Model results were compared to measured profiles at site P6 (Figure 3.1) during the four sampling campaigns (to cover temporal variability). For each modeled component (O_2, CO_2, CH_4 concentrations, and $\delta^{13}CH_4$), we calculated the R^2 and the Nash-Sutcliffe efficiency (NSE) as a goodness of fit indexes using the R package hydroGOF (Zambrano-Bigiarini, 2020). We performed sensitivity analyses to assess the relative impact of K_z, S_{CO2}, S_{CH4}, R_w, and MOX on model outputs by dividing and multiplying each of these parameters by a factor of 2. The effect of each parameter was reflected by the extent of change in model results it induced. In particular, changes in two components of the model output were examined: the change in the integrated mean CO_2 and CH_4 concentration in the deep layer, and the change in CO_2 and CH_4 concentrations at the withdrawal depth (21 m), which fuel degassing and downstream emissions.

3.4 Results and discussion

3.4.1 Physical water structure

Water temperature in the reservoir varied between 24 and 33 ºC, being the coldest in bottom waters and close to the inflow. As the distance from the river delta increases, thermocline deepened from 1.3 (± 1.6) m at the river delta, to 8 (± 2.3) m in the reservoir branch, and to 10.6 (± 1.7) m in the main basin (Figure 3.2). The maximum buoyancy frequency (N^2), observed in the metalimnion, was sufficiently large to create a strong density barrier between the epilimnion and the hypolimnion, albeit weaker in the reservoir branches compared to the main basin (Figure 3.2). This suggests a higher potential for exchanges between surface and deep waters in the branches.

Temporal variations in water temperature and stratification were mostly apparent in upstream reaches, especially at the river mouth. In Aug 2018, surface water temperatures were higher (Figure 3.2) and riverine flow rate was the lowest among sampling campaigns (49 vs 108 - 110 $m^3.s^{-1}$, Figure S3.1). This resulted in a deeper thermocline in the river delta in Aug 2018 with warm water flowing into the surface layer of the reservoir. In contrast, during the Apr-May 2017 and Feb-Mar 2018 campaigns, riverine inflows were colder and denser, thus likely plunged into the reservoir's deep layer introducing significant amounts of O_2 in the hypolimnion compared to the Aug 2018 campaign (Figure 3.2).

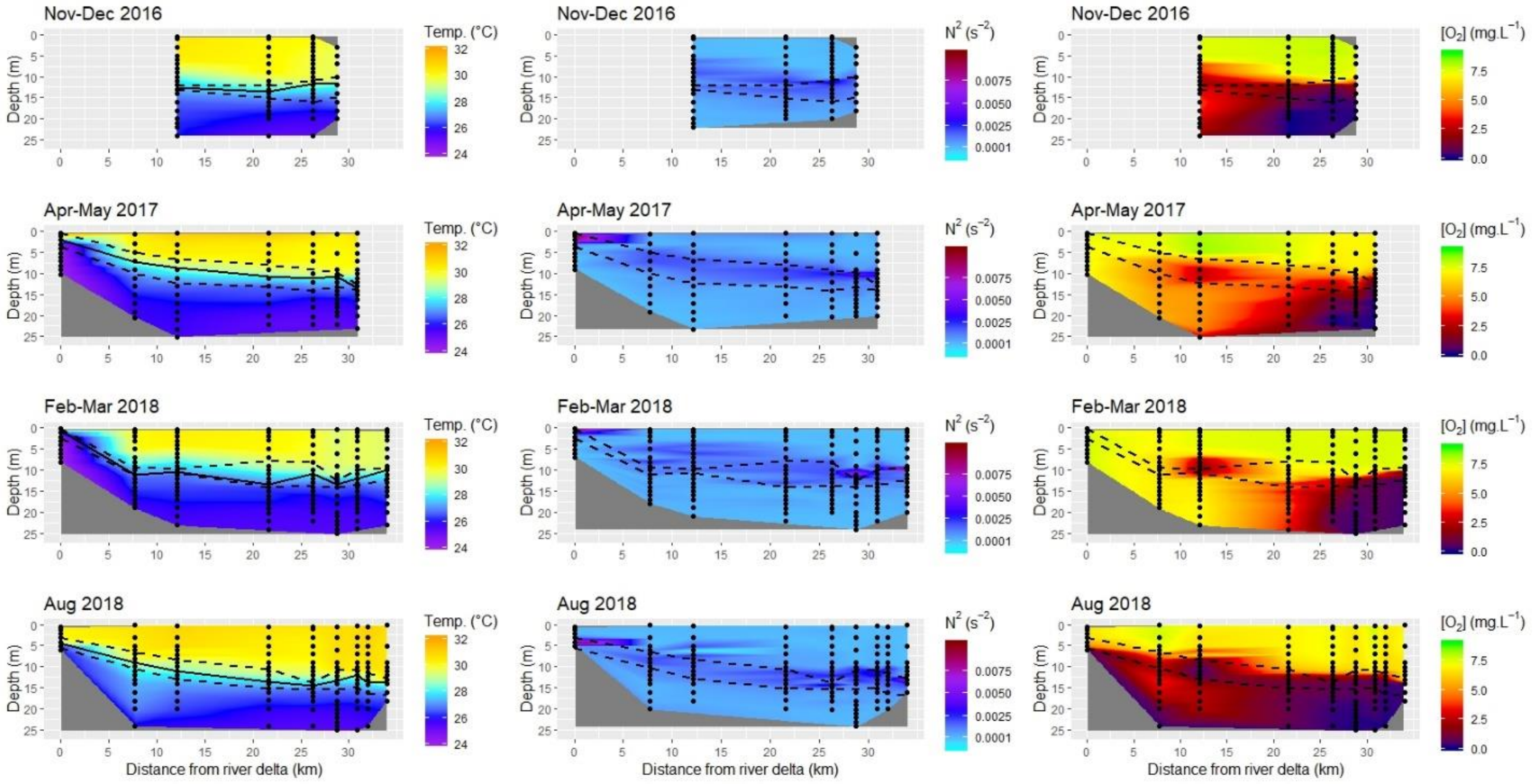

Figure 3.2: Cross-section plot of temperature (left), buoyancy frequency N^2 (middle), and dissolved O_2 concentration (right) as a function of the distance from the river delta in each sampling campaign. Interpolated data are based on measured vertical profiles (black dots). Black lines represent the thermocline (solid) and the top and bottom of the metalimnion (dashed)

3.4.2 Sediment GHG patterns

Measured CO_2 and CH_4 concentrations in the sediments ranged from 74 to 8750 $\mu mol.L^{-1}$ and 0.63 to 6800 $\mu mol.L^{-1}$ respectively, with generally increasing concentrations with sediment depth (Figure S3.4). Concentrations of CH_4 and CO_2 in the deep sediment layer (8-10 cm) were highest in the river delta, declined gradually along the reservoir branch and increased in the main basin, with a notably high value near the fish aquaculture area (Site P7, Figure 3.1 and S4). This trend could be due to higher deep sediment organic matter content in the river delta and aquaculture site promoting CO_2 and CH_4 production there. This hypothesis is in line with previous studies pointing to organic matter as a major driver of C mineralization in sediments, and identifying river deltas and aquacultures as GHG hot spots due to increased organic matter inputs (da Silva *et al.*, 2018 ; DelSontro *et al.*, 2011 ; Grinham *et al.*, 2018 ; Troell et Berg, 1997). The $\delta^{13}CO_2$ and $\delta^{13}CH_4$ signature reflect the source and biochemical processing of C. Measured $\delta^{13}CO_2$ in deep sediments was generally high (> -20, Figure S3.4 and S3.5), indicating a ^{13}C enriched source, typical of terrestrial inputs (McCallister et del Giorgio, 2008), and / or a CO_2 consuming process, like methanogenesis by CO_2 reduction. In line with that, the large difference between $\delta^{13}CH_4$ and $\delta^{13}CO_2$ (> 55 ‰) in deep sediment samples (Figure S3.5) suggests a strong isotopic fractionation typical of CH_4 production by CO_2 reduction (Whiticar, 1999). This is also supported by a strong positive correlation between CH_4 concentration and $\delta^{13}CO_2$ in the sediments (R^2_{adj}= 0.84, p-value < 0.001, Figure S3.5).

In the top sediment layer (0 - 3 cm), CO_2 concentration was lower than in deep sediments and more homogeneous across sites, while CH_4 concentration was notably lower in the reservoir branch (29 to 100 $\mu mol.L^{-1}$) compared to the main basin (254 to 857 $\mu mol.L^{-1}$). The same spatial patterns were observed for CO_2 and CH_4 sediment to water fluxes averaging 2.3 (SD ± 0.8) $mmol.m^{-2}.d^{-1}$ for CO_2, and 0.16 (SD ± 0.12) compared to 0.47 (SD ± 0.58) $mmol.m^{-2}.d^{-1}$ for CH_4 in the branches and main basin respectively. This suggests that CH_4 oxidation in the top sediment layer likely prevents the accumulation of CH_4 in the reservoir branches. That is supported by a steep increase of $\delta^{13}CH_4$ from deep sediments to the overlaying water (Figure S3.4), indicating high net CH_4 oxidation at the sediment-water interface in the branch section. This pattern likely results from higher hypolimnetic O_2 concentration in the branch compared to the main basin (Figure 3.2). In the top sediment layer, $\delta^{13}CO_2$ and $\delta^{13}CH_4$ ranged from -23.2 to -12.3 ‰ and from -76.7 to -58.1 ‰, with a difference between $\delta^{13}CH_4$ and $\delta^{13}CO_2$ lower than 55 ‰ (Figure S3.5), which is more typical of CH_4 production via acetate fermentation (Whiticar, 1999).

The generally lower $\delta^{13}CH_4$: $\delta^{13}CO_2$ ratio in the top versus deep sediment layers (Figure S3.5) likely reflects a combination of higher CH_4 oxidation in the top layer, and a change in the methanogenic pathway (acetate fermentation to CO_2 reduction). A similar shift in methanogenic pathway was reported in several other studies and related to the decreasing availability of acetate with sediment depth (Alperin *et al.*, 1992 ; Gruca-Rokosz et Tomaszek, 2015 ; Hornibrook *et al.*, 2000 ; Mandic-Mulec *et al.*, 2012). Overall, observations in Batang Ai suggest that CO_2 and CH_4 dynamics in sediments are influenced by organic matter composition and inputs (by inflows and aquaculture), as well as by benthic O_2 availability for CH_4 oxidation.

3.4.3 Hypolimnetic GHG patterns

Across all hypolimnetic samples, CO_2 and O_2 concentrations are strongly negatively correlated with a slope of 0.99 (p-value < 0.001 and $R^2_{adj} = 0.74$, Figure 3.3). This indicates that aerobic respiration, with a typical $CO_2 : O_2$ quotient close to one (Vachon *et al.*, 2020), is a major driver of CO_2 concentration in the reservoir deep layer. The average deep CO_2 concentration gradually increases from the river delta (mean of 82 $\mu mol.L^{-1}$) to the west of the main basin (mean of 368 $\mu mol.L^{-1}$), mirrored by a decrease in O_2 concentration (Figure 3.3). Based on the difference in mean deep CO_2 concentration between the river delta and the dam wall, we estimated that Batang Ai river inputs have the potential to sustain 31 % of the CO_2 concentration in deep waters discharged from the reservoir. The remaining 69 % is most likely produced by aerobic organic matter respiration along the passage of deep waters through the reservoir branch and main basin (Figure 3.3).

The $\delta^{13}CO_2$ gradually decreases along the branch section (from a mean of -19.5 to -23.3 ‰, Figure 3.3), which may reflect isotopic fractionation of aerobic respiration producing increasingly ^{13}C depleted CO_2 along this transect (Blair *et al.*, 1985). In the west section of the main basin (site P9) CO_2 concentration reaches its maximum, however, its ^{13}C signature is notably enriched, averaging -19.5 (SD ± 1.3) ‰ compared to -23.3 (SD ± 0.6) ‰ at the end of the branch section (site P4, Figure 3.1). An increase in $\delta^{13}CO_2$ indicates either a more ^{13}C enriched source of C or a process consuming CO_2. CO_2 consuming processes such as chemiolithotrophy or hydrogenotrophic methanogenesis in deep waters of the west reservoir basin could be at play. However, following this latter hypothesis, one would expect lower hypolimnetic CO_2 concentrations in the west basin whereas measured data show the opposite. A higher ^{13}C in the organic matter of the west part of the main basin could be due to a higher retention time in this area which would result in a more degraded and ^{13}C enriched organic matter over time. The west part of the main basin, being outside the pre-impoundment river channel, may have a higher water residence time, allowing for the consumption of a larger fraction of the organic carbon which becomes an increasingly ^{13}C enriched substrate for CO_2. This hypothesis is in line with results from sediment $\delta^{13}CO_2$ values which exhibit a similar spatial pattern (Figure S3.4). Also, the higher residence time would explain the higher accumulation of CO_2 in the hypolimnion of the west basin.

In the branch section, average CH_4 concentration in the deep layer remains low (mostly < 50 µmol.L^{-1}) then increases close to the dam and reaches its maximum in the west part of the main basin (Figures 3). This pattern suggests that the CH_4 exiting the reservoir was produced mostly in the main basin rather than upstream, with the hypolimnetic CH_4 concentration at the end of the branch (site P4) equal to only 5 % of the one at the dam wall (Site P6). A key element controlling CH_4 dynamics is O_2, which can inhibit its production and promote its consumption via CH_4 oxidation (Borrel *et al.*, 2011). Conversely, Figure 3.3 shows that, above a O_2 concentration threshold of about ~ 30 μmol.L^{-1} there is very little CH_4 accumulation in the deep layer (except for two outlier points), whereas under this threshold CH_4 concentrations can increase to much higher levels. In the hypolimnion of the reservoir branch, mean O_2 concentrations varied between 238 and 29 μmol.L^{-1} (Figure 3.2), which is high enough to inhibit CH_4 production while allowing for CH_4 oxidation (Borrel *et al.*, 2011 ; Thottathil *et al.*, 2019). This can explain the lack of CH_4 accumulation in the hypolimnion of the branch section. In the main basin, especially in its west section, O_2 concentrations decrease below ~30 μmol.L-1 (Figure 3.3) allowing for net CH_4 production and accumulation. Highest hypolimnetic CH_4 concentrations were found in the west part of the main basin. This observation is also in line with the hypothesis of a longer residence time in that area, which would allow for more CH_4 accumulation and O_2 depletion there.

The measured hypolimnetic $\delta^{13}CH_4$ signature was highly variable spatially (site and depth) and temporally (sampling campaigns) ranging from -77.8 to 12.7 ‰) from the river delta to the dam wall, but stabilized around an average of -58.4 ‰ in the west part of the main basin (Figure 3.3). This value of -58.4 ‰ is consistent with CH_4 originating from the sediments (pore water $\delta^{13}CH_4$ of -66 ‰) and undergoing partial oxidation (increasing its $\delta^{13}CH_4$). In the rest of the transect however, $\delta^{13}CH_4$ variability spans a range of values from lower to much higher than the typical sediment $\delta^{13}CH_4$ value. This indicates that, in those areas, both CH_4 oxidation (which increases $\delta^{13}CH_4$) and production (which decreases $\delta^{13}CH_4$) occur in the deep water column. However, the net result of these two processes is a generally low CH_4 concentration (< 50 μmol.L^{-1}, Figure 3.3) from the river delta to the dam wall.

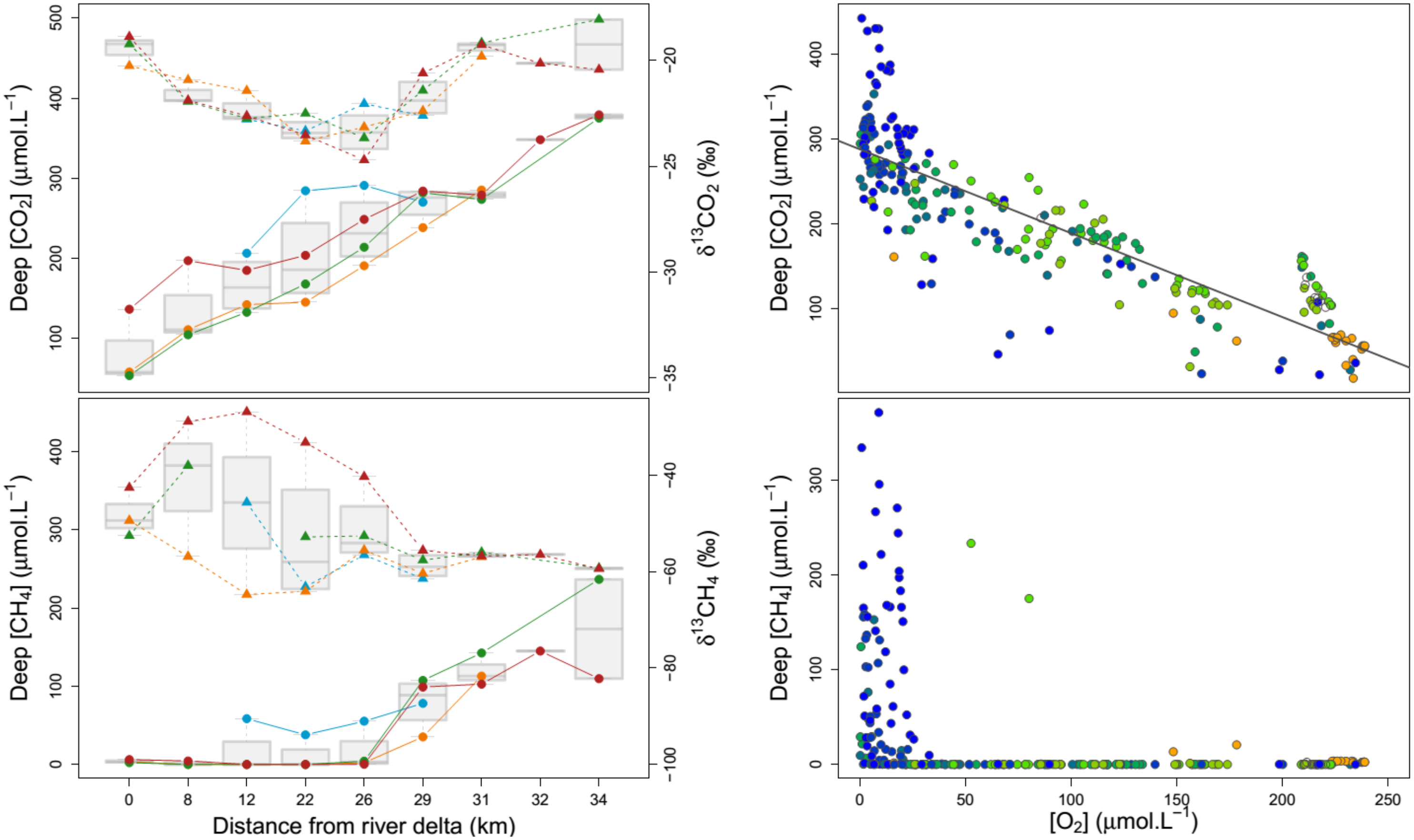

Figure 3.3: Left panels show CH_4 and CO_2 average hypolimnetic concentrations (circles) and $\delta^{13}C$ values (triangles) as a function of distance from the river delta (0 km is site P1) for each sampling campaign (blue, orange, red, and green represent Nov-Dec 2016, Apr-May 2017, Feb-Mar 2018, Aug 2018 respectively, and grey boxes are boxplots of all campaigns). The right panels show measured deep CO_2 and CH_4 concentration as a function of O_2 concentration, with a color gradient representing an increased distance from the river delta (orange to green to blue). The regression on the top right panel has a slope of 0.99, a p-value < 0.001 and a $R^2_{adj} = 0.74$.

3.4.4 Water column metabolic rates

Measured deep aerobic respiration rates based on O_2 changes in incubations averaged 15.6 (SD ± 10.5) µmol.L^{-1}.d^{-1}. These values are in the range of previously reported respiration rates in clear water oligotrophic lakes (Bogard *et al.*, 2020 ; Hanson *et al.*, 2003 ; Pace et Prairie, 2005). Due to the limited and non-normally distributed data points, it is difficult to clearly identify the factors controlling variability in measured respiration rates. Nevertheless, a non-parametric Kendall test showed a positive correlation between aerobic respiration rates and O_2 concentrations (p-value = 0.002, Figure S3.3), suggesting that O_2 can become a limiting factor for aerobic respiration in the deep layer of Batang Ai.

Net CH_4 oxidation rates (MOX) measured in *in situ* incubations ranged from 0.003 to 9.2 µmol.L^{-1}.d^{-1} (a few incubations in the epilimnetic layer showing a slight net CH_4 production were excluded from the analysis). The contribution of MOX to aerobic respiration (O_2 consumption in incubations) in the deep layer ranged from negligible (< 1 %) to more than 100 %, and increased following a near-perfect linear fit with initial CH_4 concentration ($R^2_{adj} = 0.98$, p-value < 0.001, Figure S3.6). Indeed, sites with high CH_4 concentration tend to coincide with low O_2 concentration and respiration, and high MOX rate ($R^2_{adj} = 0.78$, p-value < 0.001, Figure S3.6). This makes MOX the main O_2 consuming process in the CH_4 rich deep hypoxic sites of Batang Ai. This is in line with results of Reis et al. (2020a) (submitted) finding unprecedented high levels of abundance and activity of CH_4 oxidizing bacteria in the hypoxic hypolimnion of Batang Ai (up to 19 % of prokaryotic cell abundance and up to 60 % of rRNA sequences).

MOX dependence on CH_4 and O_2 concentrations has been previously reported, with maximum rates at high CH_4 and low O_2 concentrations (Kankaala *et al.*, 2013b ; Michaud *et al.*, 2017 ; Rudd *et al.*, 1974 ; Thottathil *et al.*, 2019). Thottathil et al. (2019) proposed a non-linear model (Eq. (3.12)) to account for the inhibitory effect of high O_2

on CH_4 specific oxidation rates (MOX_{sp}). To assess whether the same model structure was applicable to Batang Ai, we tested it on two sets of data: incubation derived MOX_{sp}, and F_{ox} (fraction of oxidized CH_4) calculated from $\delta^{13}CH_4$ data in vertical profiles (section 3.3.4). In both cases, the best fit was obtained by a unimodal curve shape with inhibition at high O_2. While the MOX_{sp}-O_2 link was not as obvious in incubations results, field-based F_{ox} estimates strongly supported a unimodal relationship between the two. Our results are in good agreement with Thottathil et al. (2019) (Figure S3.7) suggesting that the MOX_{sp}-O_2 kinetic they describe is widely applicable. Nevertheless, unexplained variance was high in both empirical models in Batang Ai (incubations and F_{ox}), which suggests other local drivers of MOX_{sp} may be at play, possibly the microbial community structure (Reis *et al.*, 2020b).

In all vertical profiles, F_{ox} reaches high values (> 0.6), indicating all sites experience substantial CH_4 oxidation at a given depth. However, the depth at which highest CH_4 oxidation states are observed differ among sites, occurring higher in the sediments and water column when moving from upstream (river delta) to downstream (main basin). Indeed, in the river delta, CH_4 oxidation is apparent mostly within the sediments and at the sediment-water interface (Figure S3.4, increase in $\delta^{13}CH_4$). Whereas in the branch, maximum F_{ox} are observed starting near the bottom of the hypolimnion, and gradually move higher in the water column, occurring at the top of the hypolimnion in the main basin (Figure S3.8). This spatial pattern of F_{ox} driven by O_2 concentrations (Figure S3.7) shapes deep CH_4 accumulation along the river to reservoir continuum (Figure 3.3). This effect is also reflected at a temporal scale, with mean hypolimnetic $\delta^{13}CH_4$ values in the reservoir branch being higher in Aug 2018 (Figure 3.3), when O_2 concentrations are lower and closer to the MOX_{sp} optimal O_2 concentration compared to other seasons (Figure 3.1). Overall, experimental and field-based data show that metabolic processing of O_2, CO_2, and CH_4 are interconnected across space and time in the deep layer of Batang Ai, with CH_4 oxidation playing a major role in the hypoxic part of the hypolimnion.

3.4.5 Temporal evolution of deep GHG

The large stocks of both CO_2 and CH_4 in the hypolimnion raise the question of whether GHG are still accumulating in the deep layers of Batang Ai or instead have reached an equilibrium. To explore this question, we combined the rates of gas diffusivity, sediment production, and water column metabolism in the model framework described above (section 3.3.5) to recreate the evolution of O_2, CO_2, CH_4 concentrations and $\delta^{13}CH_4$ through time since the impoundment of Batang Ai. Assuming that the physical and metabolic parameters have remained unchanged, results of the simulation show a rapid decrease of hypolimnetic O_2 concentration mirrored by an increase in CO_2 concentration immediately after impoundment (Figure 3.4). Within only two months, O_2 reaches a quasi-steady state being completely consumed in most of the hypolimnion due to aerobic respiration. At this stage, CO_2 production by aerobic respiration also stops in deeper layers, but CO_2 continues to accumulate due to anaerobic processes for ~10 years (Figure 3.4). Likewise, CH_4 hypolimnetic concentrations start increasing rapidly after the onset of anoxic conditions (during the first year), and continue to rise more slowly over ~10 years before reaching a quasi-steady state. Our results strongly argue that, despite the permanent stratification, the reservoir stops accumulating GHG in its hypolimnion a few years after its construction because the total amount of hypolimnetic CO_2 and CH_4 production are in a dynamic equilibrium with vertical gas transport and CH_4 oxidation in the upper portion of the deep layer.

Because of the deep water withdrawal in Batang Ai, hypolimnetic gas concentrations control GHG emissions downstream of the dam, which represent 89 % of the reservoir GHG footprint (Soued et Prairie, 2020). According to modeled deep CO_2 and CH_4 concentrations, downstream emissions increased mostly during the first year after impoundment, and then only slightly over ~10 years. Studies on Petit Saut and Eastmain-1 reservoirs both found CO_2 and CH_4 emissions below the dam to increase the first 1-2 years (Abril *et al.*, 2005 ; Teodoru *et al.*, 2012). This initial increase fits the results in Batang Ai, and illustrates the initial peak in flooded organic matter decomposition. Surface GHG emissions are thought to decrease exponentially with reservoir age due to the degradation of flooded organic matter. However, our model results, in line with previous studies, suggest that downstream emissions follow a different temporal dynamic than surface ones, being potentially higher in older reservoirs when permanently stratified.

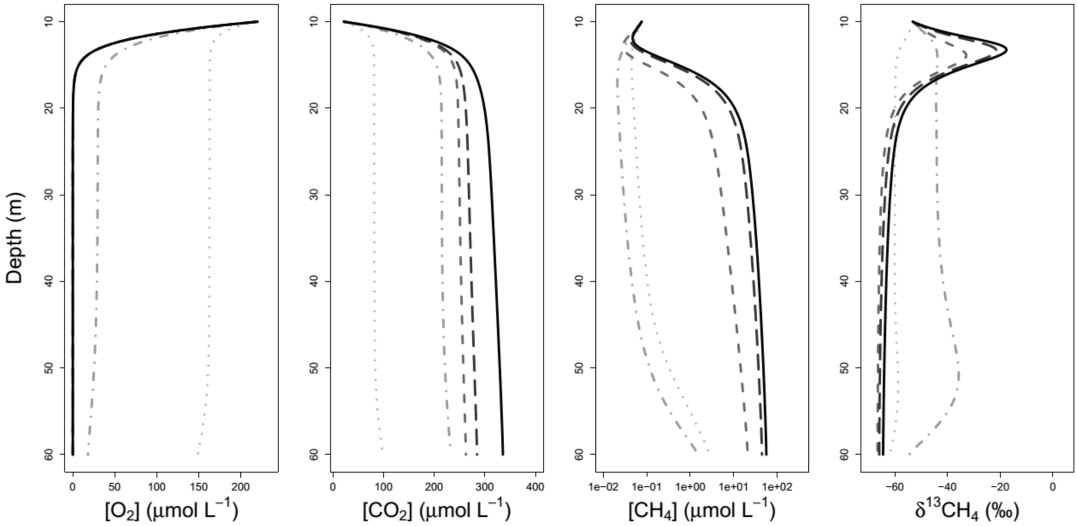

Figure 3.4: Modeled temporal evolution of O_2, CO_2, CH_4 concentrations and $\delta^{13}CH_4$ along a vertical profile in the deep layer of Batang Ai. Lines represent different times after the reservoir impoundment: 5 days (dotted), 15 days (dash and dot), 100 days (short dash), 1 year (long dash), and 10 years (solid), with the light to dark gradient in line color following the same order.

3.4.6 Modeled vs measured deep GHG

Model accuracy can be evaluated by comparing measured versus modeled results at the time of sampling. In the case of O_2, the model reproduces quite well the shape of the curve and concentrations along the depth profile (R^2 = 0.91, NSE = 0.75, Figure

3.5). Modeled CO_2 values also match well measured data ($R^2 = 0.82$, NSE = 0.50, Figure 3.5), indicating that the main processes are well formulated in the theoretical framework, with hypolimnetic CO_2 buildup originating from both aerobic and anaerobic processes. For comparison, the CO_2 profile modeling was tested without the inclusion of anaerobic production, and this scenario resulted in a large underestimation of hypolimnetic CO_2 buildup (Figure 3.5).

For CH_4, modeled and observed concentrations were well correlated but the model substantially underestimated the actual accumulation in the hypolimnion, with predicted bottom concentration reaching 56 $\mu mol.L^{-1}$ compared to a measured value of 290 $\mu mol.L^{-1}$ ($R^2 = 0.83$, NSE = 0.41 on log values, Figure 3.5). However, the model reproduced well the CH_4 isotopic signature ($\delta^{13}CH_4$) profile and exhibited the same peak at ~13 m as the one observed ($R^2 = 0.67$, NSE = 0.52, Figure 3.5). This highly enriched $\delta^{13}CH_4$ deep layer peak is the direct result of the inhibition of CH_4 oxidation at high O_2. It therefore suggests that the non-linear dependence of CH_4 oxidation on O_2 was well defined in the model.

The discrepancy in CH_4 concentrations potentially indicates an overlooked process in the theoretical model framework, which considered sediments as the sole source of CH_4. The formation and dissolution of bubbles may constitute a CH4 source not explicitly considerd in the model (McGinnis *et al.*, 2006). Another likely source of CH_4 is the production in the fully anoxic layer of the water column. While this process is much less documented than sediment production, it has been found in different systems (Biderre-Petit *et al.*, 2011 ; Iversen *et al.*, 1987 ; Winfrey et Zeikus, 1979 ; Youngblut *et al.*, 2014). The permanently anoxic hypolimnion of Batang Ai offers ideal conditions for water column CH_4 production, making it a likely process in this system. As a first-order approximation, we evaluated its potential effect on model fitness by incorporating this putative source in as a negative exponential function of O_2 concentration as follows:

$$P_{WCH4} = P_{Wmax}\ e^{-[O_2]} \tag{3.15}$$

with P_{WCH4} the potential water column CH_4 production at a given point, and P_{Wmax} the maximal value it can attain. The maximum value (P_{Wmax}) is unknown for Batang Ai so we used two values derived from the literature (0.01 and 1 µmol.L^{-1}.d^{-1}) as lower and upper bounds (Iversen *et al.*, 1987 ; Winfrey et Zeikus, 1979). Results of the simulation show that, at its upper bound, this additional source yields ~7 fold increase in mean hypolimnetic CH_4 concentration, matching well with measured data. This increase is not observed in the top part of the deep layer, where oxidation consumes excess CH_4, so it does not affect surface emissions. However, it influences CH_4 concentration at the withdrawal depth and could thus substantially influence downstream emissions. While we have no direct measurements supporting the occurrence and amplitude of deep water column CH_4 production in Batang Ai, model simulations suggest that it has the potential to drastically increase hypolimnetic CH_4 concentrations. Yet, there is very little information about this process in the literature, and it is largely overlooked in aquatic CH_4 budgets, being considered low compared to sediment production (Bastviken *et al.*, 2008 ; Eckert et Conrad, 2007 ; Liikanen *et al.*, 2002). Our results suggest that water column CH_4 production may be an important process to investigate in large systems with a higher ratio of anoxic water volume to sediment area such as Batang Ai.

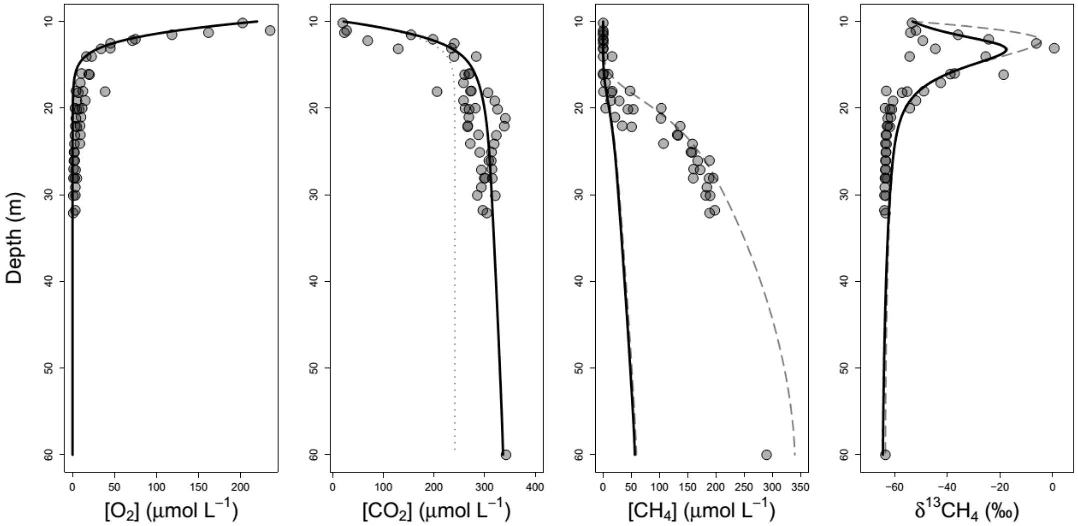

Figure 3.5: Modeled (solid line) versus measured (gray circles) O_2, CO_2, CH_4 concentrations and $\delta^{13}CH_4$ along a vertical profile in the deep layer of Batang Ai. In the [CO_2] panel, the dotted line represent a model simulation without anoxic CO_2 production. In the [CH_4] and $\delta^{13}CH_4$ panels, dashed lines represent model simulations with two levels of water column CH_4 production (note that the line for low production is hidden by the black solid lines).

3.4.7 Model sensitivity to parameters

While our model was able to capture the main features of the GHG profiles, we further investigated to which parameters it was most sensitive to and their impacts on deep CO_2 and CH_4 patterns in Batang Ai are shown in Figure 3.6. Gas diffusivity changes had the largest impact on CO_2 and CH_4 concentrations both at the withdrawal depth and as an integrated profile average. Gas diffusivity directly impacts CO_2 and CH_4 through vertical transport, which affects gas accumulation rates, and indirectly through its effect on O_2 concentration, which modulates both aerobic respiration and CH_4 oxidation. Lower gas diffusivity increases the gas residence time allowing for a higher CO_2 and CH_4 accumulation, as well as more O_2 depletion, which limits CH_4 oxidation.

The importance of gas diffusivity in Batang Ai is in line with the study of Vachon et al. (2019) which highlighted the importance of water column stability in a small lake CH_4 budget. The effect of physical water column structure on GHG emissions is also known to control variations in emissions downstream of dams (Bastien *et al.*, 2011) and to trigger emission peaks during lake turnovers (Encinas Fernández *et al.*, 2014). Given the importance of gas diffusivity, elements such as vertical advection via turbine withdrawal and thermal convection, not considered in the model, could play a large role in shaping hypolimnetic gas patterns at shorter time scales (daily to seasonal) in Batang Ai. Studies on freshwater CO_2 and CH_4 dynamics often ignore the physical dimension of their cycling, focusing mainly on their biological production and consumption. While biological factors are undoubtedly important, our results show that their interaction with gas diffusivity is a key element to consider at an ecosystem scale.

Sediment fluxes to the water column was the second most important parameter in terms of CO_2 and CH_4 deep layer concentrations (Figure 3.6). For both gases, this represents mostly the effect of anoxic processes. Indeed, for CO_2 the aerobic portion of sediment respiration is negligible in the hypoxic to anoxic water column due to its dependence on O_2 availability. While methanogenesis is extensively studied (Conrad, 2009), there is comparatively little information about the mechanisms, rates, and drivers of anaerobic CO_2 production in freshwater sediments. The latter component is a large source of uncertainty in the model due to the absence of direct measurements in Batang Ai and in other systems. Nevertheless, our modeling results in Batang Ai clearly show that anoxic sediment processes are determinants for both CO_2 and CH_4 accumulation in the deep layer and emissions to the atmosphere. Sediment processes are a particularly important component in reservoirs where the flooding of soils represent an additional substrate for anoxic GHG production (Prairie *et al.*, 2018).

Surprisingly, aerobic respiration rate had little effect on modeled CO_2 accumulation in the hypolimnion. Changing R_w resulted in small variations in O_2 and CO_2

concentrations only in the top 10 m of the deep layer (Figure 3.6) where O_2 penetration from the surface layer occurs. The rest of the water column, being anoxic, was not affected by R_w. However, R_w did have a notable effect on modeled CH_4 concentration. Indeed, by changing even slightly the O_2 profile in the top 10 m, variations in R_w induced changes in the depth of the CH_4 oxidation peak (visible on the $\delta^{13}CH_4$ graph, Figure 3.6). Lower R_w resulted in slightly more O_2 penetration in the deep layer leading to a deeper CH_4 oxidation peak reducing CH_4 accumulation and downstream emissions.

Surprisingly, the magnitude of maximum specific CH_4 oxidation had only a small impact on the CH_4 concentration profile (Figure 3.6), notably smaller than any of the other tested parameters. While counter-intuitive at first glance, MOX is largely confined to the top section (< 20 m) of the deep layer due to its dependency on O_2 availability and therefore does not affect substantially deep CH_4 accumulation that is mainly concentrated in the anoxic deep section (> 20 m). This result on model sensitivity to MOX rate indicates that the spatial interaction between MOX, O_2, and CH_4 concentrations is more important than the magnitude of MOX rate alone. In other words, where MOX occurs constrains how much CH_4 it is able to consume. Thus, doubling the MOX rate at a depth where CH_4 concentration is low has little effect on the gas profile, whereas changing the O_2 profile and hence the depth of the MOX peak (case of R_w variations, Figure 3.6) substantially affects CH_4 accumulation. This, in line with our previous results, reinforces the importance of integrative approaches considering the interactions between multiple factors to better understand and predict freshwater GHG patterns.

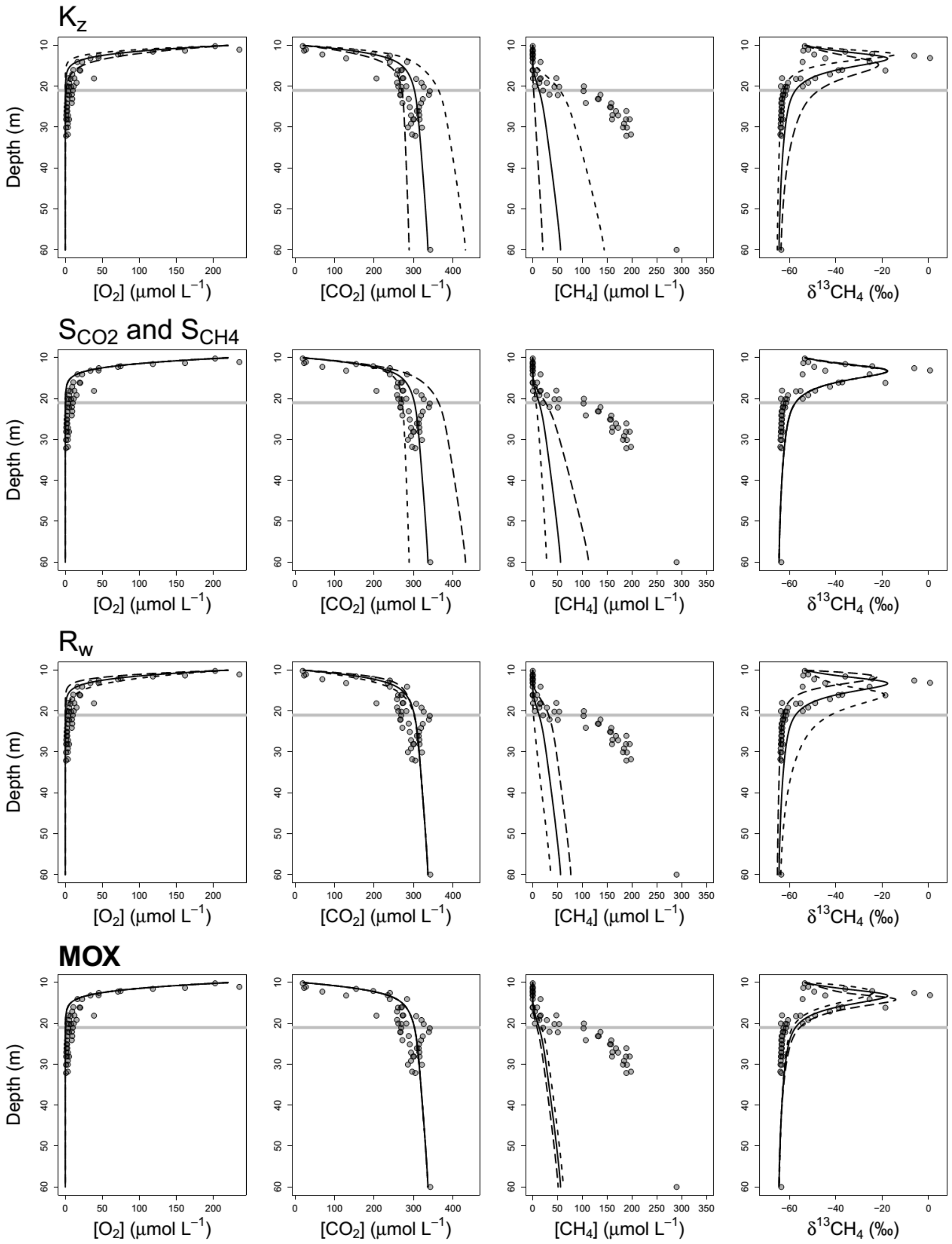

Figure 3.6: Modeled (solid line) and measured (gray circles) O_2, CO_2, CH_4 concentrations and $\delta^{13}CH_4$ along a vertical profile in the deep layer of Batang Ai. From top to bottom panels, graphs show results of sensitivity analyses of gas diffusivity (K_z), Sediment inputs (S_{CO2} and S_{CH4}), aerobic water column respiration (R_w), and CH_4 oxidation (MOX) respectively. Short and long dashed lines represent respectively halving and doubling of the parameter.

3.5 Conclusion

The general aim of this study was to improve our understanding of CO_2 and CH_4 dynamics in the deep layer of lakes and reservoirs; in particular, the spatial patterns of these gases, their temporal evolution, and their controlling factors. Our results from Batang Ai reservoir showed vertical variations in deep CO_2 and CH_4 concentrations reaching several orders of magnitude, tightly linked to O_2 concentrations. O_2 affected deep aerobic respiration, methanogenesis, and methanotrophy, and was thus a central player in the spatial structure of CO_2 and CH_4 vertically (with depth) and horizontally (along the river-reservoir continuum). Our simulations of the temporal evolution suggest that O_2 was rapidly depleted in the deep layer of the reservoir over a period of a few months after its construction. This constrained aerobic processes to the metalimnion, while anaerobic production fueled the accumulation of CO_2 and CH_4 in the hypolimnion for a decade before reaching a quasi-steady state. Comparing modeled to measured data suggested that anaerobic CO_2 production and water column methanogenesis are likely important but generally overlooked CO_2 and CH_4 sources. The importance of anaerobic CO_2 and CH_4 production in the sediments was corroborated by sensitivity analyses on the model. Latter analyses also showed that metabolic production of CO_2 (by aerobic respiration) and consumption of CH_4 (by oxidation) were highly dependent on the vertical O_2 profile. O_2, CO_2, and CH_4 profiles were all influenced by water column gas diffusivity, with higher mixing leading to less GHG accumulation and more oxygenation, which enhanced CH_4 oxidation and aerobic respiration. Thus, gas diffusivity played a paramount role in deep GHG dynamics, having a direct impact on their movement and an indirect one on their metabolism. This highlights the importance of comprehensive modeling approaches to understand the relative role and interactions between factors controlling CO_2 and CH_4 dynamics at an ecosystem level. In that sense, our integrative approach increases our ability to predict deep GHG behavior, and hence reservoirs downstream emissions.

3.6 Acknowledgments

This work was funded by Sarawak Energy Berhad and the Natural Science and Engineering Research Council of Canada (Discovery grant to Y.T.P. and BES-D scholarship to C.S.). We thank Karen Lee Suan Ping and Jenny Choo Cheng Yi for their logistic support and participation in sampling campaigns. We also thank Jessica Fong Fung Yee, Amar Ma’aruf Bin Ismawi, Gerald Tawie Anak Thomas, Hilton Bin John, Paula Reis, Sara Mercier-Blais and Karelle Desrosiers for their assistance on the field, and Katherine Velghe and Marilyne Robidoux for their help during laboratory analyses.

3.7 Supplementary information

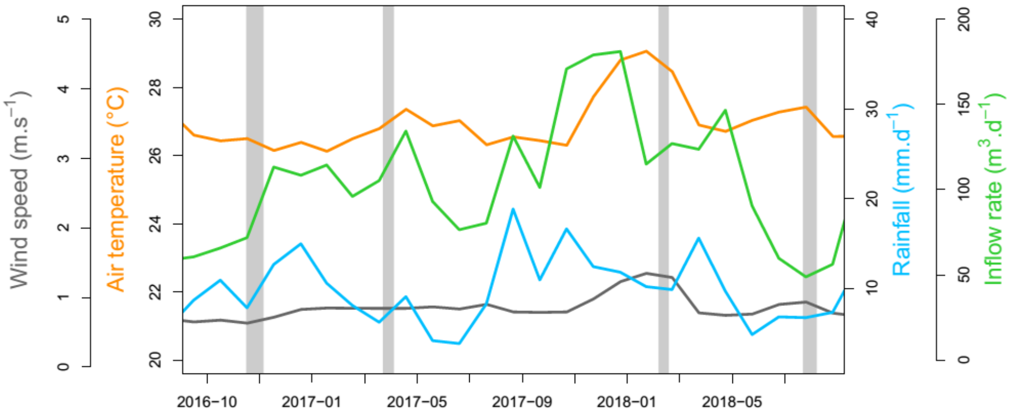

Figure S3.1: Time-series of air temperature, wind speed, rainfall, and inflow rate in Batang Ai (data provided by Sarawak Energy hydroelectric company). Gray bars represent sampling campaigns.

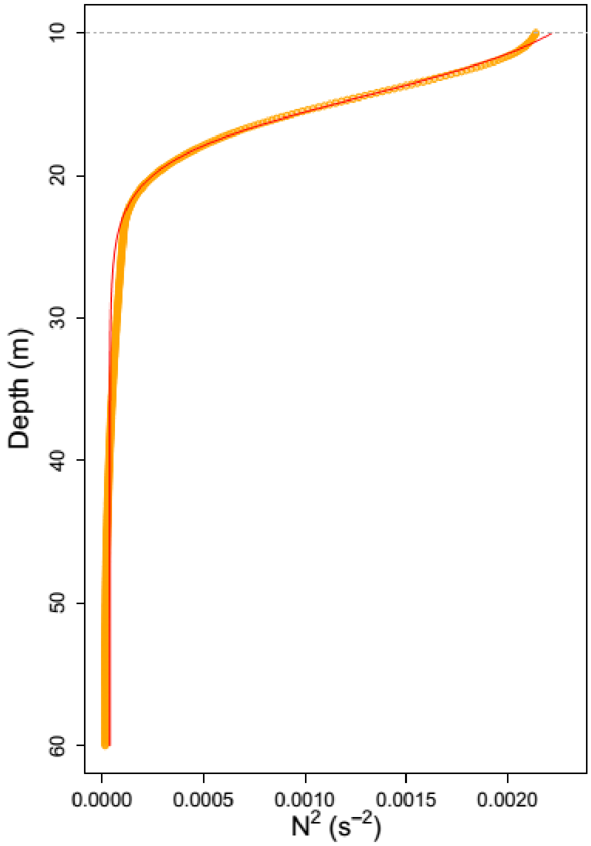

Figure S3.2: Vertical profile of N^2 in the deep layer of Batang Ai. Orange points are the result of a smooth spline applied to a measured temperature profile and the red line is the modeled N^2 derived from fitting a sigmoid curve to the orange data points. The Nash-Sutcliffe index is 0.84 (on log values). The gray dashed line indicates the top of the metalimnion.

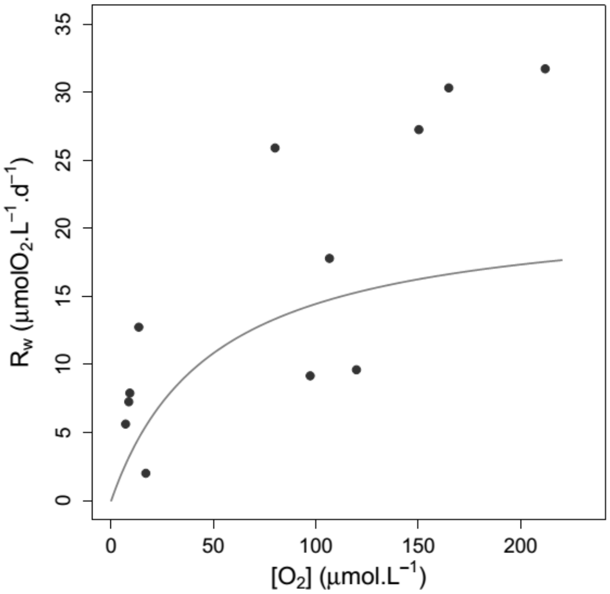

Figure S3.3: Measured (points) and modeled (line, derived from Eq. (3.10)) water column aerobic respiration rates (R_w) in Batang Ai deep layer (>10 m) as a function of available O_2 concentration.

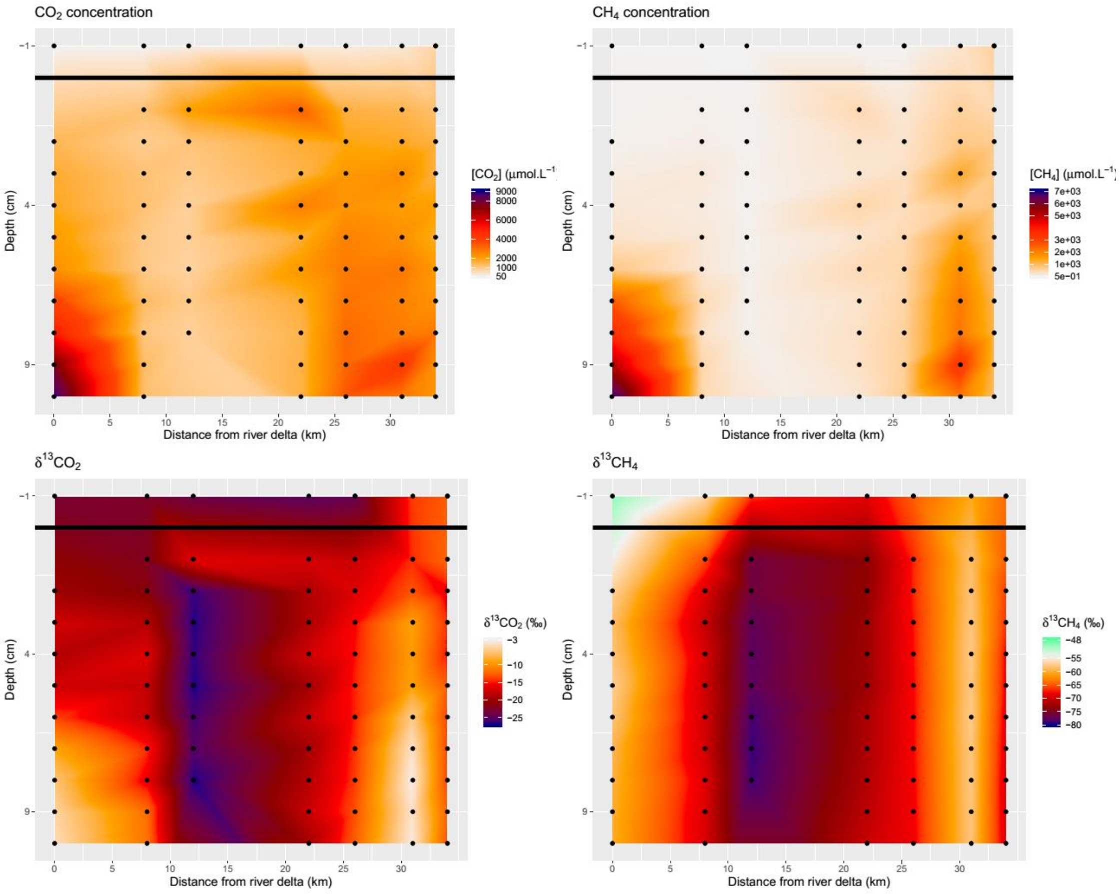

Figure S3.4: Spatial interpolation of pore water sediment CO_2 and CH_4 concentrations and isotopic signatures as a function of sediments depth (+ overlaying water 1 cm above) and distance from the river delta. The solid line represents the sediment surface, and the black circles represent the sampled points.

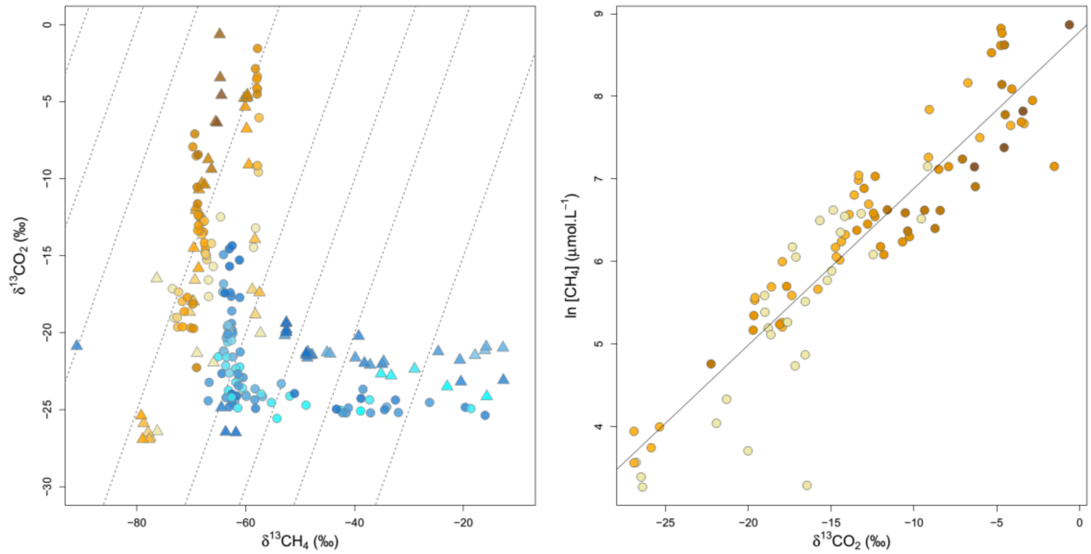

Figure S3.5: Correlation between $\delta^{13}CH_4$ and $\delta^{13}CO_2$ in sediment and deep water samples (left panel) and between CH_4 concentration and $\delta^{13}CO_2$ in the sediments (right panel, p-value < 0.001 and $R^2_{adj} = 0.84$). Light to dark blue represent shallow to deep water samples, and light to dark brown represent shallow to deep sediments samples. In the left panel, triangles and circles represents sites in the reservoir branches and main basin respectively, and dotted diagonals represent 8 different $CO_2 – CH_4$ fractionation lines (of 90, 80, 70, 55, 40, 30, 20 and 5).

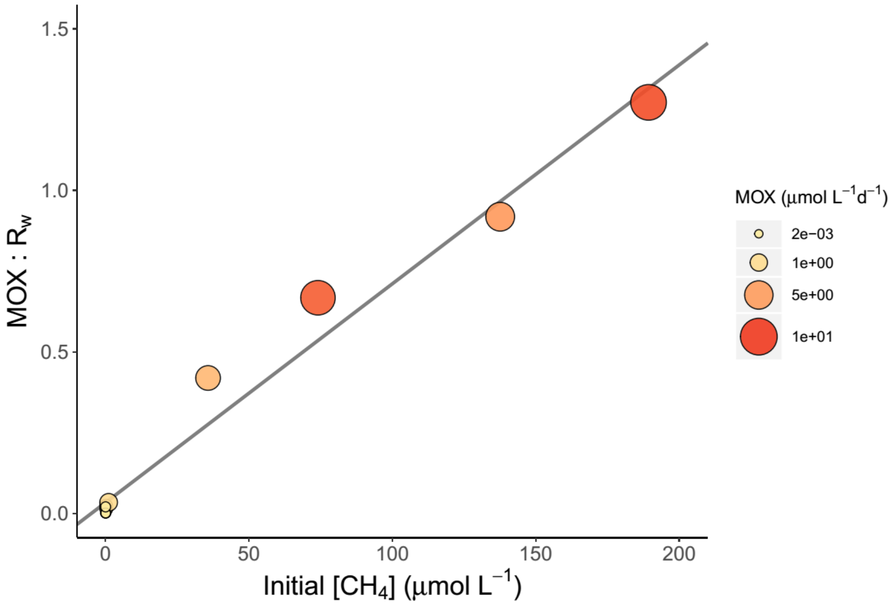

Figure S3.6: CH_4 oxidation rate (MOX, point size and color gradient) and its contribution to total O_2 consumption by aerobic respiration (MOX : R_w ratio) as a function of initial CH_4 concentration in deep water incubations in Batang Ai. The ratio of O_2 : CH_4 consumed (ranging typically from 1 to 2) was set to 1 since a higher value would make the MOX : R_w largely exceed the maximal possible limit of 1. The line represents the linear regression of the variables on the two axes (p-value < 0.001, R^2_{adj} = 0.98). The linear regression of MOX vs initial [CH4] (line not shown) had a p-value < 0.001 and an R^2_{adj} = 0.78.

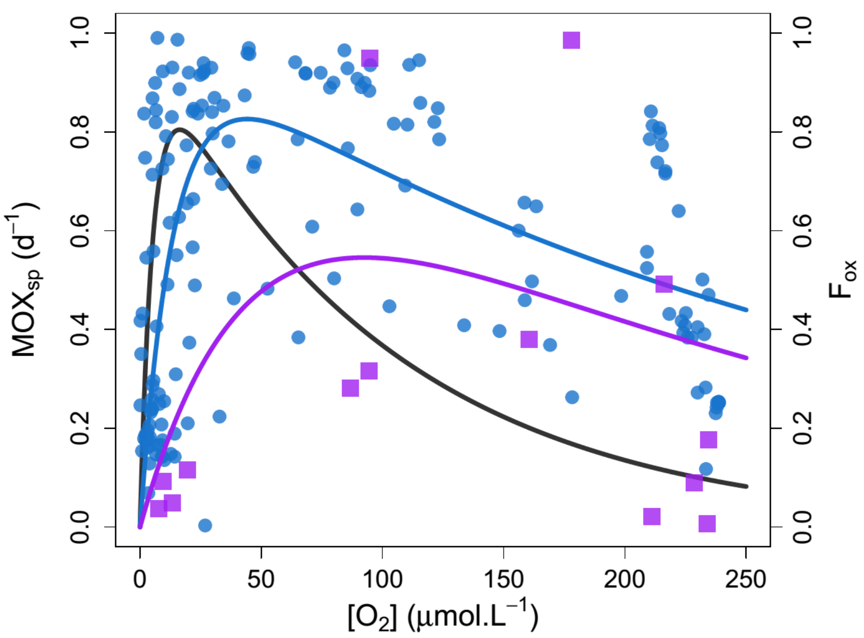

Figure S3.7: Specific CH_4 oxidation (MOX$_{sp}$, derived from incubations, purple squares) and fraction of CH_4 oxidized (F_{ox}, derived from $\delta^{13}CH_4$ in vertical profiles, blue points) as a function of O_2 concentration. Lines represent Eq. (3.14) model fitted to the data in purple (λ = 0.004 and β = 0.02, p-values of 0.01 and 0.19 respectively), and using parameter values of Thottathil *et al*., (2019) in gray (λ = 0.01 and β = 0.18).

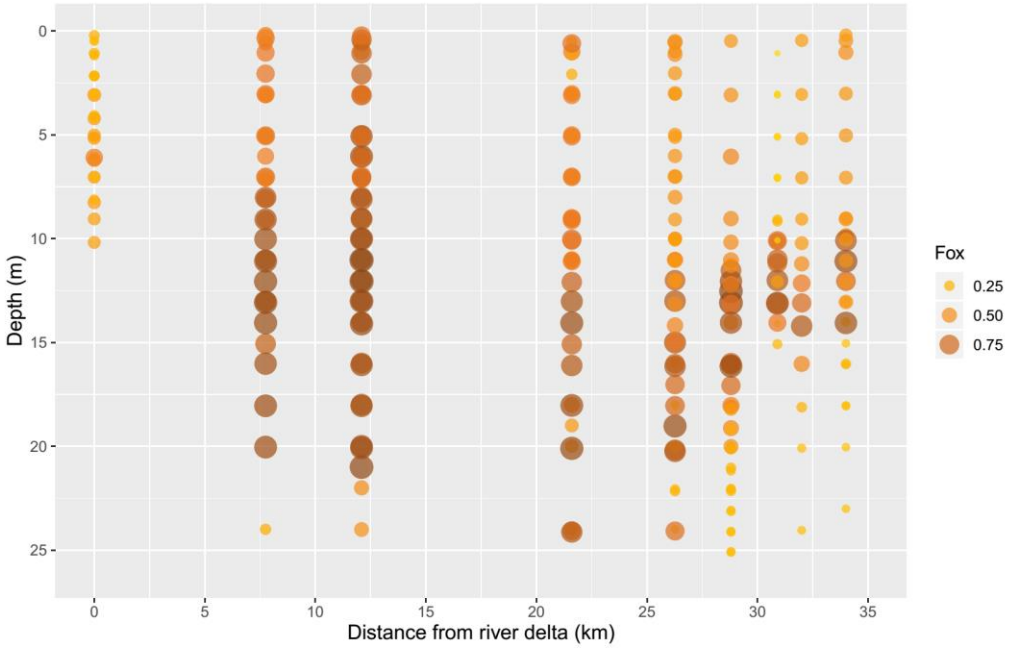

Figure S3.8: Fraction of CH_4 oxidized (F_{ox}) as a function of depth and distance from the river delta for all sites and sampling campaigns.

CONCLUSION

La recherche présentée s'inscrit dans un contexte ou les réservoirs sont des sources de GES (surtout de CO_2 et de CH_4) vers l'atmosphère, mais comprendre et prédire leurs émissions est un défi nécessitant un approfondissement des connaissances sur le sujet. L'objectif général de la thèse est d'obtenir un portrait complet de la dynamique du CO_2 et du CH_4 à l'échelle écosystémique dans un réservoir tropical. En premier lieu, nous voulions comprendre où, quand, et comment les GES sont émis à l'échelle du réservoir, et tester notre capacité actuelle à les prédire (Chapitre I). Pour cela, nous avons fait une évaluation exhaustive des flux de GES du réservoir Batang Ai, prenant en compte la variabilité spatiale et temporelle, ainsi que toutes les voies d'émission en amont et en aval du barrage. Nous avons ensuite comparé les valeurs mesurées sur le terrain aux prédictions des modèles les plus récents pour tester leur performance et identifier leurs failles. Nous voulions ensuite définir l'origine et les facteurs qui déterminent l'ampleur des flux, en surface du réservoir (Chapitre II), et en aval (Chapitre III). Nous avons donc construit un bilan de masse des apports / exports de CO_2 et de CH_4 dans l'épilimnion du réservoir pour déterminer la variabilité et la contribution relative des différentes composantes au flux de surface (Chapitre II). Nous avons ensuite mesuré les taux de production, de consommation, et de transport du CO_2 et du CH_4 dans la couche profonde (qui alimente les émissions en aval), et modélisé l'interaction de ces processus dans l'espace et dans le temps (Chaputre III).

Les résultats du Chapitre I ont révélé l'importance, souvent négligée, de la résolution spatiotemporelle de l'échantillonnage et de l'inclusion de toutes les voies d'émission de GES dans l'estimation de l'empreinte C d'un réservoir. En amont du barrage, les flux diffusifs et ebullitifs mesurés sont relativement faibles et surestimés par les modèles, dû au fait que ces derniers ne prennent pas en compte l'effet de la composition du sol argileux et de la forte pente qui empêche l'accumulation de matière organique dans la zone littorale. Cependant, la plus grande partie des émissions (89 %) ont lieu en aval du barrage, une voie d'émission rarement prise en compte dans la littérature. D'ailleurs, les modèles prédictifs testés sur Batang Ai sous-estiment largement ces émissions en aval, ne considérant que le dégazage du CH_4 dans cette section. En somme, le réservoir étudié émet une grande quantité de GES comparé à d'autres, surtout en aval du barrage et sous forme de CH_4. En effet, la construction du barrage a créé un vaste environnement anoxique (l'hypolimnion) propice à la production de CH_4, et offre aussi une échappatoire directe à ce gaz, à travers la sortie d'eau située en profondeur. Nous avons estimé qu'une sortie d'eau située 5 m plus haut réduirait drastiquement (de 77 %) l'empreinte C du réservoir.

Les résultats du Chapitre II ont mis en évidence les sources et processus régulant les flux diffusifs en surface du réservoir. Ces sources changent selon un gradient hydrologique allant des branches du réservoir au bassin principal, ce qui se reflète dans la structure spatiale des concentrations et des signatures isotopiques du CO_2 et du CH_4. Dans les branches du réservoir, l'apport de GES des flux horizontaux du milieu terrestre et riverain est élevé, et a le potentiel d'alimenter plus de 90 % des émissions de CO_2 et CH_4 dans cette section. Cependant, l'influence de ces apports provenant du bassin versant est localisée, et devient négligeable dans le bassin principal, où les sources de CO_2 et CH_4 divergent créant un découplage entre ces deux gaz. En effet, dans le bassin principal les apports verticaux des couches profondes vers l'épilimnion sont une importante source de CO_2 mais pas de CH_4, et inversement, les apports des sédiments contribuent substantiellement aux émissions de CH_4 (25 %) mais pas de CO_2 (7 %). Cependant, la dynamique des deux gaz dans l'épilimnion est fortement influencée par leur métabolisme dans la colonne d'eau, qui est en même temps un élément central, mais très variable, ajoutant une grande incertitude aux budgets de gaz dans les deux sections du réservoir. Ainsi, le métabolisme dans la colonne d'eau soutient jusqu'à 75 % des émissions de CH_4 dans le bassin principal, et module la direction et l'amplitude des flux de CO_2.

Dans la couche profonde (Chapitre III), l'influence du métabolisme sur la dynamique des GES est aussi présente, et dépend fortement de la disponibilité de l'O_2 pour la respiration aérobique (production de CO_2) et pour l'oxydation du CH_4. Le lien entre les trois gaz (O_2, CO_2, et CH_4) crée un patron spatial le long du continuum hydrologique, où la concentration de CO_2 augmente et celle de O_2 diminue graduellement dans la couche profonde, alors que le CH_4 s'accumule uniquement dans le bassin principal devenu hypoxique / anoxique. La modélisation montre que l'accumulation de GES dans le bassin principal atteint un état d'équilibre environ 10 ans après la construction du barrage, et ce malgré la stratification thermique permanente. La quantité de GES accumulée dans la couche profonde module les émissions de GES en aval du barrage, et dépend de l'interaction entre plusieurs facteurs biogéochimiques. Notamment, la diffusivité verticale des gaz qui joue un rôle prédominant dû à son influence directe sur le mouvement des gaz, mais aussi indirecte via son effet sur la pénétration de l'O_2 dans la couche profonde qui affecte le métabolisme du CO_2 et du CH_4.

Dans l'ensemble, les résultats de l'étude montrent que les émissions en surface du réservoir sont relativement faibles et reflètent en grande partie les apports du bassin versant et le métabolisme interne de la colonne d'eau, tandis que les émissions en aval du barrage sont très élevées et surtout contrôlées par l'O_2 et la le transport vertical des des gaz dans la couche profonde (Figure 4.1). À l'échelle du paysage, l'impact de la construction du barrage sur le cycle du C est surtout apparent avec la création de la couche profonde anoxique du bassin principal, qui accumule de grandes quantités de GES notamment sous forme de CH_4. Dans une perspective de gestion, nos résultats indiquent que l'empreinte climatique du réservoir serait réduite par l'élévation de la prise d'eau, l'oxygénation de l'hypolimnion, et une augmentation du mélange des eaux profondes. D'un point de vue théorique, cette thèse a permis une compréhension intégrale de la dynamique du CO_2 et du CH_4 à l'échelle de l'écosystème, et a identifié les facteurs de régulation les plus importants. L'étude a aussi mis en lumière plusieurs lacunes dans les connaissances actuelles sur le sujet: l'effet de la composition du sol et de la pente sur les flux diffusifs et ebullitifs (Chapitre I), les réactions et facteurs de contrôle du métabolisme du CO_2 et du CH_4 (Chapitre II), la production de CO_2 en anoxie et de CH_4 dans la colonne d'eau (Chapitre III). Explorer les éléments mentionnés dans des recherches futures améliorerait la modélisation des concentrations et de flux de GES dans les réservoirs.

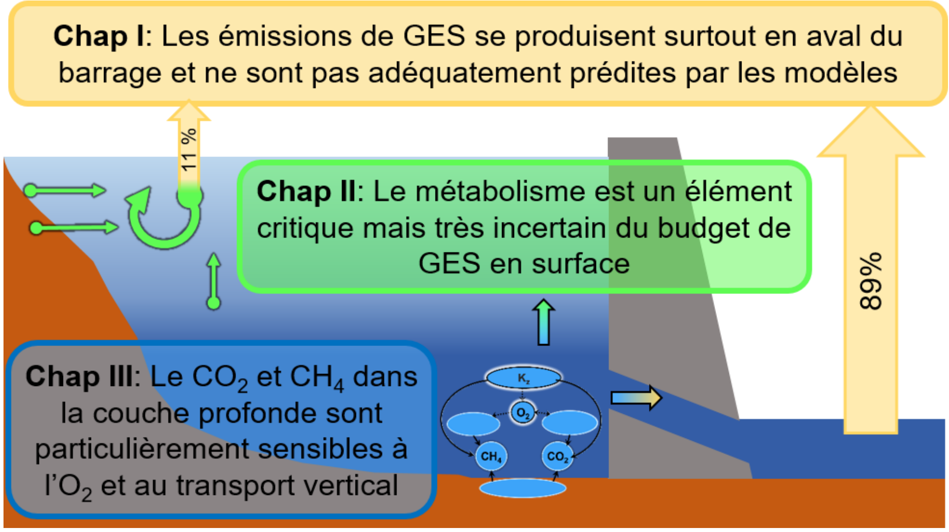

Figure 4.1: Schéma des principales conclusions des trois chapitres de la thèse.

BIBLIOGRAPHIE

Åberg, J., Bergström, A.-K., Algesten, G., Söderback, K. et Jansson, M. (2004). A comparison of the carbon balances of a natural lake (L. Örträsket) and a hydroelectric reservoir (L. Skinnmuddselet) in northern Sweden. *Water Research*, *38*(3), 531-538. doi: 10.1016/j.watres.2003.10.035

Abril, G., Guérin, F., Richard, S., Delmas, R., Galy-Lacaux, C., Gosse, P., … Matvienko, B. (2005). Carbon dioxide and methane emissions and the carbon budget of a 10-year old tropical reservoir (Petit Saut, French Guiana). *Global Biogeochemical Cycles*, *19*(4), 1-16. doi: 10.1029/2005GB002457

Adamczyk, E. M. et Shurin, J. B. (2015). Seasonal Changes in Plankton Food Web Structure and Carbon Dioxide Flux from Southern California Reservoirs. *PloS one*, 1-20. doi: 10.5061/dryad.6tn4h.Funding

Adams, D. D. (2005). Diffuse Flux of Greenhouse Gases — Methane and Carbon Dioxide — at the Sediment-Water Interface of Some Lakes and Reservoirs of the World. Dans *Greenhouse Gas Emissions - Fluxes and Processes* (p. 129-153). doi: 10.1007/978-3-540-26643-3_6

Algesten, G., Sobek, S., Bergström, A. K., Jonsson, A., Tranvik, L. J. et Jansson, M. (2005). Contribution of sediment respiration to summer CO2 emission from low productive boreal and subarctic lakes. *Microbial Ecology*, *50*(4), 529-535. doi: 10.1007/s00248-005-5007-x

Almeida, R. M., Nóbrega, G. N., Junger, P. C., Figueiredo, A. V, Andrade, A. S., Moura, C. G. B., … Kosten, S. (2016). High primary production contrasts with intense carbon emission in a eutrophic tropical reservoir. *Frontiers in Microbiology*, *7*(May), 1-13. doi: 10.3389/fmicb.2016.00717

Alperin, M. J., Blair, N. E., Albert, D. B., Hoehler, T. M. et Martens, C. S. (1992). Factors that control the stable carbon isotopic composition of methane produced in an anoxic marine sediment. *Global Biogeochemical Cycles*, *6*(3), 271-291. doi: 10.1029/92GB01650

Amarasinghe, P. B. et Vijverberg, J. (2002). Primary production in a tropical reservoir in Sri Lanka. *Hydrobiologia*, *487*, 93.

Amon, R. M. W. et Benner, R. (1996). Bacterial utilization of different size classes of dissolved organic matter. *Limnology and Oceanography*, *41*(1), 41-51. doi: 10.4319/lo.1996.41.1.0041

Appling, A. P., Hall, R. O., Arroita, M. et Yackulic, C. B. (2018). *StreamMetabolizer: Models for Estimating Aquatic Photosynthesis and Respiration* (R package version 0.10.9). Récupéré de https://github.com/USGS-R/streamMetabolizer

Barrette, N. et Laprise, R. (2005). A One-Dimensional Model for Simulating the Vertical Transport of Dissolved CO2 and CH4 in Hydroelectric Reservoirs. Dans *Greenhouse Gas Emissions - Fluxes and Processes* (p. 575-595). doi: 10.1007/978-3-540-26643-3_25

Barros, N., Cole, J. J., Tranvik, L. J., Prairie, Y. T., Bastviken, D., Huszar, V. L. M., … Roland, F. (2011). Carbon emission from hydroelectric reservoirs linked to reservoir age and latitude. *Nature Geoscience*, *4*(9), 593-596. doi:

10.1038/ngeo1211

Bastien, J. et Demarty, M. (2013). Spatio-temporal variation of gross CO2 and CH4 diffusive emissions from Australian reservoirs and natural aquatic ecosystems, and estimation of net reservoir emissions. *Lakes & Reservoirs: Research & Management, 18*(2), 115-127. doi: 10.1111/lre.12028

Bastien, J., Demarty, M. et Tremblay, A. (2011). CO2 and CH4 diffusive and degassing emissions from 2003 to 2009 at Eastmain 1 hydroelectric reservoir , Québec , Canada. *Inland waters,* (2), 113-123. doi: 10.5268/IW-1.2.349

Bastviken, D., Cole, J. J., Pace, M. L. et Van de-Bogert, M. C. (2008). Fates of methane from different lake habitats: Connecting whole-lake budgets and CH4 emissions. *Journal of Geophysical Research: Biogeosciences*, *113*(2), 1-13. doi: 10.1029/2007JG000608

Bastviken, D., Cole, J., Pace, M. et Tranvik, L. (2004). Methane emissions from lakes: Dependence of lake characteristics, two regional assessments, and a global estimate. *Global Biogeochemical Cycles*, *18*(4), 1-12. doi: 10.1029/2004GB002238

Bastviken, D., Ejlertsson, J. et Tranvik, L. (2002). Measurement of methane oxidation in lakes: A comparison of methods. *Environmental Science and Technology*, *36*(15), 3354-3361. doi: 10.1021/es010311p

Bastviken, D., Tranvik, L. J., Downing, J. A., Crill, P. M. et Enrich-Prast, A. (2011). Freshwater Methane Emissions Offset the Continental Carbon Sink. *Science, 331*(6013), 50-50. doi: 10.1126/science.1196808

Beaulieu, J. J., DelSontro, T. et Downing, J. A. (2019). Eutrophication will increase methane emissions from lakes and impoundments during the 21st century. *Nature Communications*, *10*(1), 3-7. doi: 10.1038/s41467-019-09100-5

Beaulieu, J. J., McManus, M. G. et Nietch, C. T. (2016). Estimates of reservoir methane emissions based on a spatially balanced probabilistic-survey. *Limnology and Oceanography*, *61*(S1), S27-S40. doi: 10.1002/lno.10284

Berg, A., Lindblad, P. et Svensson, B. H. (2014). Cyanobacteria as a source of hydrogen for methane formation. *World Journal of Microbiology and Biotechnology*, *30*(2), 539-545. doi: 10.1007/s11274-013-1463-5

Berg, P., Risgaard-Petersen, N. et Rysgaard, S. (1998). Interpretation of measured concentration profiles in sediment pore water. *Limnology and Oceanography*, *43*(7), 1500-1510. doi: 10.4319/lo.1998.43.7.1500

Berggren, M., Lapierre, J.-F. et del Giorgio, P. A. (2012). Magnitude and regulation of bacterioplankton respiratory quotient across freshwater environmental gradients. *The ISME Journal*, *6*(5), 984-993. doi: 10.1038/ismej.2011.157

Bergier, I., Novo, E. M. L. M., Ramos, F. M., Mazzi, E. a. et Rasera, M. F. F. L. (2011). Carbon Dioxide and Methane Fluxes in the Littoral Zone of a Tropical Savanna Reservoir (Corumbá, Brazil). *Oecologia Australis, 15*(3), 666-681. doi: 10.4257/oeco.2011.1503.17

Bergström, A.-K., Algesten, G., Sobek, S., Tranvik, L. et Jansson, M. (2004). Emission of CO2 from hydroelectric reservoirs in northern Sweden. *Archiv für Hydrobiologie*, *159*(1), 25-42. doi: 10.1127/0003-9136/2004/0159-0025

Biderre-Petit, C., Jézéquel, D., Dugat-Bony, E., Lopes, F., Kuever, J., Borrel, G., … Peyret, P. (2011). Identification of microbial communities involved in the methane cycle of a freshwater meromictic lake. *FEMS Microbiology Ecology*, *77*(3), 533-545. doi: 10.1111/j.1574-6941.2011.01134.x

Bižić, M., Klintzsch, T., Ionescu, D., Hindyieh, M., Guenthel, M., Muro-Pastor, A. M., … Grossart, H.-P. (2019). Aquatic and terrestrial Cyanobacteria produce methane. *Science Advances*, (13), In Press.

Blair, N., Leu, A., Munoz, E., Olsen, J., Kwong, E. et Des Marais, D. (1985). Carbon isotopic fractionation in heterotrophic microbial metabolism. *Applied and Environmental Microbiology*, *50*(4), 996-1001. doi: 0099-2240/85/100996-06$02.00/0

Blais, J. M. et Kalff, J. (1995). The influence of lake morphometry on sediment focusing. *Limnology and Oceanography*, *40*(3), 582-588. doi: 10.4319/lo.1995.40.3.0582

Bogard, M. J., del Giorgio, P. a, Boutet, L., Chaves, M. C. G., Prairie, Y. T., Merante, A. et Derry, A. M. (2014). Oxic water column methanogenesis as a major component of aquatic CH4 fluxes. *Nature communications*, *5*(May), 5350. doi: 10.1038/ncomms6350

Bogard, M. J. et del Giorgio, P. A. (2016). The role of metabolism in modulating CO2 fluxes in boreal lakes. *Global Biogeochemical Cycles*, *30*(10), 1509-1525. doi: 10.1002/2016GB005463

Bogard, M. J., Kuhn, C. D., Johnston, S. E., Striegl, R. G., Holtgrieve, G. W., Dornblaser, M. M., … Butman, D. E. (2019). Negligible cycling of terrestrial carbon in many lakes of the arid circumpolar landscape. *Nature Geoscience*, *12*(3), 180-185. doi: 10.1038/s41561-019-0299-5

Bogard, M. J., St-Gelais, N. F., Vachon, D. et del Giorgio, P. A. (2020). Patterns of Spring/Summer Open-Water Metabolism Across Boreal Lakes. *Ecosystems*. doi: 10.1007/s10021-020-00487-7

Borrel, G., Jézéquel, D., Biderre-Petit, C., Morel-Desrosiers, N., Morel, J. P., Peyret, P., … Lehours, A. C. (2011). Production and consumption of methane in freshwater lake ecosystems. *Research in Microbiology*, *162*(9), 832-847. doi: 10.1016/j.resmic.2011.06.004

Cammack, W. K. L., Kalff, J., Prairie, Y. T. et Smith, E. M. (2004). Fluorescent dissolved organic matter in lakes: Relationships with heterotrophic metabolism. *Limnology and Oceanography*, *49*(6), 2034-2045. doi: 10.4319/lo.2004.49.6.2034

Cardoso, S. J., Vidal, L. O., Mendon??a, R. F., Tranvik, L. J., Sobek, S. et Roland, F. (2013). Spatial variation of sediment mineralization supports differential CO2 emissions from a tropical hydroelectric reservoir. *Frontiers in Microbiology*, *4*(APR), 1-8. doi: 10.3389/fmicb.2013.000101

Carignan, R., Planas, D. et Vis, C. (2000). Planktonic production and respiration in oligotrophic Shield lakes. *Limnology and Oceanography*, *45*(1), 189-199. doi: 10.4319/lo.2000.45.1.0189

Chanudet, V., Descloux, S., Harby, A., Sundt, H., Hansen, B. H., Brakstad, O., … Guerin, F. (2011). Gross CO2 and CH4 emissions from the Nam Ngum and Nam Leuk sub-tropical reservoirs in Lao PDR. *Science of The Total Environment*, *409*(24), 5382-5391. doi: 10.1016/j.scitotenv.2011.09.018

Chen, H., Yuan, X., Chen, Z., Wu, Y., Liu, X., Zhu, D., … Li, W. (2011). Methane emissions from the surface of the Three Gorges Reservoir. *Journal of Geophysical Research: Atmospheres, 116*(21), 1-5. doi: 10.1029/2011JD016244

Chowdhury, T. R. et Dick, R. P. (2013). Ecology of aerobic methanotrophs in controlling methane fluxes from wetlands. *Applied Soil Ecology*, *65*, 8-22. doi: 10.1016/j.apsoil.2012.12.014

Ciais, P., Sabine, C., Bala, G., Bopp, L., Brovkin, V., Canadell, J., … Munhoven, G. (2013). Carbon and Other Biogeochemical Cycles. *Climate Change 2013 - The Physical Science Basis*, 465-570. doi: 10.1017/CBO9781107415324.015

Cole, J. J. et Caraco, N. F. (1998). Atmospheric exchange of carbon dioxide in a low-wind oligotrophic lake measured by the addition of SF6. *Limnology and Oceanography, 43*(4), 647-656. doi: 10.4319/lo.1998.43.4.0647

Coleman, D. D., Risatti, J. B. et Schoell, M. (1981). Fractionation of carbon and hydrogen isotopes by methane-oxidizing bacteria. *Geochimica et Cosmochimica Acta, 45*(7), 1033-1037. doi: 10.1016/0016-7037(81)90129-0

Coloso, J. J., Cole, J. J. et Pace, M. L. (2011). Difficulty in Discerning Drivers of Lake Ecosystem Metabolism with High-Frequency Data. *Ecosystems*, *14*(6), 935-948. doi: 10.1007/s10021-011-9455-5

Conrad, R. (2005). Quantification of methanogenic pathways using stable carbon isotopic signatures: A review and a proposal. *Organic Geochemistry*, *36*(5), 739-752. doi: 10.1016/j.orggeochem.2004.09.006

Conrad, R. (2009). The global methane cycle: recent advances in understanding the microbial processes involved. *Environmental Microbiology Reports*, *1*(5), 285-292. doi: 10.1111/j.1758-2229.2009.00038.x

Cory, R. M. et Kling, G. W. (2018). Interactions between sunlight and microorganisms influence dissolved organic matter degradation along the aquatic continuum. *Limnology and Oceanography Letters*. doi: 10.1002/lol2.10060

Cotner, J. B. et Biddanda, B. A. (2002). Small players, large role: Microbial influence on biogeochemical processes in pelagic aquatic ecosystems. *Ecosystems*, *5*(2), 105-121. doi: 10.1007/s10021-001-0059-3

da Silva, M. G., Packer, A. P., Sampaio, F. G., Marani, L., Mariano, E. V. C., Pazianotto, R. A. A., … Alvalá, P. C. (2018). Impact of intensive fish farming on methane emission in a tropical hydropower reservoir. *Climatic Change*, *150*(3-4), 195-210. doi: 10.1007/s10584-018-2281-4

de Mello, N. A. S. T., Brighenti, L. S., Barbosa, F. A. R., Staehr, P. A. et Bezerra Neto, J. F. (2018). Spatial variability of methane (CH4) ebullition in a tropical hypereutrophic reservoir: silted areas as a bubble hot spot. *Lake and Reservoir Management*, *34*(2), 105-114. doi: 10.1080/10402381.2017.1390018

Deemer, B. R., Harrison, J. A., Li, S., Beaulieu, J. J., DelSontro, T., Barros, N., … Vonk, J. A. (2016). Greenhouse Gas Emissions from Reservoir Water Surfaces: A New Global Synthesis. *BioScience*, *66*(11), 949-964. doi: 10.1093/biosci/biw117

DelSontro, T., Beaulieu, J. J. et Downing, J. A. (2018a). Greenhouse gas emissions from lakes and impoundments: Upscaling in the face of global change. *Limnology and Oceanography Letters*, *3*(3), 64-75. doi: 10.1002/lol2.10073

DelSontro, T., Boutet, L., St-Pierre, A., del Giorgio, P. A. et Prairie, Y. T. (2016a). Methane ebullition and diffusion from northern ponds and lakes regulated by the interaction between temperature and system productivity. *Limnology and Oceanography*, *61*(S1), S62-S77. doi: 10.1002/lno.10335

DelSontro, T., del Giorgio, P. A. et Prairie, Y. T. (2018b). No Longer a Paradox: The Interaction Between Physical Transport and Biological Processes Explains the Spatial Distribution of Surface Water Methane Within and Across Lakes. *Ecosystems*, *21*(6), 1073-1087. doi: 10.1007/s10021-017-0205-1

DelSontro, T., Kunz, M. J., Kempter, T., Wüest, A., Wehrli, B. et Senn, D. B. (2011). Spatial Heterogeneity of Methane Ebullition in a Large Tropical Reservoir. *Environmental Science & Technology*, *45*(23), 9866-9873. doi: 10.1021/es2005545

DelSontro, T., McGinnis, D. F., Sobek, S., Ostrovsky, I. et Wehrli, B. (2010). Extreme Methane Emissions from a Swiss Hydropower Reservoir: Contribution from Bubbling Sediments. *Environmental Science & Technology*, *44*(7), 2419-2425. doi: 10.1021/es9031369

DelSontro, T., Perez, K. K., Sollberger, S. et Wehrli, B. (2016b). Methane dynamics downstream of a temperate run-of-the-river reservoir. *Limnology and Oceanography, 61*, S188-S203. doi: 10.1002/lno.10387

Demarty, M. et Bastien, J. (2011). GHG emissions from hydroelectric reservoirs in tropical and equatorial regions: Review of 20 years of CH4 emission measurements. *Energy Policy*, *39*(7), 4197-4206. doi: 10.1016/j.enpol.2011.04.033

Demarty, M., Bastien, J. et Tremblay, a. (2011). Annual follow-up of gross diffusive carbon dioxide and methane emissions from a boreal reservoir and two nearby lakes in Québec, Canada. *Biogeosciences, 8*(3), 41-53. doi: 10.5194/bg-8-41-2011

Demarty, M., Bastien, J., Tremblay, A., Hesslein, R. H. et Gill, R. (2009). Greenhouse gas emissions from boreal reservoirs in Manitoba and Québec, Canada, measured with automated systems. *Environmental Science and Technology*, *43*(23), 8908-8915. doi: 10.1021/es8035658

Demirel, B. et Scherer, P. (2008). The roles of acetotrophic and hydrogenotrophic methanogens during anaerobic conversion of biomass to methane: A review. *Reviews in Environmental Science and Biotechnology*, *7*(2), 173-190. doi: 10.1007/s11157-008-9131-1

Donis, D., Flury, S., Stöckli, A., Spangenberg, J. E., Vachon, D. et McGinnis, D. F. (2017). Full-scale evaluation of methane production under oxic conditions in a mesotrophic lake. *Nature Communications, 8*(1), 1-11. doi: 10.1038/s41467-017-01648-4

dos Santos, M. A., Rosa, L. P., Sikar, B., Sikar, E. et dos Santos, E. O. (2006). Gross greenhouse gas fluxes from hydro-power reservoir compared to thermo-power plants. *Energy Policy, 34*(4), 481-488. doi: 10.1016/j.enpol.2004.06.015

Duarte, C. M. et Agustí, S. (1998). The CO2 balance of unproductive aquatic ecosystems. *Science*, *281*(5374), 234-236. doi: 10.1126/science.281.5374.234

Ducharme-Riel, V., Vachon, D., del Giorgio, P. A. et Prairie, Y. T. (2015). The Relative Contribution of Winter Under-Ice and Summer Hypolimnetic CO2 Accumulation to the Annual CO2 Emissions from Northern Lakes. *Ecosystems*, *18*(4), 547-559. doi: 10.1007/s10021-015-9846-0

Eckert, W. et Conrad, R. (2007). Sulfide and methane evolution in the hypolimnion of a subtropical lake: A three-year study. *Biogeochemistry*, *82*(1), 67-76. doi: 10.1007/s10533-006-9053-3

Encinas Fernández, J., Peeters, F. et Hofmann, H. (2014). Importance of the autumn overturn and anoxic conditions in the hypolimnion for the annual methane emissions from a temperate lake. *Environmental Science and Technology*, *48*(13), 7297-7304. doi: 10.1021/es4056164

R. Douglas Evans, Joe Wisniewski, Jan R. Wisniewski. (1997). *The Interactions Between Sediments and Water*. Dordrecht : Springer Netherlands. doi: 10.1007/978-94-011-5552-6

Fahrner, S., Radke, M., Karger, D. et Blodau, C. (2008). Organic matter mineralisation in the hypolimnion of an eutrophic Maar lake. *Aquatic Sciences*, *70*(3), 225-237. doi: 10.1007/s00027-008-8008-2

Fearnside, P. M. (2006). Greenhouse gas emissions from hydroelectric dams: Reply to Rosa et al. *Climatic Change*, *75*(1-2), 103-109. doi: 10.1007/s10584-005-9016-z

Fearnside, P. M. et Pueyo, S. (2012). Greenhouse-gas emissions from tropical dams. *Nature Climate Change*, *2*(6), 382-384. doi: 10.1038/nclimate1540

Fekete, B. M., Vörösmarty, C. J. et Grabs, W. (2002). High-resolution fields of global runoff combining observed river discharge and simulated water balances. *Global Biogeochemical Cycles*, *16*(3), 15-1-15-10. doi: 10.1029/1999GB001254

Ferland, M. E., Prairie, Y. T., Teodoru, C. et Del Giorgio, P. A. (2014). Linking organic carbon sedimentation, burial efficiency, and long-term accumulation in boreal lakes. *Journal of Geophysical Research: Biogeosciences*, *119*(5), 836-847. doi: 10.1002/2013JG002345

Ferry, J. (2012). *Methanogenesis: Ecology, Physiology, Biochemistry & Genetics*. (s. l. : n. é.).

Galy-Lacaux, C., Delmas, R., Jambert, C., Dumestre, J.-F., Labroue, L., Richard, S. et Gosse, P. (1997). Gaseous emissions and oxygen consumption in hydroelectric dams: A case study in French Guyana. *Global Biogeochemical Cycles*, *11*(4), 471-483. doi: 10.1029/97GB01625

Galy-Lacaux, C., Delmas, R., Kouadio, G., Richard, S. et Gosse, P. (1999). Long-term greenhouse gas emissions from hydroelectric reservoirs in tropical forest regions. *Global Biogeochemical Cycles*, *13*(2), 503-517.

Gebert, J., Köthe, H. et Gröngröft, A. (2006). Prognosis of methane formation by river sediments. *Journal of Soils and Sediments*, *6*(2), 75-83. doi: 10.1065/jss2006.04.153

Giles, J. (2006). Methane quashes green credentials of hydropower. *Nature*, *444*(7119), 524-5. doi: 10.1038/444524a

Giorgio, P. A. Del, Cole, J. J., Caraco, N. F. et Peters, R. H. (1999). Linking Planktonic Biomass and Metabolism to Net Gas Fluxes in Northern Temperate Lakes. *Ecology*, *80*(4), 1422. doi: 10.2307/177085

Grinham, A., Dunbabin, M. et Albert, S. (2018). Importance of sediment organic matter to methane ebullition in a sub-tropical freshwater reservoir. *Science of The Total*

Environment, *621*, 1199-1207. doi: 10.1016/j.scitotenv.2017.10.108

Grinham, A., Dunbabin, M., Gale, D. et Udy, J. (2011). Quantification of ebullitive and diffusive methane release to atmosphere from a water storage. *Atmospheric Environment*, *45*(39), 7166-7173. doi: 10.1016/j.atmosenv.2011.09.011

Grossart, H.-P., Frindte, K., Dziallas, C., Eckert, W. et Tang, K. W. (2011). Microbial methane production in oxygenated water column of an oligotrophic lake. *Proceedings of the National Academy of Sciences*, *108*(49), 19657-19661. doi: 10.1073/pnas.1110716108

Gruca-Rokosz, R. et Tomaszek, J. A. (2015). Methane and carbon dioxide in the sediment of a eutrophic reservoir: Production pathways and diffusion fluxes at the sediment-water interface. *Water, Air, and Soil Pollution*, *226*(2). doi: 10.1007/s11270-014-2268-3

Guérin, F. et Abril, G. (2007). Significance of pelagic aerobic methane oxidation in the methane and carbon budget of a tropical reservoir. *Journal of Geophysical Research: Biogeosciences*, *112*(G3), n/a-n/a. doi: 10.1029/2006JG000393

Guérin, F., Abril, G., Richard, S., Burban, B., Reynouard, C., Seyler, P. et Delmas, R. (2006). Methane and carbon dioxide emissions from tropical reservoirs: Significance of downstream rivers. *Geophysical Research Letters*, *33*(21), L21407. doi: 10.1029/2006GL027929

Guérin, F., Deshmukh, C., Labat, D., Pighini, S., Vongkhamsao, A., Guédant, P., … Serça, D. (2016). Effect of sporadic destratification, seasonal overturn, and artificial mixing on CH4 emissions from a subtropical hydroelectric reservoir. *Biogeosciences*, *13*(12), 3647-3663. doi: 10.5194/bg-13-3647-2016

Hall, R. O. et Hotchkiss, E. R. (2017). Stream Metabolism. Dans *Methods in Stream Ecology* (vol. 2, p. 219-233). Elsevier. doi: 10.1016/B978-0-12-813047-6.00012-7

Hanson, P. C., Bade, D. L., Carpenter, S. R. et Kratz, T. K. (2003). Lake metabolism: Relationships with dissolved organic carbon and phosphorus. *Limnology and Oceanography*, *48*(3), 1112-1119. doi: 10.4319/lo.2003.48.3.1112

Hofmann, H., Federwisch, L. et Peeters, F. (2010). Wave-induced release of methane: Littoral zones as source of methane in lakes. *Limnology and Oceanography*, *55*(5), 1990-2000. doi: 10.4319/lo.2010.55.5.1990

Holmer, M. et Storkholm, P. (2001). Sulphate reduction and sulphur cycling in lake sediments: A review. *Freshwater Biology*, *46*(4), 431-451. doi: 10.1046/j.1365-2427.2001.00687.x

Hondzo, M. et Stefan, H. G. (1993). Lake Water Temperature Simulation Model. *Journal of Hydraulic Engineering*, *119*(11), 1251-1273. doi: 10.1061/(ASCE)0733-9429(1993)119:11(1251)

Hornibrook, E. R. C., Longstaffe, F. J. et Fyfe, W. S. (2000). Evolution of stable carbon isotope compositions for methane and carbon dioxide in freshwater wetlands and other anaerobic environments. *Geochimica et Cosmochimica Acta*, *64*(6), 1013-1027. doi: 10.1016/S0016-7037(99)00321-X

Hotchkiss, E. R., Hall Jr, R. O., Sponseller, R. A., Butman, D., Klaminder, J., Laudon, H., … Karlsson, J. (2015). Sources of and processes controlling CO2 emissions change with the size of streams and rivers. *Nature Geoscience*, *8*(9), 696-699. doi: 10.1038/ngeo2507

Humborg, C., Mörth, C., Sundbom, M., Borg, H., Blenckner, T., Giesler, R. et Ittekkot, V. (2010). CO2 supersaturation along the aquatic conduit in Swedish watersheds as constrained by terrestrial respiration, aquatic respiration and weathering. *Global Change Biology*, *16*(7), 1966-1978. doi: 10.1111/j.1365-2486.2009.02092.x

Huotari, J., Ojala, A., Peltomaa, E., Pumpanen, J., Hari, P. et Vesala, T. (2009). Temporal variations in surface water CO2 concentration in a boreal humic lake based on high-frequency measurements. *Boreal environment research*, *14*, 48-60.

Huttunen, J. T., Väisänen, T. S., Hellsten, S. K. et Martikainen, P. J. (2006). Methane fluxes at the sediment-water interface in some boreal lakes and reservoirs. *Boreal Environment Research*, *11*(1), 27-34.

ICOLD. (2019). *International commission on large dams*. Récupéré de http://www.icold-cigb.net/GB/Dams/role_of_dams.asp

Imboden, D. M. (1973). Limnologische Transport- und Nährstoffmodelle. *Schweizerische Zeitschrift für Hydrologie*, *35*(1), 29-68. doi: 10.1007/BF02502063

International Hydropower Association (IHA). (2015). *A brief history of hydropower*. Récupéré de https://www.hydropower.org/a-brief-history-of-hydropower

Isidorova, A., Grasset, C., Mendonça, R. et Sobek, S. (2019). Methane formation in tropical reservoirs predicted from sediment age and nitrogen. *Scientific Reports*, *9*(1), 1-9. doi: 10.1038/s41598-019-47346-7

ISRIC - World Soil Information. (2019). *SoilGrids v0.5.3*. Récupéré de https://soilgrids.org/#!/?layer=ORCDRC_M_sl4_250m&vector=1

Iversen, N., Oremland, R. S. et Klug, M. J. (1987). Big Soda Lake (Nevada). 3. Pelagic methanogenesis and anaerobic methane oxidation. *Limnology and Oceanography*, *32*(4), 804-814. doi: 10.4319/lo.1987.32.4.0804

Jones, J. R. et Knowlton, M. F. (1993). Limnology Of Missouri Reservoirs: An Analysis of Regional Patterns. *Lake and Reservoir Management*, *8*(1), 17-30. doi: 10.1080/07438149309354455

Joyce, J. (2003). Physical Controls on Methane Ebullition from Reservoirs and Lakes. *Environmental and Engineering Geoscience*, *9*(2), 167-178. doi: 10.2113/9.2.167

Kankaala, P., Huotari, J., Peltomaa, E., Saloranta, T. et Ojala, A. (2006). Methanotrophic activity in relation to methane efflux and total heterotrophic bacterial production in a stratified, humic, boreal lake. *Limnology and Oceanography*, *51*(2), 1195-1204. doi: 10.4319/lo.2006.51.2.1195

Kankaala, P., Huotari, J., Tulonen, T. et Ojala, A. (2013a). Lake-size dependent physical forcing drives carbon dioxide and methane effluxes from lakes in a boreal landscape. *Limnology and Oceanography*, *58*(6), 1915-1930. doi: 10.4319/lo.2013.58.6.1915

Kankaala, P., Lopez Bellido, J., Ojala, A., Tulonen, T. et Jones, R. I. (2013b). Variable Production by Different Pelagic Energy Mobilizers in Boreal Lakes. *Ecosystems*, *16*(6), 1152-1164. doi: 10.1007/s10021-013-9674-z

Karlsson, J., Jansson, M. et Jonsson, A. (2007). Respiration of allochthonous organic carbon in unproductive forest lakes determined by the Keeling plot method.

Limnology and Oceanography, *52*(2), 603-608. doi: 10.4319/lo.2007.52.2.0603

Keller, M. et Stallard, R. F. (1994). Methane emission by bubbling from Gatun Lake, Panama. *Journal of Geophysical Research*, *99*(D4), 8307. doi: 10.1029/92JD02170

Kelly, C. a. et Chynoweth, D. P. (1981). The contributions of temperature and of the input of organic matter in controlling rates of sediment methanogenesis1. *Limnology and Oceanography*, *26*(5), 891-897. doi: 10.4319/lo.1981.26.5.0891

Kemenes, A., Forsberg, B. R. et Melack, J. M. (2007). Methane release below a tropical hydroelectric dam. *Geophysical Research Letters*, *34*(12), 1-5. doi: 10.1029/2007GL029479

Kemenes, A., Forsberg, B. R. et Melack, J. M. (2016). Downstream emissions of CH4 and CO2 from hydroelectric reservoirs (Tucuruí, Samuel, and Curuá-Una) in the Amazon basin. *Inland Waters*, *6*(3), 295-302. doi: 10.1080/IW-6.3.980

Kim, B., Choi, K., Kim, C., Lee, U. H. et Kim, Y. H. (2000). Effects of the summer monsoon on the distribution and loading of organic carbon in a deep reservoir, Lake Soyang, Korea. *Water Research*, *34*(14), 3495-3504. doi: 10.1016/S0043-1354(00)00104-4

Kimmel, B. L. et Groeger, A. W. (1984). Factors Controlling Primary Production in Lakes and Reservoirs: a Perspective. *Lake and Reservoir Management*, *1*(1), 277-281. doi: 10.1080/07438148409354524

Kimmel, Bruce L., Lind, O. et Paulson, L. J. (1990). Reservoir primary production. Dans *Reservoir Limnology: Ecological Perspectives* (chap. 6, p. 133-). (s. l. : n.

é.).

Kindler, R., Siemens, J., Kaiser, K., Walmsley, D. C., Bernhofer, C., Buchmann, N., … Kaupenjohann, M. (2011). Dissolved carbon leaching from soil is a crucial component of the net ecosystem carbon balance. *Global Change Biology*, *17*(2), 1167-1185. doi: 10.1111/j.1365-2486.2010.02282.x

Knoll, L. B., Vanni, M. J. et Renwick, W. H. (2003). Phytoplankton primary production and photosynthetic parameters in reservoirs along a gradient of watershed land use. *Limnology and Oceanography*, *48*(2), 608-617. doi: 10.4319/lo.2003.48.2.0608

Knox, M., Quay, P. D. et Wilbur, D. (1992). Kinetic isotopic fractionation during air-water gas transfer of O2 , N2 , CH4 , and H2. *Journal of Geophysical Research*, *97*(C12), 20335. doi: 10.1029/92JC00949

Kreling, J., Bravidor, J., McGinnis, D. F., Koschorreck, M. et Lorke, A. (2014). Physical controls of oxygen fluxes at pelagic and benthic oxyclines in a lake. *Limnology and Oceanography*, *59*(5), 1637-1650. doi: 10.4319/lo.2014.59.5.1637

Lapierre, J.-F. et del Giorgio, P. A. (2012). Geographical and environmental drivers of regional differences in the lake pCO2 versus DOC relationship across northern landscapes. *Journal of Geophysical Research: Biogeosciences*, *117*(G3), n/a-n/a. doi: 10.1029/2012JG001945

Ledwell, J. J. (1984). The Variation of the Gas Transfer Coefficient with Molecular Diffusity. Dans *Gas Transfer at Water Surfaces* (p. 293-302). Dordrecht : Springer Netherlands. doi: 10.1007/978-94-017-1660-4_27

Lee, K., Matsuno, T., Endoh, T., Ishizaka, J., Zhu, Y., Takeda, S. et Sukigara, C. (2017). A role of vertical mixing on nutrient supply into the subsurface chlorophyll maximum in the shelf region of the East China Sea. *Continental Shelf Research, 143*(October), 139-150. doi: 10.1016/j.csr.2016.11.001

Lefèvre, N. et Merlivat, L. (2012). Carbon and oxygen net community production in the eastern tropical Atlantic estimated from a moored buoy. *Global Biogeochemical Cycles*, *26*(1), n/a-n/a. doi: 10.1029/2010GB004018

Lehmusluoto, P., Machbub, B., Terangna, N., Rusmiputro, S., Achmad, F., Boer, L., … Margana, a. (1997). *National inventory of the major lakes and reservoirs in Indonesia. General limnology*. Récupéré de http://www.kolumbus.fi/pasi.lehmusluoto/210_expedition_indodanau_report1997.PDF

Lehner, B., Liermann, C. R., Revenga, C., Vörösmarty, C., Fekete, B., Crouzet, P., … Wisser, D. (2011). High-resolution mapping of the world’s reservoirs and dams for sustainable river-flow management. *Frontiers in Ecology and the Environment*, *9*(9), 494-502. doi: 10.1890/100125

Lemoalle, J. (1981). Photosynthetic production and phytoplankton in the euphotic zone of some African and temperate lakes. *Revue d’Hydrobiologie Tropicale*.

Lenhart, K., Klintzsch, T., Langer, G., Nehrke, G., Bunge, M., Schnell, S. et Keppler, F. (2015). Evidence for methane production by marine algae (*Emiliana huxleyi*) and its implication for the methane paradox in oxic waters. *Biogeosciences Discussions*, *12*(24), 20323-20360. doi: 10.5194/bgd-12-20323-2015

Lewis, W. M. (2010). Biogeochemistry of tropical lakes. *SIL Proceedings, 1922-2010*, *30*(10), 1595-1603. doi: 10.1080/03680770.2009.11902383

Li, M., Peng, C., Wang, M., Xue, W., Zhang, K., Wang, K., … Zhu, Q. (2017). The carbon flux of global rivers: A re-evaluation of amount and spatial patterns. *Ecological Indicators*, *80*(April), 40-51. doi: 10.1016/j.ecolind.2017.04.049

Lide, D. (2005). *CRC Handbook of Chemistry and Physics*. Boca Raton, FL. Récupéré de http://www.hbcpnetbase.com

Liikanen, A., Huttunen, J. T., Valli, K. et Martikainen, P. J. (2002). Methane cycling in the sediment and water column of mid-boreal hyper-eutrophic Lake Kevätön, Finland. *Fundamental and Applied Limnology*, *154*(4), 585-603. doi: 10.1127/archiv-hydrobiol/154/2002/585

Likens, G. E. (1975). Primary production of inland aquatic ecosystems. *Primary productivity of the biosphere. Springer-Verlag, New York*, 185-202. doi: 10.1007/978-3-642-80913-2_9

Lima, I. B. T. (2005). Biogeochemical distinction of methane releases from two Amazon hydroreservoirs. *Chemosphere*, *59*(11), 1697-1702. doi: 10.1016/j.chemosphere.2004.12.011

Lind, O. T., Terrell, T. T. et Kimmel, B. L. (1993). Problems in reservoir trophic-state classification and implications for reservoir management. Dans *Comparative Reservoir Limnology and Water Quality Management* (vol. 23, p. 57-67). Dordrecht : Springer Netherlands. doi: 10.1007/978-94-017-1096-1_3

Ling, T.-Y., Gerunsin, N., Soo, C.-L., Nyanti, L., Sim, S.-F. et Grinang, J. (2017). Seasonal Changes and Spatial Variation in Water Quality of a Large Young

Tropical Reservoir and Its Downstream River. *Journal of Chemistry*, *2017*, 1-16. doi: 10.1155/2017/8153246

Lliros, M., Gich, F., Plasencia, A., Auguet, J.-C., Darchambeau, F., Casamayor, E. O., … Borrego, C. (2010). Vertical Distribution of Ammonia-Oxidizing Crenarchaeota and Methanogens in the Epipelagic Waters of Lake Kivu (Rwanda-Democratic Republic of the Congo). *Applied and Environmental Microbiology*, *76*(20), 6853-6863. doi: 10.1128/AEM.02864-09

Loken, L. C., Crawford, J. T., Schramm, P. J., Stadler, P., Desai, A. R. et Stanley, E. H. (2019). Large Spatial and Temporal Variability of Carbon Dioxide and Methane in a Eutrophic Lake. *Journal of Geophysical Research: Biogeosciences*, *124*(7), 2248-2266. doi: 10.1029/2019JG005186

Lupon, A., Denfeld, B. A., Laudon, H., Leach, J., Karlsson, J. et Sponseller, R. A. (2019). Groundwater inflows control patterns and sources of greenhouse gas emissions from streams. *Limnology and Oceanography*, *64*(4), 1545-1557. doi: 10.1002/lno.11134

Maavara, T., Lauerwald, R., Regnier, P. et Van Cappellen, P. (2017). Global perturbation of organic carbon cycling by river damming. *Nature Communications*, *8*(May), 1-10. doi: 10.1038/ncomms15347

Maberly, S. C. (2008). Diel, episodic and seasonal changes in pH and concentrations of inorganic carbon in a productive lake. *Freshwater Biology*, *35*(3), 579-598. doi: 10.1111/j.1365-2427.1996.tb01770.x

Macklin, P. A., Suryaputra, I. G. N. A., Maher, D. T. et Santos, I. R. (2018). Carbon dioxide dynamics in a lake and a reservoir on a tropical island (Bali, Indonesia).

PLOS ONE, *13*(6), e0198678. doi: 10.1371/journal.pone.0198678

Mandic-Mulec, I., Gorenc, K., Petrišič, M. G., Faganeli, J. et Ogrinc, N. (2012). Methanogenesis pathways in a stratified eutrophic alpine lake (Lake Bled, Slovenia). *Limnology and Oceanography*, *57*(3), 868-880. doi: 10.4319/lo.2012.57.3.0868

Marotta, H., Pinho, L. et Gudasz, C. (2014). Greenhouse gas production in low-latitude lake sediments responds strongly to warming. *Nature Climate Change*, *4*(May), 11-14. doi: 10.1038/NCLIMATE2222

Martin, P., Cherukuru, N., Tan, A. S. Y., Sanwlani, N., Mujahid, A. et Müller, M. (2018). Distribution and cycling of terrigenous dissolved organic carbon in peatland-draining rivers and coastal waters of Sarawak, Borneo. *Biogeosciences*, *15*(22), 6847-6865. doi: 10.5194/bg-15-6847-2018

Martinsen, K. T., Kragh, T. et Sand-Jensen, K. (2020). Carbon dioxide efflux and ecosystem metabolism of small forest lakes. *Aquatic Sciences*, *82*(1), 9. doi: 10.1007/s00027-019-0682-8

Matthews, C. J. D., Joyce, E. M., St. Louis, V. L., Schiff, S. L., Venkiteswaran, J. J., Hall, B. D., … Beaty, K. G. (2005). Carbon dioxide and methane production in small reservoirs flooding upland boreal forest. *Ecosystems*, *8*, 267-285. doi: 10.1007/s10021-005-0005-x

McCallister, S. L. et del Giorgio, P. a. (2008). Direct measurement of the d13C signature of carbon respired by bacteria in lakes: Linkages to potential carbon sources, ecosystem baseline metabolism, and CO2 fluxes. *Limnology and Oceanography*, *53*(4), 1204-1216. doi: 10.4319/lo.2008.53.4.1204

McGinnis, D. F., Greinert, J., Artemov, Y., Beaubien, S. E. et Wüest, A. (2006). Fate of rising methane bubbles in stratified waters: How much methane reaches the atmosphere? *Journal of Geophysical Research*, *111*(C9), C09007. doi: 10.1029/2005JC003183

Michaud, A. B., Dore, J. E., Achberger, A. M., Christner, B. C., Mitchell, A. C., Skidmore, M. L., … Priscu, J. C. (2017). Microbial oxidation as a methane sink beneath the West Antarctic Ice Sheet. *Nature Geoscience*, *10*(8), 582-586. doi: 10.1038/NGEO2992

Monteith, D. T., Stoddard, J. L., Evans, C. D., De Wit, H. A., Forsius, M., Høgåsen, T., … Vesely, J. (2007). Dissolved organic carbon trends resulting from changes in atmospheric deposition chemistry. *Nature*, *450*(7169), 537-540. doi: 10.1038/nature06316

Murase, J. et Sugimoto, A. (2005). Inhibitory effect of light on methane oxidation in the pelagic water column of a mesotrophic lake (Lake Biwa, Japan). *Limnology and Oceanography*, *50*(4), 1339-1343. doi: 10.4319/lo.2005.50.4.1339

Musenze, R. S., Fan, L., Grinham, A., Werner, U., Gale, D., Udy, J. et Yuan, Z. (2016). Methane dynamics in subtropical freshwater reservoirs and the mediating microbial communities. *Biogeochemistry*, *128*(1-2), 233-255. doi: 10.1007/s10533-016-0206-8

Musenze, R. S., Grinham, A., Werner, U., Gale, D., Sturm, K., Udy, J. et Yuan, Z. (2014). Assessing the Spatial and Temporal Variability of Diffusive Methane and Nitrous Oxide Emissions from Subtropical Freshwater Reservoirs. *Environmental Science & Technology*, *48*, 14499-14507.

Myhre, G., Shindell, D., Bréon, F.-M., Collins, W., Fuglestvedt, J., Huang, J., … Zhang, H. (2013). Anthropogenic and Natural Radiative Forcing. Dans *Climate Change 2013: The Physical Science Basis. Contribution of Working Group I to the Fifth Assessment Report of the Intergovernmental Panel on Climate Change* (p. 659-740). Cambridge, United Kindom. Récupéré de http://www.climatechange2013.org/images/report/WG1AR5_Chapter08_FINAL.pdf

NASA. (2008). *Surface meteorology and Solar Energy (SSE) Release 6.0 Data set*. Récupéré de http://eosweb.larc.nasa.gov/sse/

Natchimuthu, S., Sundgren, I., Gålfalk, M., Klemedtsson, L. et Bastviken, D. (2017). Spatiotemporal variability of lake pCO2 and CO2 fluxes in a hemiboreal catchment. *Journal of Geophysical Research: Biogeosciences*, *122*(1), 30-49. doi: 10.1002/2016JG003449

Oades, J. M. (1988). The retention of organic matter in soils. *Biogeochemistry*, *5*(1), 35-70. doi: 10.1007/BF02180317

Oakey, N. S. (1982). Determination of the Rate of Dissipation of Turbulent Energy from Simultaneous Temperature and Velocity Shear Microstructure Measurements. *Journal of Physical Oceanography*, *12*(3), 256-271. doi: 10.1175/1520- 0485(1982)012<0256:DOTROD>2.0.CO;2, 1982

Odum, H. T. (1956). Primary Production in Flowing Waters1. *Limnology and Oceanography*, *1*(2), 102-117. doi: 10.4319/lo.1956.1.2.0102

Ometto, J. P., Cimbleris, A. C. P., Dos Santos, M. a., Rosa, L. P., Abe, D., Tundisi, J. G., … Roland, F. (2013). Carbon emission as a function of energy generation in hydroelectric reservoirs in Brazilian dry tropical biome. *Energy Policy, 58*, 109-116. doi: 10.1016/j.enpol.2013.02.041

Osborn, T. R. (1980). Estimates of the Local Rate of Vertical Diffusion from Dissipation Measurements. *Journal of Physical Oceanography*, *10*(1), 83-89. doi: 10.1175/1520-0485(1980)010<0083:EOTLRO>2.0.CO;2

Oswald, K., Milucka, J., Brand, A., Littmann, S., Wehrli, B., Kuypers, M. M. M. et Schubert, C. J. (2015). Light-Dependent Aerobic Methane Oxidation Reduces Methane Emissions from Seasonally Stratified Lakes. *PLOS ONE*, *10*(7), e0132574. doi: 10.1371/journal.pone.0132574

Pace, M. L. et Prairie, Y. T. (2005). Respiration in lakes. Dans *Respiration in Aquatic Ecosystems* (p. 103-121). Oxford University Press. doi: 10.1093/acprof:oso/9780198527084.003.0007

Pacheco, F. S., Soares, M. C. S., Assireu, A. T., Curtarelli, M. P., Roland, F., Abril, G., … Ometto, J. P. (2015). The effects of river inflow and retention time on the spatial heterogeneity of chlorophyll and water–air CO2 fluxes in a tropical hydropower reservoir. *Biogeosciences*, *12*(1), 147-162. doi: 10.5194/bg-12-147-2015

Paranaíba, J. R., Barros, N., Mendonça, R., Linkhorst, A., Isidorova, A., Roland, F., … Sobek, S. (2018). Spatially Resolved Measurements of CO2 and CH4 Concentration and Gas-Exchange Velocity Highly Influence Carbon-Emission Estimates of Reservoirs. *Environmental Science & Technology*, *52*(2), 607-615. doi: 10.1021/acs.est.7b05138

Pasche, N., Hofmann, H., Bouffard, D., Schubert, C. J., Lozovik, P. A. et Sobek, S.

(2019). Implications of river intrusion and convective mixing on the spatial and temporal variability of under-ice CO2. *Inland Waters, 2041*. doi: 10.1080/20442041.2019.1568073

Patton, C. et Kryskalla, J. (2003). *Methods of analysis by the U.S. Geological Survey National Water Quality Laboratory : evaluation of alkaline persulfate digestion as an alternative to Kjeldahl digestion for determination of total and dissolved nitrogen and phosphorus in water*. doi: 10.3133/wri034174

Pebesma, E. J. (2004). Multivariable geostatistics in S: the gstat package. *Computers & Geosciences, 30*(7), 683-691. doi: 10.1016/j.cageo.2004.03.012

Pollard, P. C. (2013). In situ rapid measures of total respiration rate capture the super labile DOC bacterial substrates of freshwater. *Limnology and Oceanography: Methods, 11*(11), 584-593. doi: 10.4319/lom.2013.11.584

Prairie, Y. T., Alm, J., Beaulieu, J., Barros, N., Battin, T., Cole, J., … Vachon, D. (2018). Greenhouse Gas Emissions from Freshwater Reservoirs: What Does the Atmosphere See? *Ecosystems, 21*(5), 1058-1071. doi: 10.1007/s10021-017-0198-9

Prairie, Y. T., Alm, J., Mercier-Blais, S. et Nahas, R. (2017). *The GHG Reservoir Tool (G-res) Technical documentation, UNESCO/IHA research project on the GHG status of freshwater reservoirs. Version 1.13*.

Prairie, Y. T., Bird, D. F. et Cole, J. J. (2002). The summer metabolic balance in the epilimnion of southeastern Quebec lakes. *Limnology and Oceanography, 47*(1), 316-321. doi: 10.4319/lo.2002.47.1.0316

Prairie, Y. T., Duarte, C. M. et Kalff, J. (1989). Unifying Nutrient–Chlorophyll Relationships in Lakes. *Canadian Journal of Fisheries and Aquatic Sciences*, *46*(7), 1176-1182. doi: 10.1139/f89-153

Pu, J., Li, J., Zhang, T., Martin, J. B. et Yuan, D. (2020). Varying thermal structure controls the dynamics of CO2 emissions from a subtropical reservoir, south China. *Water Research*, 115831. doi: 10.1016/j.watres.2020.115831

R Core Team. (2017). *R: A language and environment for statistical computing*. Vienna, Austria : R Foundation for Statistical Computing. Récupéré de https://www.r-project.org/

Rasilo, T., Hutchins, R. H. S., Ruiz-González, C. et del Giorgio, P. A. (2017). Transport and transformation of soil-derived CO2, CH4 and DOC sustain CO2 supersaturation in small boreal streams. *Science of The Total Environment*, *579*, 902-912. doi: 10.1016/j.scitotenv.2016.10.187

Rasilo, T., Prairie, Y. T. et Del Giorgio, P. A. (2014). Large-scale patterns in summer diffusive CH4 fluxes across boreal lakes, and contribution to diffusive C emissions. *Global change biology*, *1*, 1-16. doi: 10.1111/gcb.12741

Raymond, P. A., Hartmann, J., Lauerwald, R., Sobek, S., McDonald, C., Hoover, M., … Guth, P. (2013). Global carbon dioxide emissions from inland waters. *Nature*, *503*(7476), 355-359. doi: 10.1038/nature12760

Reis, P. C. J., Ruiz-González, C., Soued, C., Crevecoeur, S. et Prairie, Y. T. (2020a). Rapid shifts in methanotrophic bacterial communities mitigate methane emissions from a tropical hydropower reservoir and its downstream river. *submitted manuscript*.

Reis, P. C. J., Thottathil, S. D., Ruiz-González, C. et Prairie, Y. T. (2020b). Niche separation within aerobic methanotrophic bacteria across lakes and its link to methane oxidation rates. *Environmental Microbiology*, *22*(2), 738-751. doi: 10.1111/1462-2920.14877

Riera, J. L., Schindler, J. E. et Kratz, T. K. (1999). Seasonal dynamics of carbon dioxide and methane in two clear-water lakes and two bog lakes in northern Wisconsin, U.S.A. *Can J Fish Aquat Sci*, *274*, 1-10. doi: 10.1139/f98-182

Rimmer, A., Eckert, W., Nishri, A. et Agnon, Y. (2006). Evaluating hypolimnetic diffusion parameters in thermally stratified lakes. *Limnology and Oceanography*, *51*(4), 1906-1914. doi: 10.4319/lo.2006.51.4.1906

Roberts, B. J. et Howarth, R. W. (2006). Nutrient and light availability regulate the relative contribution of autotrophs and heterotrophs to respiration in freshwater pelagic ecosystems. *Limnology and Oceanography*, *51*(1), 288-298. doi: 10.4319/lo.2006.51.1.0288

Roland, F., Vidal, L. O., Pacheco, F. S., Barros, N. O., Assireu, A., Ometto, J. P. H. B., … Cole, J. J. (2010). Variability of carbon dioxide flux from tropical (Cerrado) hydroelectric reservoirs. *Aquatic Sciences*, *72*(3), 283-293. doi: 10.1007/s00027-010-0140-0

Rosa, L. P., Aurelio, M., Santos, D. O. S., Matvienko, B., Oliveira, E. et Sikar, E. (2004). Reservoirs in Tropical Regions. *Climatic Change*, *66*, 9-21.

Rosa, L. P., Dos Santos, M. A., Matvienko, B., Sikar, E., Lourenço, R. S. M. et Menezes, C. F. (2003). Biogenic gas production from major Amazon reservoirs, Brazil. *Hydrological Processes*, *17*(October 2002), 1443-1450. doi:

10.1002/hyp.1295

Rowan, D. J., Kalff, J. et Rasmussen, J. B. (1992). Estimating the Mud Deposition Boundary Depth in Lakes from Wave Theory. *Canadian Journal of Fisheries and Aquatic Sciences*, *49*(12), 2490-2497. doi: 10.1139/f92-275

Rudd, J. W. M., Hamilton, R. D. et Campbell, N. E. R. (1974). Measurement of microbial oxidation of methane in lake water. *Limnology and Oceanography*, *19*(3), 519-524. doi: 10.4319/lo.1974.19.3.0519

Rudd, J. W. M., Harris, R., Kelly, C. A. et Hecky, R. E. (1993). Are Hydroelectric Reservoirs Significant Sources of Greenhouse Gases? *Ambio*, *22*(4), 246-248. Récupéré de http://www.jstor.org/stable/4314078

Rudd, J. W. M. M. et Hamilton, R. D. (1978). Methane cycling in a eutrophic shield lake and its effects on whole lake metabolism. *Limnology and Oceanography*, *23*(2), 337-348. doi: 10.4319/lo.1978.23.2.0337

Rudorff, C. M., Melack, J. M., MacIntyre, S., Barbosa, C. C. F. et Novo, E. M. L. M. (2011). Seasonal and spatial variability of CO2 emission from a large floodplain lake in the lower Amazon. *Journal of Geophysical Research: Biogeosciences*, *116*(4), 1-12. doi: 10.1029/2011JG001699

Sand-Jensen, K. et Staehr, P. A. (2009). Net heterotrophy in small danish lakes: A widespread feature over gradients in trophic status and land cover. *Ecosystems*, *12*(2), 336-348. doi: 10.1007/s10021-008-9226-0

Sarawak Government. (2019). *The Geography of Sarawak*. Récupéré de https://www.sarawak.gov.my/web/home/article_view/159/176/

Sartory, D. P. et Grobbelaar, J. U. (1984). Extraction of chlorophyll a from freshwater phytoplankton for spectrophotometric analysis. *Hydrobiologia*, *114*(3), 177-187. doi: 10.1007/BF00031869

Schmid, M., De Batist, M., Granin, N. G., Kapitanov, V. A., McGinnis, D. F., Mizandrontsev, I. B., … Wüest, A. (2007). Sources and sinks of methane in Lake Baikal: A synthesis of measurements and modeling. *Limnology and Oceanography*, *52*(5), 1824-1837. doi: 10.4319/lo.2007.52.5.1824

Schmid, M., Halbwachs, M., Wehrli, B. et Wüest, A. (2005). Weak mixing in Lake Kivu: New insights indicate increasi risk of uncontrolled gas eruption. *Geochemistry, Geophysics, Geosystems*, *6*(7), 1-11. doi: 10.1029/2004GC000892

Schmid, M., Halbwachs, M. et Wüest, A. (2006). Simulation of CO2 concentrations, temperature, and stratification in Lake Nyos for different degassing scenarios. *Geochemistry, Geophysics, Geosystems*, *7*(6). doi: 10.1029/2005GC001164

Scott Winton, R., Calamita, E. et Wehrli, B. (2019). Reviews and syntheses: Dams, water quality and tropical reservoir stratification. *Biogeosciences*, *16*(8), 1657-1671. doi: 10.5194/bg-16-1657-2019

Sellers, P., Hesslein, R. H. et Kelly, C. a. (1995). Continuous measurement of CO2 for estimation of air-water fluxes in lakes: An in situ technique. *Limnology and Oceanography*, *40*(3), 575-581. doi: 10.4319/lo.1995.40.3.0575

Shelley, F., Ings, N., Hildrew, A. G., Trimmer, M. et Grey, J. (2017). Bringing methanotrophy in rivers out of the shadows. *Limnology and Oceanography*, *62*(6), 2345-2359. doi: 10.1002/lno.10569

Sherman, B. et Ford, P. (2011). Methane Emissions from Two reservoirs in a steep, sub- Tropical rainforest catchment. Dans D. K. Begbie et S. L. Wakem (dir.), *Science Forum and Stakeholder Engagement: Building Linkages, Collaboration and Science Quality* (p. 1-9). Brisbane, Queensland : Urban Water Security Research Alliance.

Skeel, R. D. et Berzins, M. (1990). A Method for the Spatial Discretization of Parabolic Equations in One Space Variable. *SIAM Journal on Scientific and Statistical Computing*, *11*(1), 1-32. doi: 10.1137/0911001

Sobek, S., Delsontro, T., Wongfun, N. et Wehrli, B. (2012). Extreme organic carbon burial fuels intense methane bubbling in a temperate reservoir. *Geophysical Research Letters*, *39*(1), 2-5. doi: 10.1029/2011GL050144

Sobek, S., Tranvik, L. J. et Cole, J. J. (2005). Temperature independence of carbon dioxide supersaturation in global lakes. *Global Biogeochemical Cycles*, *19*(2), n/a-n/a. doi: 10.1029/2004GB002264

Sobek, S., Tranvik, L. J., Prairie, Y. T., Kortelainen, P. et Cole, J. J. (2007). Patterns and regulation of dissolved organic carbon: An analysis of 7,500 widely distributed lakes. *Limnology and Oceanography*, *52*(3), 1208-1219. doi: 10.4319/lo.2007.52.3.1208

Solomon, C. T., Bruesewitz, D. A., Richardson, D. C., Rose, K. C., Van de Bogert, M. C., Hanson, P. C., … Zhu, G. (2013). Ecosystem respiration: Drivers of daily variability and background respiration in lakes around the globe. *Limnology and Oceanography*, *58*(3), 849-866. doi: 10.4319/lo.2013.58.3.0849

Soued, C., del Giorgio, P. A. et Maranger, R. (2016). Nitrous oxide sinks and emissions in boreal aquatic networks in Québec. *Nature Geoscience*, *9*(2), 116-120. doi: 10.1038/ngeo2611

Soued, C. et Prairie, Y. T. (2020). The carbon footprint of a Malaysian tropical reservoir: measured versus modelled estimates highlight the underestimated key role of downstream processes. *Biogeosciences*, *17*(2), 515-527. doi: 10.5194/bg-17-515-2020

St. Louis, V. L., Kelly, C. A., Duchemin, É., Rudd, J. W. M. et Rosenberg, D. M. (2000). Reservoir Surfaces as Sources of Greenhouse Gases to the Atmosphere: A Global Estimate. *Bioscience*, *50*(9), 766–775. doi: 10.1641/0006-3568(2000)050[0766:RSASOG]2.0.CO;2

Staehr, P. A. et Sand-Jensen, K. (2007). Temporal dynamics and regulation of lake metabolism. *Limnology and Oceanography*, *52*(1), 108-120. doi: 10.4319/lo.2007.52.1.0108

Tamooh, F., Borges, A. V., Meysman, F. J. R., Van Den Meersche, K., Dehairs, F., Merckx, R. et Bouillon, S. (2013). Dynamics of dissolved inorganic carbon and aquatic metabolism in the Tana River basin, Kenya. *Biogeosciences*, *10*(11), 6911-6928. doi: 10.5194/bg-10-6911-2013

Tan, A. C. (2015). *Water and sediment quality of Batang Ai Reservoir*. Récupéré de https://ir.unimas.my/id/eprint/10428/

Tang, K. W., McGinnis, D. F., Frindte, K., Brüchert, V. et Grossart, H. P. (2014). Paradox reconsidered: Methane oversaturation in well-oxygenated lake waters. *Limnology and Oceanography*, *59*(1), 275-284. doi: 10.4319/lo.2014.59.1.0275

Tank, J. L., Rosi-Marshall, E. J., Griffiths, N. A., Entrekin, S. A. et Stephen, M. L. (2010). A review of allochthonous organic matter dynamics and metabolism in streams. *Journal of the North American Benthological Society, 29*(1), 118-146. doi: 10.1899/08-170.1

Teodoru, C. R., Bastien, J., Bonneville, M.-C., del Giorgio, P. A., Demarty, M., Garneau, M., … Tremblay, A. (2012). The net carbon footprint of a newly created boreal hydroelectric reservoir. *Global Biogeochemical Cycles, 26*(2). doi: 10.1029/2011GB004187

Teodoru, C. R., Prairie, Y. T. et del Giorgio, P. A. (2011). Spatial Heterogeneity of Surface CO2 Fluxes in a Newly Created Eastmain-1 Reservoir in Northern Quebec, Canada. *Ecosystems, 14*(1), 28-46. doi: 10.1007/s10021-010-9393-7

Thérien, N. et Morrison, K. (2005). Production of GHG from the Decomposition of in vitro Inundated Phytomass and Soil. Dans *Greenhouse Gas Emissions — Fluxes and Processes* (p. 315-338). doi: 10.1007/978-3-540-26643-3_14

Thornton, K. W., Kimmel, B. L. et Payne, F. E. (1990). *Reservoir Limnology: Ecological Perspectives*. (s. l.) : John Wiley & Sons, Inc.

Thottathil, S. D., Reis, P. C. J., del Giorgio, P. A. et Prairie, Y. T. (2018). The Extent and Regulation of Summer Methane Oxidation in Northern Lakes. *Journal of Geophysical Research: Biogeosciences, 123*(10), 3216-3230. doi: 10.1029/2018JG004464

Thottathil, S. D., Reis, P. C. J. et Prairie, Y. T. (2019). Methane oxidation kinetics in northern freshwater lakes. *Biogeochemistry*, *143*(1), 105-116. doi: 10.1007/s10533-019-00552-x

Tranvik, L. J., Cole, J. J. et Prairie, Y. T. (2018). The study of carbon in inland waters-from isolated ecosystems to players in the global carbon cycle. *Limnology and Oceanography Letters*, *3*(3), 41-48. doi: 10.1002/lol2.10068

Tremblay, A., Therrien, J., Hamlin, B., Wichmann, E. et LeDrew, L. J. (2005). GHG Emissions from Boreal Reservoirs and Natural Aquatic Ecosystems. Dans *Environmental Science and Engineering* (chap. 8, p. 209-232). doi: 10.1007/978-3-540-26643-3_9

Troell, M. et Berg, H. (1997). Cage fish farming in the tropical Lake Kariba, Zimbabwe: Impact and biogeochemical changes in sediment. *Aquaculture Research*, *28*(7), 527-544. doi: 10.1046/j.1365-2109.1997.00889.x

UNESCO/IHA. (2017). *The GHG Reservoir Tool (G- res)*. Récupéré de https://g-res.hydropower.org/

Vachon, D. et del Giorgio, P. A. (2014). Whole-Lake CO2 Dynamics in Response to Storm Events in Two Morphologically Different Lakes. *Ecosystems*, *17*(8), 1338-1353. doi: 10.1007/s10021-014-9799-8

Vachon, D., Langenegger, T., Donis, D. et McGinnis, D. F. (2019). Influence of water column stratification and mixing patterns on the fate of methane produced in deep sediments of a small eutrophic lake. *Limnology and Oceanography*, *64*(5), 2114-2128. doi: 10.1002/lno.11172

Vachon, D., Sadro, S., Bogard, M. J., Lapierre, J., Baulch, H. M., Rusak, J. A., … Giorgio, P. A. (2020). Paired O 2 –CO 2 measurements provide emergent insights into aquatic ecosystem function. *Limnology and Oceanography Letters*. doi: 10.1002/lol2.10135

Valentine, D. L. (2002). Biogeochemistry and microbial ecology of methane oxidation in anoxic environments: A review. *Antonie van Leeuwenhoek, International Journal of General and Molecular Microbiology, 81*(1-4), 271-282. doi: 10.1023/A:1020587206351

Venkiteswaran, J. J., Schiff, S. L., St. Louis, V. L., Matthews, C. J. D., Boudreau, N. M., Joyce, E. M., … Bodaly, R. A. (2013). Processes affecting greenhouse gas production in experimental boreal reservoirs. *Global Biogeochemical Cycles*, *27*(2), 567-577. doi: 10.1002/gbc.20046

Walker, W. W. (1984). Empirical Prediction of Chlorophyll in Reservoirs. *Lake and Reservoir Management*, *1*(1), 292-297. doi: 10.1080/07438148409354527

Wang, F., Wang, B., Liu, C. Q., Wang, Y., Guan, J., Liu, X. et Yu, Y. (2011). Carbon dioxide emission from surface water in cascade reservoirs-river system on the Maotiao River, southwest of China. *Atmospheric Environment*, *45*(23), 3827-3834. doi: 10.1016/j.atmosenv.2011.04.014

Wang, Q., Dore, J. E. et McDermott, T. R. (2017). Methylphosphonate metabolism by Pseudomonas sp. populations contributes to the methane oversaturation paradox in an oxic freshwater lake. *Environmental Microbiology*, *19*(6), 2366-2378. doi: 10.1111/1462-2920.13747

Wanninkhof, R. (1992). Relationship between wind speed and gas exchange over the ocean. *Journal of Geophysical Research*, *97*(C5), 7373. doi: 10.1029/92JC00188

Wasli, M. E., Tanaka, S., Kendawang, J. J., Abdu, A., Lat, J., Morooka, Y., … Sakurai, K. (2011). Soils and Vegetation Condition of Natural Forests and Secondary Fallow Forests within Batang Ai National Park Boundary , Sarawak , Malaysia.

Kuroshio Science, *5*(1), 67-76.

Weather Spark. (s. d.). *Average Weather at Simanggang Malaysia*. Récupéré de https://weatherspark.com/y/149163/Average-Weather-at-Simanggang-Malaysia-Year-Round

Webb, J. R., Hayes, N. M., Simpson, G. L., Leavitt, P. R., Baulch, H. M. et Finlay, K. (2019). Widespread nitrous oxide undersaturation in farm waterbodies creates an unexpected greenhouse gas sink. *Proceedings of the National Academy of Sciences*, *116*(20), 9814-9819. doi: 10.1073/pnas.1820389116

West, W. E., Coloso, J. J. et Jones, S. E. (2012). Effects of algal and terrestrial carbon on methane production rates and methanogen community structure in a temperate lake sediment. *Freshwater Biology*, *57*(5), 949-955. doi: 10.1111/j.1365-2427.2012.02755.x

Wetzel, R. G. et Likens, G. E. (2000). *Limnological Analyses* (3^e éd.). New York, NY : Springer New York. doi: 10.1007/978-1-4757-3250-4

Whiticar, M. J. (1999). Carbon and hydrogen isotope systematics of bacterial formation and oxidation of methane. *Chemical Geology*, *161*(1-3), 291-314. doi: 10.1016/S0009-2541(99)00092-3

Wik, M., Thornton, B. F., Bastviken, D., MacIntyre, S., Varner, R. K. et Crill, P. M. (2014). Energy input is primary controller of methane bubbling in subarctic lakes. *Geophysical Research Letters*, *41*(2), 555-560. doi: 10.1002/2013GL058510

Wilkinson, G. M., Buelo, C. D., Cole, J. J. et Pace, M. L. (2016). Exogenously produced CO2 doubles the CO2 efflux from three north temperate lakes.

Geophysical Research Letters, *43*(5), 1996-2003. doi: 10.1002/2016GL067732

Williams, P. J. I. et Robertson, J. E. (1991). Overall planktonic oxygen and carbon dioxide metabolisms: the problem of reconciling observations and calculations of photosynthetic quotients. *Journal of Plankton Research*. doi: 10.1093/oxfordjournals.plankt.a042366

Winfrey, M. R. et Zeikus, J. G. (1979). Microbial Methanogenesis and Acetate Metabolism in a meromictic lake. *Applied and Environmental Microbiology*, *37*(2), 213-221. doi: 10.1128/aem.37.2.213-221.1979

Winslow, L., Read, J., Woolway, R., Brentrup, J., Leach, T., Zwart, J., … Collinge, D. (2018). *rLakeAnalyzer: Lake Physics Tools* (R package version 1.11.4). Récupéré de https://cran.r-project.org/package=rLakeAnalyzer

Wüest, A. et Lorke, A. (2009). Small-Scale Turbulence and Mixing: Energy Fluxes in Stratified Lakes. Dans *Encyclopedia of Inland Waters* (p. 628-635). Elsevier. doi: 10.1016/B978-012370626-3.00084-3

Yao, M., Henny, C. et Maresca, J. A. (2016). Freshwater Bacteria Release Methane as a By-Product of Phosphorus Acquisition. *Applied and Environmental Microbiology*, *82*(23), 6994-7003. doi: 10.1128/AEM.02399-16

Youngblut, N. D., Dell'Aringa, M. et Whitaker, R. J. (2014). Differentiation between sediment and hypolimnion methanogen communities in humic lakes. *Environmental Microbiology*, *16*(5), 1411-1423. doi: 10.1111/1462-2920.12330

Yvon-Durocher, G., Allen, A. P., Bastviken, D., Conrad, R., Gudasz, C., St-Pierre, A., … del Giorgio, P. a. (2014). Methane fluxes show consistent temperature dependence across microbial to ecosystem scales. *Nature*, *507*(7493), 488-91. doi: 10.1038/nature13164

Zambrano-Bigiarini, M. (2020). *hydroGOF: Goodness-of-fit functions for comparison of simulated and observed hydrological time series* (v0.4-0). doi: 10.5281/zenodo.839854

Zarfl, C., Lumsdon, A. E., Berlekamp, J., Tydecks, L. et Tockner, K. (2015). A global boom in hydropower dam construction. *Aquatic Sciences*, *77*(1), 161-170. doi: 10.1007/s00027-014-0377-0

Zhang, Q., Tao, Z., Ma, Z., Gao, Q., Deng, H., Xu, P., … Lin, Y. (2019). Hydro-ecological controls on riverine organic carbon dynamics in the tropical monsoon region. *Scientific Reports*, *9*(1), 1-11. doi: 10.1038/s41598-019-48208-y

Zhao, Y., Wu, B. F. et Zeng, Y. (2013). Spatial and temporal patterns of greenhouse gas emissions from Three Gorges Reservoir of China. *Biogeosciences*, *10*(2), 1219-1230. doi: 10.5194/bg-10-1219-2013

Zigah, P. K., Oswald, K., Brand, A., Dinkel, C., Wehrli, B. et Schubert, C. J. (2015). Methane oxidation pathways and associated methanotrophic communities in the water column of a tropical lake. *Limnology and Oceanography*, *60*(2), 553-572. doi: 10.1002/lno.10035